Combined inversion methods for inverse conductivity problems

Rahma Jerbi

University of Sfax

Faculty of Sciences of Sfax

Department of Mathematics

DOCTORAL THESIS

For the degree of

Doctor of Philosophy in Mathematics

Presented by

Rahma Jerbi

Combined inversion methods for inverse conductivity problems

Defended on October 28, 2023, in front of the jury:

Mr. Afif Masmoudi	**University of Sfax**	**President**
Mrs. Amel Ben Abda	**University of Tunis El Manar**	**Reviewer**
Mr. Maher Moakher	**University of Tunis El Manar**	**Reviewer**
Mr. Mondher Benjemaa	**University of Sfax**	**Examiner**
Mr. Slim Chaabane	**University of Sfax**	**Supervisor**
Mr. Houssem Haddar	**INRIA & Institut Polytechnique de Paris**	**Supervisor**
Mr. Mohamed Hbaib	**University of Sfax**	**Invited**

Acknowledgments

First, I would like to express my profound gratitude to my PhD supervisors, Prof. Slim Chaabane and Prof. Houssem Haddar. I sincerely thank you both for your trust, granting me research freedom, your invaluable guidance and mentorship, and most importantly, for standing by my side during all the difficult moments.

I would also like to extend my thanks to Professors Amel Ben Abda and Maher Moakher for agreeing to review this work and for the time they dedicated to reading and assessing this thesis, as well as for preparing their reports. I am deeply grateful to Professors Afif Masmoudi, Mondher Benjemaa, and Mohamed Hbaib for agreeing to be part of the jury.

My appreciation extends to all the members of the Mathematics Department at the Faculty of Sciences of Sfax and the LAMHA laboratory for providing me with such a friendly and supportive environment. Special thanks to Bilel Charfi and Zouhour Jlali for our enjoyable discussions, and to Assistant Fatma Abid for her valuable administrative assistance. I also want to acknowledge my doctoral friends, Mariem Ammar, Yosra Barkaoui, Khouloud Dammak, and Chaima Hmani, with whom I shared many cherished moments during my thesis.

Additionally, I want to express my gratitude to all the members of the IDEFIX team for their warmth and friendliness. A special thanks goes to Marcella, who provided invaluable assistance during my internship when we shared the same office, and to my doctoral and post-doctoral friends, Amal, Nouha, and Mohamed Aziz, for the fantastic moments we shared during my internships.

A huge thank you to my friends Yassmine, Vanessa and Walid, who provided invaluable assistance during my stays in France and with whom I shared wonderful moments.

Before I wrap up, I want to thank my friends whom I met in Albania during my participation in the CIMPA summer school and who have remained in contact with me, especially Ina Hila, Gazi Ozdemir and Destiny S. Lutero.

Finally, I want to express my deepest gratitude to my family, with a special mention of my sister Hanen, for their unwavering support during these years of my thesis.

Abstract

In this thesis, we develop an inversion method that combines the use of a Kohn-Vogelius type cost functional with a non-overlapping domain decomposition method as an iterative solver. The idea behind this method is to iterate simultaneously on the solution of the direct problem using the domain decomposition method and on the unknown of the inverse problem using gradient descent on the Kohn-Vogelius cost functional. This type of approach falls into the category of "one-shot inversion methods," and its use has the potential to significantly reduce the cost of inversion when the numerical solution of the direct problem is costly. We are particularly interested in the case of geometric inverse problems where the unknown of the inverse problem is the support of a physical parameter's discontinuity. The developments made in this area were modeled on the inverse electrical conductivity problem, where the goal is to reconstruct the conductivity discontinuity interface from Cauchy data on the domain boundary. We prove the local convergence of the method in simplified cases and numerically show its efficiency for some two dimensional experiments with synthetic data. Additionally, we extend our approach to the more complex case where we also iterate on the value of conductivity. In this context, we have also developed an alternating inversion algorithm between the geometry and the inner value of the conductivity, with an adaptive descent step.

Keywords: Inverse conductivity problem, Kohn-Vogelius cost functional, domain decomposition method, combined inversion method, convergence analysis, identification.

Résumé

Dans cette thèse, nous développons une méthode d'inversion qui combine l'utilisation d'une fonctionnelle coût de type Kohn-Vogelius avec une méthode de décomposition de domaine sans recouvrement en tant que solveur itératif. L'idée derrière cette méthode est d'itérer simultanément sur la solution du problème direct via la méthode de décomposition de domaine et sur l'inconnue du problème inverse en utilisant une descente de gradient sur la fonctionnelle de Kohn-Vogelius. Ce type d'approche fait partie de la famille des méthodes dites "one-shot inversion methods", et son utilisation a le potentiel de réduire sensiblement le coût de l'inversion lorsque la résolution du problème direct est coûteuse. Nous nous intéressons plus particulièrement au cas des problèmes inverses géométriques où l'inconnue du problème inverse est le support d'une discontinuité d'un paramètre physique. Les développements réalisés sur cette thématique ont pris pour modèle inverse le problème inverse de conductivité électrique, où l'on cherche à reconstruire l'interface de discontinuité de la conductivité à partir de données de Cauchy sur la frontière du domaine. Nous prouvons un résultat de convergence locale de la méthode dans des cas simplifiés et l'avons validée numériquement pour certaines expériences bidimensionnelles avec des données synthétiques. De plus, nous étendons notre approche au cas plus complexe où l'on itère également sur la valeur de la conductivité. Dans ce contexte, nous avons également développé un algorithme d'inversion alternée entre la géométrie et la valeur intérieure de la conductivité, avec un pas de descente adaptatif.

Mots-clés : Problème inverse de conductivité, fonctionnelle coût de Kohn-Vogelius, méthode de décomposition de domaine, méthode d'inversion combinée, analyse de convergence, identification.

Contents

Abstract **3**

Résumé **4**

Introduction **11**

1 A Kohn-Vogelius method for an inverse conductivity problem **17**

1.1 Introduction 17

1.2 Some technical tools 18

1.3 The direct problem 19

1.3.1 Existence and uniqueness of the solution 21

1.3.2 Multi-domain formulation using the natural transmission conditions . 23

1.4 The inverse conductivity problem 26

1.5 The Kohn-Vogelius cost function 27

1.6 Differentiability of the Kohn-Vogelius cost function 29

1.6.1 Derivative with respect to conductivity values 29

1.6.2 Derivative with respect to the singularity interface 33

1.7 The gradient algorithm in the case of starlike domains and a local convergence analysis 34

1.7.1 The one dimensional case 36

1.7.2 The case of an annulus 40

1.7.3 The case of an open disk 43

1.8 Numerical experiments and validation 46
1.8.1 Scenario 1: only $\overline{\sigma_1}$ is unknown 49
1.8.2 Scenario 2: only $\overline{\sigma_2}$ is unknown 49
1.8.3 Scenario 3: both $\overline{\sigma_1}$ and $\overline{\sigma_2}$ are unknown 50
1.8.4 Scenario 4: only $\Sigma_{\overline{R}}$ is unknown 50
1.9 Conclusion 51

2 A non-overlapping Domain Decomposition Method 53
2.1 Introduction 53
2.2 On the domain decomposition methods 53
2.3 Multidomain formulation using OSM 56
2.3.1 The case of the direct problem (N_σ) 57
2.3.2 The case of the Dirichlet problem (D_σ) 60
2.4 Convergence rate for OSM in some particular domains 61
2.4.1 The one dimensional case 61
2.4.2 The case of an annulus 65
2.4.3 The case of an open disk 70
2.5 Numerical illustrations 75
2.6 Conclusion 81

3 A combined inversion method for a geometrical inverse conductivity problem 82
3.1 Introduction 82
3.2 Combined inversion algorithm 83
3.3 Local convergence analysis in some particular cases 86
3.3.1 The one dimensional case 86
3.3.2 The case of an annulus 92
3.3.3 The case of an open disk 99
3.4 Numerical experiments and validation 110
3.4.1 Discussion of Algorithm 2 for a kite shape 111
3.4.2 The example of other geometries 113
3.4.3 Discussion on the choice of L and τ 114
3.5 Conclusion 117

4 A combined inversion method for the full inverse conductivity problem 118
4.1 Introduction 118
4.2 Identifiability 119
4.3 Numerical algorithm in the case of starlike domains 120
4.3.1 An alternating gradient descent algorithm 120
4.3.2 An alternating combined inversion algorithm 124
4.3.3 On the local convergence study of the non-alternating version of Algorithm 4. 126
4.4 Numerical validation and results 130
4.5 Conclusion 134

Conclusion and perspectives 136

Bibliography 137

List of Figures

1.1 Representative diagram for the decomposed problem where the domain Ω is divided into two subdomains Ω_1 and Ω_2. 24

1.2 Description of the geometry in the case of a starlike geometry parameterized by (1.29), where the arc S_i is shown in blue, and the interface Σ_R is shown in red. 34

1.3 Description of the geometry in the case of an annulus domain. $\Omega_1 : R_1 < r < R$ and $\Omega_2 : R < r < R_2$. 40

1.4 Description of the geometry in the case of an open disk domain of center $(0, 0)$ and radius R_2. Ω_1 is an open disk of center $(0, 0)$ and radius R. 43

1.5 Description of the geometry for the numerical experiments. 47

1.6 Convexity of the function J with respect to σ_1. 48

1.7 Convexity of the function J with respect to σ_2 48

1.8 Identification of $\overline{\sigma_1}$ is shown on the left, and the evolution of J versus the number of iterations is shown on the right. 49

1.9 Identification of $\overline{\sigma_2}$ is shown on the left, and the evolution of J versus the number of iterations is shown on the right. 49

1.10 Values of σ at the location where $\Sigma_{\overline{R}}$ intersects the x-axis at the two singularity points A and B with different noisy data: noise-free data (left), noise level $\epsilon = 1\%$ (middle), and $\epsilon = 3\%$ (right). 50

1.11 Reconstruction of $\Sigma_{\overline{R}}$ by Algorithm 1 for different noisy data: free noisy data (b), noise level $\epsilon = 3\%$ (c) and $\epsilon = 5\%$ (d). The exact shape and initial guess are shown in Figure (a). 51

2.1 Typical example of domain decomposition method with overlap (left), as it appears in Schwarz's article in 1870, and without overlap (right). 54
2.2 Outward normals for overlapping (left) and nonoverlapping (right) subdomains for Optimized Schwarz Method. Image from the book of V. Dolean et al. [21]. 56
2.3 Outward normals for nonoverlapping subdomains Ω_1 and Ω_2 for OSM. 57
2.4 Evolution of the convergence rate ρ_m^α (left) and $\hat{\rho}_m^\alpha$ (right) as a function of $m \in \mathbb{N}^*$. The OSM parameter $\alpha = 2$. 74
2.5 Evolution of the convergence rate ρ_m^α (left) and $\hat{\rho}_m^\alpha$ (right) as a function of $\alpha \in [0.1, 5]$. 75
2.6 Evolution of the convergence rate ρ_m^α (left) and $\hat{\rho}_m^\alpha$ (right) as a function of $\alpha \in [5, 200]$. 75
2.7 Example of meshes used for the circular geometry problem. Subdomain Ω_1 is on the left and subdomain Ω_2 is on the right. 77
2.8 Isovalues of the solution obtained by OSM (2.6)-(2.7) at different OSM iterations are displayed: at iteration 0 (a), at iteration 1 (b), and at iteration 9 (c). The exact solution is shown in Figure (d). The current flux is given by $\phi(\theta) = \cos(\theta)$, $\theta \in [0, 2\pi]$. 78
2.9 Convergence curve for the example depicted in Figure 2.8: Evolution of the relative error e^ℓ versus the number of OSM iterations ℓ. 79
2.10 Convergence curves of the approximation errors e_Σ^ℓ and $\hat{e}_\Sigma^\ell$ versus the number of OSM iterations. 80
2.11 Convergence curves for different refinements: error e^ℓ versus the number of OSM iterations ℓ. 81

3.1 Comparison between Algorithm 1 and Algorithm 2 with $L = 1$ for the case of the kite parameterized by (3.58) and for noise free data. The exact shape and initial guess are shown in Figure (a). The gradient descent parameter $\tau = 0.05$ for both algorithms. 112
3.2 Comparison of the evolution of $\log_{10}(\sqrt{\mathcal{J}/\mathcal{J}_0})$ between Algorithm 1 and Algorithm 2 with $L = 1$ (left), $L = 2$ (middle) and $L = 5$ (right) for the example shown in Figure 3.1. The gradient descent parameter is $\tau = 0.05$. 112

3.3 Reconstructions obtained by Algorithm 2 with $L = 1$ for the example discussed in Figure 3.1 but for noisy data with noise level $\epsilon = 1\%$ (left), $\epsilon = 3\%$ (middle) and $\epsilon = 5\%$ (right). 113
3.4 Reconstructions obtained by Algorithm 2 for the geometries discussed in Table 3.1 but for noisy data with noise level $\epsilon = 3\%$. 114
3.5 Reconstructions obtained by Algorithm 2 for the geometries discussed in Table 3.1 but for noisy data with noise level $\epsilon = 5\%$. 114
3.6 Comparison between Algorithm 1 and Algorithm 2 with $L = 1$ to achieve 5% relative accuracy in the case of the geometry given by Figure (a) and for noise free data. The gradient descent parameter $\tau = 0.1$ for both algorithms. . . . 115
3.7 Comparison of the evolution of $\log_{10}(\sqrt{\mathcal{J}/\mathcal{J}_0})$ between Algorithm 1 and Algorithm 2 applied to the example of Figure 3.6 with different gradient descent parameter $\tau = 0.1$ (left), $\tau = 0.05$ (middle) and $\tau = 0.005$ (right). 116

4.1 The two partitions of Ω for the counterexample. 119
4.2 Description of the geometry for the kite parameterized by (4.16) 131
4.3 Reconstructions obtained by Algorithm 3 using flux ϕ_1 and for noise-free data. The initial guess is shown in Figure 4.2. 132
4.4 Reconstructions obtained by Algorithm 4 with $L = 1$ using flux ϕ_1 and for noise-free data. The initial guess is shown in Figure 4.2. 132
4.5 Reconstructions obtained by Algorithm 3 using two fluxes ϕ_1 and ϕ_2, and for noise-free data. The initial guess is shown in Figure 4.2. 133
4.6 Reconstructions obtained by Algorithm 4 with $L = 1$ using two fluxes ϕ_1 and ϕ_2, and for noise-free data. The initial guess is shown in Figure 4.2. 133
4.7 Comparison of the evolution of $\log_{10}(\mathcal{J})$ between Algorithm 3 and Algorithm 4 with $L = 1$ for the example shown in Figures 4.5 and 4.6. 134

Introduction

The goal of this thesis is to introduce and study a combined iterative inversion method that uses an incomplete solver for the direct problem at each iteration for the inverse problem parameter. This type of approach has the advantage of reducing the iterative cost and speeding up the convergence rate. Many variants of these combinations have been proposed in the literature [30, 14, 29, 32, 27, 42, 11]. We develop here an algorithm in the vein of so-called one-shot iterative methods for optimization problems and we address two novel aspects for this type of methods. The first one is to use a combination of the Khon-Vogelius energy functional and a non overlapping domain decomposition method as an iterative solver. The second one is that the inverse parameter is the geometry of an unknown object used as a part of the domain partitioning. We study all theses aspects in the framework of the inverse conductivity problem, where the electric conductivity σ is a piecewise constant function with a regular unknown discontinuity interface Σ. This is a classic inverse problem that has many applications and has been extensively studied in the literature (we refer to [44, 45, 36, 37, 12, 7, 33, 50, 38, 43]). The assumption on the conductivity is rather natural and arises, for example, in geophysical applications, medical imaging and nondestructive testing of materials where the medium under investigation contains regions with different electric conducting properties. We are particularly interested in the case of geometric inverse problems where one would like to identify the discontinuity curve Σ of σ from boundary measurements. Our goal here is not to address issues specific to this inverse problem but to rather use it as a toy model to illustrate the feasibility of the combined inversion scheme and study convergence in some simplified configurations.

The Kohn-Vogelius cost functional has been used in the solution of various inverse geometrical problems [46, 18, 7, 34]. It has been specifically applied to inverse conductivity problem in [46, 7, 2, 3]. This functional seems to provide better stability and precision as compared with a classical least squares cost functional [16, 2]. From the theoretical point of view, it also has the advantage of being differentiable with respect to the discontinuity curve under less restrictive smoothness assumptions [15, 17]. We shall review some results from the literature on this functional and study its local convergence for the inverse conductivity problem in the case of circular domains.

The implementation of this method requires the solution of two direct problems, one associated with Neumann data and the other one associated with Dirichlet data coming from the measurements. In order to evaluate these solutions we employ a non overlapping domain decomposition method. We employ the so-called Optimized Schwarz Method (OSM) where communications at the interfaces of the domains are enforced through Robin type boundary conditions [48, 39, 40, 25, 21]. We here study the case where the inverse problem unknown Σ is part of the partitioning used in the domain decomposition method. We propose a combined inverse algorithm where the Kohn-Vogelius cost functional is minimized using a gradient descent scheme. At each gradient step, the exact solutions of the Neumann and Dirichlet problems are approximated using only one or a few iterations of the OSM. Two difficulties arise in this coupling. The first one is that the domain partitioning changes after a gradient descent step which requires modifications in the OSM scheme. The second one is that the gradient cannot be evaluated exactly and therefore a choice has to be made. One should either evaluate the shape gradient with respect to incomplete exact solutions or propose an approximation of the gradient of the exact cost functional. The first option would require the introduction of two adjoint problems and therefore may render the method more costly. This is why we adopt the second approach, that indeed lead to an incorrect gradient at first iterations, but this gradient becomes closer to the exact one as the iterations number increases. Concerning the first issue related to OSM, we solve it by rewriting the OSM as an iterative scheme on the interface values. These values are then transported by the gradient flow in the same way as the unknown geometry Σ. We explicit this scheme in the case of star shaped interfaces, but the approach can be easily extended to other type or shape parametrizations. We study and prove local convergence of the resulting algorithm in the very simplified case where the geometry is circular and the inverse shape problem is the radius of the inner circle. We then numerically investigate the effectiveness and the accuracy of this algorithm in the case of star shaped domains. We show in particular that

only one OSM iteration would achieve a converge rate similar to classical gradient (where the solutions are evaluated exactly at each iteration). Determining the optimal choice of OSM iteration number in order to have the best convergence rate is an open issue. Numerical tests suggests that this optimal choice is among the one using few number of OSM iterations. These investigations are then partially extended to the more complex inverse problem where both the discontinuity interface and the conductivity value in the inner domain are unknown and have to be determined from boundary Cauchy data.

This thesis is composed of 4 chapters, and in the following, we detail the contributions of each chapter.

Chapter 1: A Kohn-Vogelius method for an inverse conductivity problem.

In this chapter, we introduce the direct and inverse problems together with the Kohn-Vogelius cost functional. The chapter is organized as follows:

The first part is dedicated to the study of the existence and uniqueness of the solution of the following Neumann boundary value problem

$$(N_\sigma)\begin{cases} -\mathrm{div}(\sigma\nabla u) = 0 & \text{in } \Omega, \\ \sigma\dfrac{\partial u}{\partial \nu} = \phi & \text{on } \Gamma, \end{cases}$$

where Ω is a simply connected bounded domain of $\mathbb{R}^d$, $d = 1, 2$ or 3, with $\mathcal{C}^{1,\beta}$ boundary $\Gamma := \partial\Omega$, $\beta \in]0,1[$, ν denotes the outward unit normal on Γ and $\phi \in L^2(\Gamma)$ the current flux through Γ that satisfies the compatibility condition: $\displaystyle\int_\Gamma \phi \, ds = 0$. Indeed, to ensure uniqueness of the solution to problem (N_σ), we impose that $\displaystyle\int_\Omega u \, dx = 0$.

The second part of this chapter is dedicated to the study of the inverse conductivity problem based on the Kohn-Vogelius approach for the identification of $\sigma \in \mathcal{S}^1_{ad}$ where

$$\mathcal{S}^1_{ad} := \left\{\sigma = \sigma_1\chi_{\Omega_1} + \sigma_2\chi_{\Omega_2};\ \sigma_1 > 0; \sigma_2 > 0;\ \Omega_1 \subset \Omega;\ \Sigma = \partial\Omega_1 \text{ a } \mathcal{C}^{1,\beta} \text{ Jordan curve; } \Omega_2 = \Omega \setminus \overline{\Omega_1}\right\}.$$

The inverse problem $(\mathcal{I}.\mathcal{P})$ that we are investigating is formulated as follows:

$$(\mathcal{I}.\mathcal{P})\begin{cases} \text{Given the prescribed flux } \phi \text{ together with the potential measurement } f, \\ \text{recover the function } \overline{\sigma} \in S^1_{ad} \text{ such that the solution of } (N_\sigma) \text{ also verifies } f := u_{\overline{\sigma}|_\Gamma}. \end{cases}$$

Our adopted approach consists of transforming the inverse problem into an optimization one by constructing a cost function J modeling the energy gap between the solution of the Neumann problem and the solution of the following Dirichlet problem:

$$(D_\sigma) \begin{cases} -\mathrm{div}(\sigma \nabla v) = 0 & \text{in } \Omega, \\ v = f & \text{on } \Gamma. \end{cases}$$

More precisely, we define the Kohn-Vogelius cost function as

$$J(\sigma) := \int_\Omega \sigma \mid \nabla(u_\sigma - v_\sigma) \mid^2 \; dx,$$

where $u_\sigma \in \mathcal{H}^1(\Omega)$ the solution of the Neumann problem (N_σ) and $v_\sigma \in \mathcal{H}^1(\Omega)$, the solution of the Dirichlet problem(D_σ). Indeed, we prove that the solution $\overline{\sigma}$ of the inverse problem is a minimizer of J.

To numerically minimize the function J, we shall use a gradient descent algorithm based on the derivative of J with respect to σ. For that, we calculate its derivative with respect to the conductivity values σ_1 and σ_2 in Section 1.6, while the existence and expression of the shape derivative of J with respect to the singularity surface Σ of σ have been studied by Afraites et al. in [2].

Furthermore, as a preparatory step for the combined inversion algorithm introduced in Chapter 3, addressing the geometrical inverse conductivity problem, we explicitly present in Section 1.7 the gradient descent algorithm tailored to starlike interfaces Σ. The ongoing development of this gradient descent scheme, summarized in Algorithm 1, aims to effectively identify the singularity curve Σ of σ with an exact direct solver. Additionally, we analyze the convergence of this algorithm in some simplified geometries. This study serves as a first step for the convergence analysis of the combined inverse scheme.

In the last part of the chapter, we present some numerical experiments obtained using this inversion method.

Chapter 2: A non-overlapping Domain Decomposition Method.

In order to evaluate the solutions of the direct problems (N_σ) and (D_σ) studied in Chapter 1, this chapter employs a non-overlapping Domain Decomposition Method (DDM) known as the Optimized Schwarz Method (OSM). The OSM enforces communications at the interfaces of the domains through Robin-type boundary conditions [48, 39, 40, 25, 21]. The chapter begins with a brief introduction to Domain Decomposition Methods (DDMs) and then presents the

OSM as the chosen non-overlapping DDM. Next, we reformulate the direct problems (N_σ) and (D_σ) as an equivalent multi-domain problem using Robin transmission conditions. The convergence rate of OSM is investigated in one dimension and in the case of circular interfaces. These findings are valuable for analyzing the convergence of the combined inversion algorithm. Finally, we present some numerical illustrations on the convergence of OSM.

Chapter 3: A combined inversion method for a geometrical inverse conductivity problem.

The content of this chapter is partially extracted from [19], in collaboration with S. Chaabane and H. Haddar, published in Inverse Problems, 2023. It contains additional materials to those in [19] on the convergence analysis for simplified geometries.

In this chapter, we assume that σ_1 and σ_2 are known bounded regular functions on Ω and are positive definite and we will study the shape inverse problem which consists in identifying the singularity support Σ of σ from the knowledge of the flux ϕ together with the potential $f = u_{\overline{\sigma}|\Gamma}$. For this, we develop in this chapter some inversion algorithms combining the previous gradient algorithm as defined by Algorithm 1 in Section 1.7 of Chapter 1 with a non-overlapping domain decomposition method (Optimized Schwarz Method) described in Chapter 2, that respects the partitioning of the domain Ω into $\Omega_1 \cup \Omega_2 \cup \Sigma$. The main idea consists in approximating the direct problems $(N_{\sigma(R^k)})$ and $(D_{\sigma(R^k)})$ (at each iteration k of Algorithm 1) using only one or a few OSM steps.

We shall present first the combined inversion algorithm in Section 3.2. We provide in particular a local convergence result for some simplified cases in Section 3.3. Section 3.4 is dedicated to some numerical experiments for testing the efficiency of the combined algorithm and comparing with the classical one.

Chapter 4: A combined inversion method for the full inverse conductivity problem

In this chapter, we extend the approach proposed in the previous one to a more complex case involving iteration on the conductivity values. Specifically, we assume that σ_2 is known, and we aim to identify the conductivity σ_1 and the interface Σ by developing an alternating inversion algorithm that incorporates both the geometry and the conductivity value with an adaptive step descent to enhance its performance.

The chapter is organized as follows. First, we discuss the issue of identifiability in the case of piecewise constant conductivity, where we present a counterexample to illustrate that a single or two pairs (ϕ, f) are not sufficient to uniquely determine the unknown parameters σ_1 and the geometry Σ. To address this, one needs to increase the number of linearly independent pairs of measurements used. These additional measurements would enable a more reliable and accurate resolution of the inverse problem. In this context, we reformulate the Kohn-Vogelius cost function to develop an alternating inversion descent algorithm, which iteratively updates the geometry Σ and the conductivity value σ_1 using an adaptive step descent. This algorithm is summarized in Algorithm 3 and detailed in Subsection 4.3.1. Additionally, in Subsection 4.3.2, we introduce a combined inversion algorithm, summarized in Algorithm 4, that incorporates coupling with OSM. In Subsection 4.3.3, we specifically prove in the one-dimensional case that with only one flux, the non-alternating version of Algorithm 4 may not converge. However, the convergence behavior in cases with multiple fluxes is more complex and is still under investigation. To assess the performance and convergence of the proposed algorithms, we conduct several numerical experiments in Section 4.4 and compare the efficiency of the combined algorithm (Algorithm 4) to the full gradient algorithm (Algorithm 3).

In the last part of the thesis, we give a general conclusion and some perspectives.

CHAPTER 1

A Kohn-Vogelius method for an inverse conductivity problem

1.1 Introduction

The Kohn-Vogelius method is an identification technique that has been extensively used in recent years to solve various types of inverse problems, particularly those involving the retrieval of discontinuous parameters. For instance, in [17], the method is applied to impedance coefficient inverse problems, while in [15], it is used for generalized impedance coefficient problems. Additionally, the Kohn-Vogelius method has been effectively employed in solving different types of geometrical inverse problems as well [46, 18, 7, 34]. It has been specifically applied to the inverse conductivity problem in [46, 7, 2, 3]. In comparison to classical least squares cost functionals, the Kohn-Vogelius method seems to provide better stability and precision [16, 2]. From a theoretical standpoint, it also has the advantage of being differentiable with respect to the discontinuity curve, under less restrictive smoothness assumptions [2, 15, 17].

In this chapter, we are interested in using this approach in the framework of the inverse conductivity problem, which aims to recover the electrical conductivity $\overline{\sigma} \in S_{ad}^1$ from the known flux ϕ together with the potential $f = u_{\overline{\sigma}|\Gamma}$, where $u_{\overline{\sigma}}$ is the solution of $(N_{\overline{\sigma}})$. We start this chapter by studying the existence and uniqueness of the solution of the direct problem (N_σ). Subsequently, we introduce the Kohn-Vogelius method, which consists of transforming the inverse problem into an optimization one by constructing a cost function J that models

the energy gap between the solution of the Neumann problem (N_σ) and the solution of the Dirichlet problem (D_σ). More precisely, the latter is obtained by replacing the Neumann condition $\sigma\dfrac{\partial u}{\partial \nu} = \phi$ on Γ with a Dirichlet condition $u = f$ on Γ, where f represents the potential measurement. Furthermore, we prove that the solution $\overline{\sigma}$ of the inverse problem is a minimizer of J. To numerically minimize the function J, we shall use a gradient descent algorithm based on the derivative of J with respect to σ. For that, in Section 1.6, we calculate its derivative with respect to the conductivity values σ_1 and σ_2, while the existence and expression of the shape derivative of J with respect to the singularity surface Σ of σ have been studied by Afraites et al. in [2].

Furthermore, as a preparatory step for the combined inversion algorithm introduced in Chapter 3, addressing the geometrical inverse conductivity problem, we explicitly present in Section 1.7 the gradient descent algorithm tailored to starlike interfaces Σ. The ongoing development of this gradient descent scheme, summarized in Algorithm 1, aims to effectively identify the singularity curve Σ of σ with an exact direct solver. Additionally, we analyze the convergence of this algorithm in some simplified geometries. This study serves as a first step for the convergence analysis of the combined inverse scheme. We conclude this chapter by providing some numerical experiments obtained using this inversion method.

1.2 Some technical tools

In this section, we will present some technical tools needed in some proofs of this chapter. We start by some theorems.

Theorem 1.2.1. *(Rellich)[1] Let Ω be a regular bounded open domain of $\mathbb{R}^d$, $d \geq 1$, then the injection map $\mathcal{H}^1(\Omega) \hookrightarrow L^2(\Omega)$ is a compact operator.*

Theorem 1.2.2. *(trace operator) Let Ω be a $\mathcal{C}^1$ bounded open domain of $\mathbb{R}^d$, $d \geq 1$. Then, the trace operator*

$$\begin{array}{rccc} \tau: & \mathcal{H}^1(\Omega) \cap \mathcal{C}^0(\overline{\Omega}) & \longrightarrow & L^2(\partial\Omega) \cap \mathcal{C}^0(\overline{\partial\Omega}) \\ & v & \longmapsto & v_{|\partial\Omega} \end{array}$$

can be extended by density into a continuous linear operator from $\mathcal{H}^1(\Omega)$ in $L^2(\partial\Omega)$, also noted τ. Hence, there exists a constant $C > 0$, such that, for every $v \in \mathcal{H}^1(\Omega)$, we have

$$\|v\|_{L^2(\partial\Omega)} \leq C\|v\|_{\mathcal{H}^1(\Omega)} \tag{1.1}$$

Lemma 1.2.1. *[13]*

- *Let E be a Banach space, then E is reflexive if and only if the closed unit ball $B_E = \{x \in E$ such that $\|x\| \leq 1\}$ is compact for the weak topology.*
- *Let F be a convex part of a reflexive Banach space. Then, F is weakly closed if and only if F is strongly closed.*

Proposition 1.2.2. *[5] Let Ω be a compound domain of two distinct regular open domains Ω_1 and Ω_2 separated by an interface Σ. Then, $u \in \mathcal{H}^1(\Omega)$ if and only if:*

$$\begin{cases} u_1 = u_{|\Omega_1} \in \mathcal{H}^1(\Omega_1), \\ u_2 = u_{|\Omega_2} \in \mathcal{H}^1(\Omega_2), \\ u_1 = u_2 \ on \ \Sigma. \end{cases}$$

1.3 The direct problem

Let Ω be a simply connected bounded domain of $\mathbb{R}^2$ or $\mathbb{R}^3$ with $\mathcal{C}^{1,\beta}$ boundary $\Gamma := \partial\Omega$, $\beta \in]0,1[$. We denote by $\sigma : \Omega \longrightarrow \mathbb{R}$ the electric conductivity of Ω. Let $\sigma_* > 0$ and $\mathcal{S}_{ad}$ be the set of admissible parameters:

$$\mathcal{S}_{ad} = \{\sigma \in L^\infty(\Omega) \text{ such that } \sigma \geq \sigma_* \text{ a.e. in } \Omega\}.$$

We denote by $u \in \mathcal{H}^1(\Omega)$ the electric potential which satisfies the following Neumann boundary value problem

$$(N_\sigma) \begin{cases} -\mathrm{div}(\sigma \nabla u) = 0 & \text{in } \Omega, \\ \sigma \dfrac{\partial u}{\partial \nu} = \phi & \text{on } \Gamma, \end{cases}$$

where ν denotes the outward unit normal on Γ (see Figure 1.1) and $\phi \in L^2(\Gamma)$ the current flux through Γ that satisfies the compatibility condition:

$$\int_\Gamma \phi \, ds = 0. \tag{1.2}$$

To ensure uniqueness of the solution to problem (N_σ), we impose that

$$\int_\Omega u \, dx = 0. \tag{1.3}$$

We denote by V the following set:

$$V = \left\{ v \in \mathcal{H}^1(\Omega), \text{ such that } \int_\Omega v = 0 \, dx \right\}.$$

One can see that the space V endowed with the following inner product:

$$\langle u, v \rangle = \int_\Omega \nabla u \cdot \nabla v \, dx$$

is a Hilbert space.

In the sequel, we denote by $|.|_{1,\Omega}$ the norm associated with this inner product. This gives the following lemma:

Lemma 1.3.1. *The application*

$$\begin{array}{rccl} N: & V & \longrightarrow & \mathbb{R}_+ \\ & v & \longmapsto & |.|_{1,\Omega} = \left(\int_\Omega |\nabla v|^2 \, dx \right)^{\frac{1}{2}} \end{array}$$

is a norm on V equivalent to the usual norm $\|.\|_{\mathcal{H}^1(\Omega)}$.

Proof. One can clearly see that

$$N(v) = |v|_{1,\Omega} \ \leq \ \|v\|_{\mathcal{H}^1(\Omega)} \ \forall \ v \in V.$$

Let us then show that there exists a constant $\beta > 0$, such that for every $v \in V$, we get

$$\|v\|_{H^1(\Omega)} \leq \beta N(v).$$

Assuming by contradiction that there exists a sequence $(u_n)_{n \in \mathbb{N}^*}$ of V, such that

$$N(u_n) < \frac{1}{n} \|u_n\|_{\mathcal{H}^1(\Omega)},$$

and let $W_n = \dfrac{u_n}{\|u_n\|_{\mathcal{H}^1(\Omega)}}$. According to Rellich's Theorem 1.2.1 and Lemma 1.2.1, there exists a function $W \in \mathcal{H}^1(\Omega)$ and a sub-sequence of W_n still denoted by W_n, such that

$$\begin{cases} W_n \rightharpoonup W \ \text{ weakly in } \mathcal{H}^1(\Omega), \\ W_n \to W \ \text{ strongly in } L^2(\Omega). \end{cases}$$

Since $N(W_n) \leq \dfrac{1}{n}$,

$$\nabla W_n \to 0 \text{ strongly in } L^2(\Omega), \tag{1.4}$$

and by uniqueness of the limit, we deduce that $\nabla W = 0$ in Ω. As Ω is a connected domain, there exists a constant $C \in \mathbb{R}$, such that $W = C$ in Ω and that we have

$$\begin{cases} W_n \to W = C \text{ strongly in } L^2(\Omega), \\ \nabla W_n \to \nabla W = 0 \text{ strongly in } L^2(\Omega). \end{cases}$$

So

$$W_n \to W = C \text{ strongly in } \mathcal{H}^1(\Omega).$$

As V is a closed subspace of $\mathcal{H}^1(\Omega)$, therefore $W \in V$ and so

$$\int_\Omega W \, dx = \int_\Omega C \, dx = 0,$$

then $C = 0$, and consequently

$$W \equiv 0 \text{ in } \Omega.$$

We deduce that the sequence W_n converges to 0 strongly in $\mathcal{H}^1(\Omega)$, which contradicts the fact that $\|W_n\|_{\mathcal{H}^1(\Omega)} = 1 \; \forall \, n \in \mathbb{N}$.

□

1.3.1 Existence and uniqueness of the solution

Proposition 1.3.1. *Let $\sigma \in \mathcal{S}_{ad}$ and $\phi \in L^2(\Gamma)$ which verifies the compatibility condition* (1.2)*, then the problem (N_σ) has a unique solution in V denoted by u_σ.*

Proof. Let $u \in V$ be a solution of (N_σ), we multiply the equation $-\mathrm{div}(\sigma \nabla u) = 0$ by a test function $v \in \mathcal{H}^1(\Omega)$ and we integrate, we obtain by using Green's formula:

$$\int_\Omega \sigma \nabla u \cdot \nabla v \, dx - \int_\Gamma \sigma \frac{\partial u}{\partial n} v \, ds = 0.$$

As $\sigma \dfrac{\partial u}{\partial \nu} = \phi$ on Γ, we obtain

$$\int_\Omega \sigma \nabla u \cdot \nabla v \, dx = \int_\Gamma \phi \, v \, ds. \tag{1.5}$$

Therefore, the variational problem of (N_σ) with the additionally condition (1.3) is given by

$$(VN_\sigma)\begin{cases} \text{Find } u \in V, \text{ such that :} \\ a_\sigma(u,v) = \ell(v) \ \text{ for all } v \in V. \end{cases}$$

where:

$$a_\sigma(u,v) = \int_\Omega \sigma \nabla u \cdot \nabla v \, dx \ \text{ and } \ \ell(v) = \int_\Gamma \phi \, v \, ds. \tag{1.6}$$

First, we can see from the Cauchy-Schwarz inequality that

$$|a_\sigma(u,v)| \leq \|\sigma\|_{L^\infty(\Omega)} |u|_{1,\Omega} |v|_{1,\Omega}.$$

Consequently, the bilinear form a_σ is continuous on $V \times V$. Moreover, from the condition $\sigma \geq \sigma_* > 0$, we deduce that a_σ is a coercive bilinear form on $V \times V$.
Using again the Cauchy-Schwarz inequality and the continuity of the trace operator described in Theorem 1.2.2, ℓ is a continuous linear form on V.

Then, by the Lax-Milgram theorem, the problem (VN_σ) has a unique solution.

Reciprocally:

Let u be the solution of (VN_σ), $\varphi \in \mathcal{D}(\Omega)$ and $\tilde{\varphi} = \varphi - C$, where

$$C = \frac{1}{\mu(\Omega)} \int_\Omega \varphi \, dx.$$

As $\tilde{\varphi} \in V$, we get

$$a_\sigma(u, \tilde{\varphi}) = \ell(\tilde{\varphi})$$

Replacing $\tilde{\varphi}$ by $\varphi - C$, we obtain

$$\int_\Omega \sigma \nabla u \cdot \nabla \varphi \, dx = \int_\Gamma \phi \, \varphi \, ds - C \int_\Gamma \phi \, ds.$$

Therefore, $\displaystyle\int_\Omega \sigma \nabla u \cdot \nabla \varphi \, dx = 0$ from the compatibility condition (1.2), then we get

$$< \sigma \nabla u, \nabla \varphi >= 0, \text{ in the sense of distribution.}$$

Then we get

$$-\text{div}(\sigma \nabla u) = 0 \ \text{ in } \ \Omega. \tag{1.7}$$

Let $v \in \mathcal{H}^1(\Omega)$ and $\tilde{v} = (v - K)$, where

$$K = \frac{1}{\mu(\Omega)} \int_\Omega v \, dx,$$

then we have $\tilde{v} \in V$ and

$$\int_\Omega \sigma \nabla u \cdot \nabla \tilde{v} \, dx = \int_\Gamma \phi \, \tilde{v} \, ds,$$

therefore

$$\int_\Omega \sigma \nabla u \cdot \nabla v \, dx = \int_\Gamma \phi \, v \, ds - K \int_\Gamma \phi \, ds,$$

or $\int_\Gamma \phi \, ds = 0$ from (1.2). Consequently

$$\int_\Omega \sigma \nabla u \cdot \nabla v \, dx = \int_\Gamma \phi \, v \, ds.$$

Applying Green's formula, we obtain

$$\int_\Omega -\mathrm{div}(\sigma \nabla u) v \, dx + \int_\Gamma \sigma \frac{\partial u}{\partial n} v \, ds = \int_\Gamma \phi \, v \, ds \quad \forall v \in \mathcal{H}^1(\Omega),$$

and according to (1.7), we get

$$\int_\Gamma \left(\sigma \frac{\partial u}{\partial n} - \phi \right) v \, ds = 0, \forall v \in \mathcal{H}^1(\Omega).$$

Hence

$$\sigma \frac{\partial u}{\partial n} = \phi \ \text{ on } \Gamma. \tag{1.8}$$

Then, u is the unique solution of (N_σ) which satisfies the compatibility condition (1.2).

□

1.3.2 Multi-domain formulation using the natural transmission conditions

In this part, we assume that the domain Ω is composed of two distinct regular open domains Ω_1 and Ω_2 separated by an interface Σ where Ω_1 is the inner domain (see Figure 1.1 for an illustration). Moreover, we also assume that the conductivity σ is a piecewise constant

function which take only two distinct values $\sigma_1 > 0, \sigma_2 > 0$:

$$\sigma = \sigma_1 \chi_{\Omega_1} + \sigma_2 \chi_{\Omega_2}, \tag{1.9}$$

where χ_{Ω_i} denotes the characteristic function of the domain Ω_i, i=1, 2.

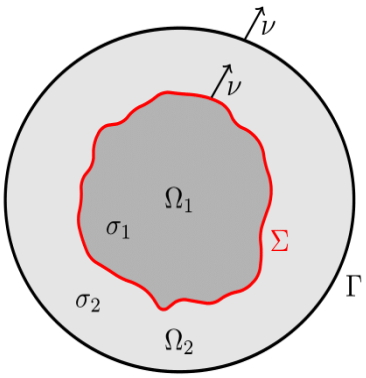

Figure 1.1: Representative diagram for the decomposed problem where the domain Ω is divided into two subdomains Ω_1 and Ω_2.

We denote by $u_i := u_{|_{\Omega_i}}$, the restriction of u to Ω_i, $i = 1, 2$. We then have the following lemma.

Lemma 1.3.2. *The problem (N_σ) can be reformulated as an equivalent multidomain problem consisting of the following subdomain problems*

$$\begin{aligned} -\sigma_i \Delta u_i &= 0 \quad \text{in } \Omega_i, \\ \sigma_2 \frac{\partial u_2}{\partial \nu} &= \phi \quad \text{on } \Gamma, \end{aligned} \tag{1.10}$$

together with the transmission conditions on the interface Σ

$$u_1 = u_2 \qquad \text{on } \Sigma, \tag{1.11}$$

$$\sigma_1 \frac{\partial u_1}{\partial \nu} = \sigma_2 \frac{\partial u_2}{\partial \nu} \quad \text{on } \Sigma. \tag{1.12}$$

Proof. Let $u \in \mathcal{H}^1(\Omega)$ be a solution of the direct problem (N_σ). According to the Proposition 1.2.2, we obtain

$$u_1 = u_2 \ \text{ on } \Sigma.$$

As $-div(\sigma\nabla u) = 0$ in Ω and using the conductivity distribution which defined by (1.9), we obtain

$$-\sigma_i \Delta u_i = 0 \quad \text{in } \Omega_i, i = 1, 2, \tag{1.13}$$

then by Green's formula, we can easily see that:

$$\sigma_2 \frac{\partial u_2}{\partial n} = \phi \ \text{ on } \Gamma. \tag{1.14}$$

From the compatibility condition (1.2) and the variational formulation (VN_σ) of (N_σ), we obtain

$$\int_{\Omega_1} \sigma_1 \nabla u_1 \cdot \nabla v \, dx + \int_{\Omega_2} \sigma_2 \nabla u_2 \cdot \nabla v \, dx = \int_\Gamma \phi \, v \, ds \quad \forall v \in \mathcal{H}^1(\Omega),$$

and by Green's formula, we get

$$\int_{\Omega_1} -\sigma_1 \Delta u_1 \, v \, dx + \int_\Sigma \sigma_1 \frac{\partial u_1}{\partial \nu} \, v \, ds - \int_{\Omega_2} \sigma_2 \Delta u_2 \, v \, dx - \int_\Sigma \sigma_2 \frac{\partial u_2}{\partial \nu} \, v \, ds + \int_\Gamma \sigma_2 \frac{\partial u_2}{\partial \nu} \, v \, ds = \int_\Gamma \phi \, v \, ds,$$

using equations (1.13) and (1.14), we obtain

$$\int_\Sigma \left(\sigma_1 \frac{\partial u_1}{\partial \nu} - \sigma_2 \frac{\partial u_2}{\partial \nu} \right) v \, ds = 0 \ \forall v \in \mathcal{H}^1(\Omega),$$

then

$$\sigma_1 \frac{\partial u_1}{\partial \nu} = \sigma_2 \frac{\partial u_2}{\partial \nu} \quad \text{on } \Sigma.$$

Reciprocally:

Let $u_i \in \mathcal{H}^1(\Omega)$, $i = 1, 2$ a solution of (1.10)-(1.12), and u is the function defined as u_1 in Ω_1 and u_2 in Ω_2, so according to the transmission condition (1.11) and Proposition 1.2.2, we deduce that $u \in \mathcal{H}^1(\Omega)$.
Moreover, we have

$$\int_\Omega \sigma \nabla u \cdot \nabla v \, dx = \int_{\Omega_1} \sigma_1 \nabla u_1 \cdot \nabla v \, dx + \int_{\Omega_2} \sigma_2 \nabla u_2 \cdot \nabla v \, dx \ \ \forall v \in \mathcal{H}^1(\Omega),$$

then by Green's formula and equation (1.10), we get

$$\begin{aligned}\int_\Omega \sigma\nabla u\cdot\nabla v\,dx &= \int_{\Omega_1} -\sigma_1\Delta u_1\, v\,dx + \int_\Sigma \sigma_1\frac{\partial u_1}{\partial\nu}\, v\,ds - \int_{\Omega_2}\sigma_2\Delta u_2\, v\,dx\\ &- \int_\Sigma \sigma_2\frac{\partial u_2}{\partial\nu}\, v\,ds + \int_\Gamma \sigma_2\frac{\partial u_2}{\partial\nu}\, v\,ds\\ &= \int_\Sigma\left(\sigma_1\frac{\partial u_1}{\partial\nu}\,ds - \sigma_2\frac{\partial u_2}{\partial\nu}\right) v\,ds + \int_\Gamma \phi\, v\,ds,\end{aligned}$$

and by the transmission condition (1.12), we obtain

$$\int_\Omega \sigma\nabla u\cdot\nabla v\,dx = \int_\Gamma \phi\, v\,ds\ \ \forall v\in\mathcal{H}^1(\Omega)$$

which concludes the proof. □

Remark 1.3.2. *Equations* (1.11) *and* (1.12) *are the "natural" transmission conditions which ensure the continuity of the electric potential* u *and the flux* $\sigma\dfrac{\partial u}{\partial\nu}$ *on the interface* Σ.

For the numerical solution of the direct problem (N_σ), we computed an approximate solution using the finite element method $\mathbb{P}_1$. Some numerical experiments of (N_σ) were already investigated in my master dissertation [41] for both one-dimensional and two-dimensional domain cases. Additionally, we studied the effect of the refinement of the mesh on the accuracy of the approximate solution. Furthermore, we investigated the impact of the discontinuity in σ on the state u_σ. To accomplish this, we introduced the coefficient $\kappa = \dfrac{\sigma_1}{\sigma_2}$ as the ratio of the discontinuity in σ and studied its influence on the regularity of the solution u_σ of the direct problem (N_σ) across Σ by fixing for example $\sigma_1 = 1$ and varying σ_2, we examined the effect in detail. To conclude this part, we would like to briefly summarize the findings from these tests. We observed that as the ratio κ approaches 1, the solution u_σ becomes more regular and the accuracy improves. Consequently, the state u_σ is highly sensitive to the jumps of σ.

1.4 The inverse conductivity problem

In this section, we assume that the electric conductivity σ of Ω is a piecewise constant function with a regular discontinuity surface Σ. More specifically, $\sigma\in\mathcal{S}^1_{ad}$ where

$$\mathcal{S}^1_{ad} := \left\{\sigma=\sigma_1\chi_{\Omega_1}+\sigma_2\chi_{\Omega_2};\ \sigma_i>0, i=1,2;\ \Sigma=\partial\Omega_1\cap\partial\Omega_2 \text{ a } \mathcal{C}^{4,\beta} \text{ Jordan curve; } \Omega_2=\Omega\setminus\overline{\Omega_1}\right\},$$

The inverse conductivity source problem reads:

$$(\mathcal{I}.\mathcal{P}) \begin{cases} \text{Given the prescribed flux } \phi \text{ together with the potential measurement } f, \\ \text{recover the function } \overline{\sigma} \in S^1_{ad} \text{ such that the solution of } (N_\sigma) \text{ also verifies } u_{\overline{\sigma}|\Gamma} = f. \end{cases}$$

Note that, in general, a single couple (ϕ, f) is not sufficient to uniquely determine the unknown parameter $\overline{\sigma}$ (see for instance the counterexample presented in Chapter 4, Section 4.2 for the full inverse conductivity problem, and we refer to [31] for the geometrical inverse conductivity problem).

In the following paragraphs, we shall provide a brief overview of the identifiability and Lipschitz stability aspects related to the inverse conductivity problem, using the Dirichlet-to-Neumann map Λ_σ defined by

$$\Lambda_\sigma : \quad f \quad \longrightarrow \quad \sigma \frac{\partial u}{\partial \nu}|_\Gamma, \quad \text{where } \; u_{|\Gamma} = f.$$

In general, the inverse conductivity problem consists of determining the conductivity σ from the knowledge of the Dirichlet-to-Neumann map Λ_σ and Electrical Impedance Tomography (EIT) is an imaging technique used to reconstruct an image of the conductivity distribution σ from the knowledge of Λ_σ. When σ is smooth enough, one can reconstruct σ from Λ_σ (see the works of Sylvester and Uhlmann [55], Nachmann [51, 52] and Novikov [53]). However, when the conductivity distribution is only L^∞, Astala and Päivärinta have shown in [7] that in dimension 2, the map Λ_σ determines $\sigma \in L^\infty$.

Noting that, in the case of piecewise constant conductivity parameters, some Lipschitz stability results using the Dirichlet to Neumann map Λ_σ have been established in [4, 8, 24]. Additionally, recent studies have extended some Lipschitz stability results to the inverse geometrical problem, considering polygonal interfaces in [9], and further extending to polyhedral interfaces for 3D problems in [6].

1.5 The Kohn-Vogelius cost function

We present in this section a numerical method based on the Kohn-Vogelius cost function that allows us to determine the unknown piecewise constant parameter $\overline{\sigma}$, which consists in transforming the inverse conductivity problem $(\mathcal{I}.\mathcal{P})$ into an optimization one by constructing

a cost function J measures the energy gap between the solution of the Neumann problem (N_σ) and that of the following Dirichlet problem:

$$(D_\sigma)\begin{cases} -\mathrm{div}(\sigma\nabla v) = 0 & \text{in } \Omega, \\ v = f & \text{on } \Gamma. \end{cases}$$

In the sequel, we denote by

$$K = \{w \in H^1(\Omega)/w_{|\Gamma} = f\} \text{ and } K_0 = \{w \in H^1(\Omega)/w_{|\Gamma} = 0\}.$$

The variational problem of (D_σ) is given by

$$(VD_\sigma)\begin{cases} \text{Find } v \in K, \text{ such that :} \\ a_\sigma(v, w) = 0 \ \forall\ w \in K_0, \end{cases}$$

where the bilinear form a_σ is the same as in (1.6). Consequently, (D_σ) admits only one solution in $\mathcal{H}^1(\Omega)$ denoted by v_σ or also v for simplicity.

We now define the Kohn-Vogelius cost function as

$$\begin{array}{rccl} J: & \mathcal{S}_{ad} & \longrightarrow & \mathbb{R} \\ & \sigma & \longmapsto & \displaystyle\int_\Omega \sigma\nabla(u_\sigma - v_\sigma)\cdot\nabla(u_\sigma - v_\sigma)\,dx, \end{array} \tag{1.15}$$

where u_σ is the solution of the Neumann problem (N_σ) and v_σ is the solution of the Dirichlet problem (D_σ). We then have the following proposition.

Proposition 1.5.1. *The solution $\overline{\sigma}$ of the inverse problem $(\mathcal{I}.\mathcal{P})$ is a minimizer of J.*

Proof. We have $J(\sigma) \geq 0$ for every $\sigma \in \mathcal{S}_{ad}$, and for $\sigma = \overline{\sigma}$, we obtain:

$$u_{\overline{\sigma}} = v_{\overline{\sigma}} = f \text{ on } \Gamma.$$

Then, $u_{\overline{\sigma}}$ is also a solution of the boundary value problem $(D_{\overline{\sigma}})$ which admits only one solution. Therefore, $u_{\overline{\sigma}} = v_{\overline{\sigma}}$ on the whole domain Ω. Consequently, $J(\overline{\sigma}) = 0$ and then $\overline{\sigma}$ is a minimizer of J.

□

To numerically minimize the function J, we shall use a gradient descent algorithm based on the differentiability of J with respect to $\sigma \in \mathcal{S}^1_{ad}$.

1.6 Differentiability of the Kohn-Vogelius cost function

We study in this part the differentiability of J with respect to the parameter σ.

1.6.1 Derivative with respect to conductivity values

In this section, we establish a first-order asymptotic expansion of the solutions u_σ and v_σ with respect to σ. We begin by proving the following lemma:

Lemma 1.6.1. *Let $\phi \in L^2(\Gamma)$, then there exists a constant $\alpha > 0$ such that for all $\sigma \in \mathcal{S}_{ad}$ we have*

$$|u_\sigma|_{1,\Omega} \leq \alpha \|\phi\|_{L^2(\Gamma)}.$$

Proof. Let $\sigma \in \mathcal{S}_{ad}$ and $\phi \in L^2(\Gamma)$, then the solution u_σ of the direct problem (N_σ) verifying

$$\int_\Omega \sigma |\nabla u_\sigma|^2 \, dx = \int_\Gamma \phi \, u_\sigma \, ds, \tag{1.16}$$

From the condition $\sigma \geq \sigma_* > 0$ and the Cauchy-Schwarz inequality, we obtain

$$|u_\sigma|^2_{1,\Omega} \leq \frac{1}{\sigma_*} \, \|\phi\|_{L^2(\Gamma)} \|u_\sigma\|_{L^2(\Gamma)}.$$

The continuity of the trace operator implies that there exists a constant $\alpha_0 > 0$, such that

$$|u_\sigma|^2_{1,\Omega} \leq \frac{\alpha_0}{\sigma_*} \, \|\phi\|_{L^2(\Gamma)} \|u_\sigma\|_{\mathcal{H}^1(\Omega)}.$$

By using the Lemma 1.3.1, there exists a constant $\alpha_1 > 0$, such that

$$|u_\sigma|_{1,\Omega} \leq \alpha \, \|\phi\|_{L^2(\Gamma)}, \quad \text{where} \quad \alpha = \frac{\alpha_0 \alpha_1}{\sigma_*}.$$

□

Proposition 1.6.2. *Let $\sigma \in \mathcal{S}_{ad}$ and $d \in L^\infty(\Omega)$, then there exists a unique function $u^1(d) \in V$ verifying*

$$\int_\Omega \sigma \nabla u^1(d) \cdot \nabla v \, dx = -\int_\Omega d \, \nabla u_\sigma \cdot \nabla v \, dx \quad \forall v \in V. \tag{1.17}$$

Moreover, the mapping:

$$\begin{array}{rccc} \delta : & L^\infty(\Omega) & \longrightarrow & V \\ & d & \longmapsto & u^1(d) \end{array}$$

is linear and continuous.

Proof. For every $d \in L^\infty(\Omega)$, the linear mapping b_d defined on V by:

$$b_d(v) = -\int_\Omega d\, \nabla u_\sigma \cdot \nabla v\, dx$$

is continuous, then by using the Lax-Milgram Theorem, there exists a unique function $u^1(d) \in V$ verifying (1.17). Moreover, the mapping δ is linear, and from the Cauchy-Schwarz inequality and the condition $\sigma \geq \sigma_*$, we have

$$\sigma_* |u^1(d)|^2_{1,\Omega} \leq \|d\|_{L^\infty(\Omega)} |u_\sigma|_{1,\Omega} |u^1(d)|_{1,\Omega},$$

we then have

$$|u^1(d)|_{1,\Omega} \leq \frac{1}{\sigma_*}\, \|d\|_{L^\infty(\Omega)} |u_\sigma|_{1,\Omega}.$$

□

Theorem 1.6.1. *Let $\sigma \in \mathcal{S}_{ad}$, $d \in L^\infty(\Omega)$ and h a small enough positive real. Let $\sigma_h = \sigma + hd$, we then have:*

$$u_{\sigma_h} = u_\sigma + h\, u^1(d) + h\epsilon_1(h), \text{ where } \lim_{h\to 0} |\epsilon_1(h)| = 0. \tag{1.18}$$

Proof. From the variational problem (VN_σ) we have:

$$\int_\Omega \sigma_h \nabla u_{\sigma h} \cdot \nabla v\, dx = \int_\Gamma \phi\, v\, ds \qquad \forall\, v \in V, \tag{1.19}$$

$$\int_\Omega \sigma \nabla u_\sigma \cdot \nabla v\, dx = \int_\Gamma \phi\, v\, ds \qquad \forall\, v \in V, \tag{1.20}$$

then,

$$\int_\Omega \sigma(\nabla u_{\sigma_h} - \nabla u_\sigma) \cdot \nabla v\, dx = -\int_\Omega h\, d\, \nabla u_{\sigma_h} \cdot \nabla v\, dx. \tag{1.21}$$

Moreover, if we denote by $w_h = \dfrac{u_{\sigma_h} - u_\sigma}{h}$ and $z_h = w_h - u^1(d)$, we obtain

$$\int_\Omega \sigma \nabla w_h \cdot \nabla v\, dx = -\int_\Omega d\, \nabla u_{\sigma_h} \cdot \nabla v\, dx \quad \forall\, v \in V,$$

$$\int_\Omega \sigma \nabla z_h \cdot \nabla v\, dx = -\int_\Omega d\, (\nabla u_{\sigma_h} - \nabla u_\sigma) \cdot \nabla v\, dx \quad \forall\, v \in V. \tag{1.22}$$

Replacing v by z_h and using the condition $\sigma \geq \sigma_* > 0$, we obtain from the Cauchy-Schwarz inequality:

$$|z_h|_{1,\Omega} \leq \frac{1}{\sigma_*} \|d\|_{L^\infty(\Omega)} |u_{\sigma_h} - u_\sigma|_{1,\Omega}, \tag{1.23}$$

Similarly, replacing v by $(u_{\sigma_h} - u_\sigma)$ in the equation (1.21), we obtain

$$|u_{\sigma_h} - u_\sigma|_{1,\Omega} \leq \frac{1}{\sigma_*}|h| \ \|d\|_{L^\infty(\Omega)}|u_{\sigma_h}|_{1,\Omega}. \tag{1.24}$$

Hence,

$$|z_h|_{1,\Omega} \leq \left(\frac{1}{\sigma_*}\|d\|_{L^\infty(\Omega)}\right)^2 |h| \ |u_{\sigma_h}|_{1,\Omega},$$

and from the Lemma 1.6.1, we get

$$\lim_{h\to 0} |z_h|_{1,\Omega} = 0.$$

□

Similarly to above, we also establish the following two results allowing us to show the asymptotic expansion of the state v_σ.

Proposition 1.6.3. *Let $\sigma \in \mathcal{S}_{ad}$ and $d \in L^\infty(\Omega)$, then there is a unique function $v^1(d) \in K_0$ verifying*

$$\int_\Omega \sigma \nabla v^1(d) \cdot \nabla w \, dx = -\int_\Omega d \ \nabla v_\sigma \cdot \nabla w \, dx \quad \forall w \in K_0. \tag{1.25}$$

Moreover, the mapping δ defined by

$$\begin{array}{rccc} \delta: & L^\infty(\Omega) & \longrightarrow & K_0 \\ & d & \longmapsto & v^1(d) \end{array}$$

is linear and continuous.

Theorem 1.6.2. *Let $\sigma \in \mathcal{S}_{ad}$, $d \in L^\infty(\Omega)$ and h a small enough positive real. Let $\sigma_h = \sigma + hd$, we then have:*

$$v_{\sigma h} = v_\sigma + h \ v^1(d) + h\epsilon_2(h), \quad \textit{where } \lim_{h\to 0} |\epsilon_2(h)| = 0, \tag{1.26}$$

As a consequence of the two previous theorems, we deduce that the function J is differentiable at every parameter σ, and we have the following theorem:

Theorem 1.6.3. *Let $\sigma \in \mathcal{S}_{ad}$, $d \in L^\infty(\Omega)$ and h a small enough positive real. Let $\sigma_h = \sigma + hd$, we then have*

$$\lim_{h\to 0} \frac{J(\sigma_h) - J(\sigma)}{h} = \int_\Omega d \ (|\nabla v_\sigma|^2 - |\nabla u_\sigma|^2) \ dx.$$

Proof. We have $J(\sigma) = J_N(\sigma) + J_D(\sigma) - 2J_{ND}(\sigma)$, where

$$J_N(\sigma) = \int_\Omega \sigma |\nabla u_\sigma|^2 \, dx \quad ; \quad J_D(\sigma) = \int_\Omega \sigma |\nabla v_\sigma|^2 \, dx \quad ; \quad J_{ND}(\sigma) = \int_\Omega \sigma \nabla u_\sigma . \nabla v_\sigma \, dx.$$

For every $\sigma \in \mathcal{S}_{ad}$, we have $J_{ND}(\sigma) = \int_\Gamma \phi f \, ds$, then

$$\lim_{h \to 0} \frac{J_{ND}(\sigma_h) - J_{ND}(\sigma)}{h} = 0.$$

Moreover, we have from (1.18)

$$J_N(\sigma_h) = \int_\Omega (\sigma + hd) |\nabla (u_\sigma + hu^1(d) + h\epsilon(h))|^2 \, dx,$$

where $u^1(d)$ satisfy the variational problem (1.17). Then,

$$J_N(\sigma_h) \;=\; \int_\Omega \sigma |\nabla u_\sigma|^2 \, dx \; + h \left(\int_\Omega d \, |\nabla u_\sigma|^2 \, dx + 2 \int_\Omega \sigma \nabla u_\sigma \cdot \nabla u^1(d) \, dx \right) + h\epsilon(h),$$

where $\lim_{h \to 0} |\epsilon(h)| = 0$. By replacing v by u_σ in the equation (1.17), we then get

$$J_N(\sigma_h) = J_N(\sigma) - h \int_\Omega d \, |\nabla u_\sigma|^2 \, dx + h\epsilon(h), \;\; \text{where } \lim_{h \to 0} |\epsilon(h)| = 0.$$

Therefore,

$$\lim_{h \to 0} \frac{J_N(\sigma_h) - J_N(\sigma)}{h} = - \int_\Omega d \, |\nabla u_\sigma|^2 \, dx.$$

Similarly, by using equations (1.25) and (1.26), we can also prove

$$\lim_{h \to 0} \frac{J_D(\sigma_h) - J_D(\sigma)}{h} = \int_\Omega d \, |\nabla v_\sigma|^2 \, dx.$$

Hence

$$\lim_{h \to 0} \frac{J(\sigma_h) - J(\sigma)}{h} = \int_\Omega d \, (|\nabla v_\sigma|^2 - |\nabla u_\sigma|^2) \, dx.$$

□

As a consequence of Theorem 1.6.3 with a direction $d = \chi_{\Omega_i}$, we have the following corollary.

Corollary 1.6.4. *The mapping*

$$\begin{array}{rccl} \psi: &]\sigma_*,+\infty[\times]\sigma_*,+\infty[& \longrightarrow & \mathbb{R} \\ & (\sigma_1,\sigma_2) & \longmapsto & \psi(\sigma_1,\sigma_2)=J(\sigma_1\chi_{\Omega_1}+\sigma_2\chi_{\Omega_2}) \end{array}$$

is differentiable at every points $(\sigma_1,\sigma_2)\in]\sigma_*,+\infty[\times]\sigma_*,+\infty[$*, and we have*

$$\frac{\partial\psi}{\partial\sigma_i}(\sigma_1,\sigma_2)=\int_{\Omega_i}(|\nabla v_\sigma|^2-|\nabla u_\sigma|^2)\,dx, i=1,2. \tag{1.27}$$

In order to recover the shape Σ of σ, a usual strategy consists to minimize a cost function like J. Many choices are possible, however, it turns out that the Kohn-Vogelius type function leads to a minimization problem with nicer properties than the least squares fitting approaches (we refer to [2] for a comparison of different objectives with one order methods).

1.6.2 Derivative with respect to the singularity interface

We present in this part the shape derivative of the Kohn-Vogelius cost function J with respect to the singularity surface Σ of σ. However, the existence and expression of the shape derivative has been studied in [2] and we outline in the following the main related results.

Let $\sigma\in S^1_{ad}$ with $\Sigma=\overline{\Omega_1}\cap\overline{\Omega_2}$, $h>0$ and $\zeta:\mathbb{R}^2\longrightarrow\mathbb{R}^2$ a $\mathcal{C}^{4,\beta}$ vector field such that $\zeta=0$ in a neighborhood of the boundary Γ. Then, there exists $h_0>0$, such that for all $h<h_0$, the mapping $\mathcal{F}_h=Id+h\zeta$ is a $\mathcal{C}^{4,\beta}$ diffeomorphism transforming the domain Ω into itself. We denote by $\Omega_{1,h}:=\mathcal{F}_h(\Omega_1)$, $\Omega_{2,h}:=\mathcal{F}_h(\Omega_2)$ and $\sigma_h=\sigma_1\chi_{\Omega_{1,h}}+\sigma_2\chi_{\Omega_{2,h}}$. Referring to [2, 3], the shape derivative of the cost function J is given by the following theorem.

Theorem 1.6.5. *The Kohn-Vogelius cost function J is differentiable with respect to the shape Σ and its derivative in the direction ζ is given by:*

$$DJ(\sigma)\cdot\zeta=[\sigma]\int_\Sigma\left[\frac{1}{\sigma_1\sigma_2}\left(\left|\sigma\frac{\partial v_\sigma}{\partial\nu}\right|^2-\left|\sigma\frac{\partial u_\sigma}{\partial\nu}\right|^2\right)+\left(|\nabla_\tau v_\sigma|^2-|\nabla_\tau u_\sigma|^2\right)\right]\zeta\cdot\nu\,ds,$$

where $[\sigma]:=\sigma_1-\sigma_2$ and ∇_τ denotes the tangential gradient operator. Noting that, the shape derivative is to be understood in the sense that

$$\frac{J(\sigma_h)-J(\sigma)}{h}=DJ(\sigma)\cdot\zeta+\epsilon(h)\ \ \textit{where}\ \lim_{h\to0}|\epsilon(h)|=0.$$

1.7 The gradient algorithm in the case of starlike domains and a local convergence analysis

As a preparatory step to the combined algorithm we explicit the gradient descent algorithm in the case of starlike interfaces Σ. Let $\mathcal{C}$ be the set of $\mathcal{C}^1$ piecewise Jordan curves of $\mathbb{R}^2$, $n \in \mathbb{N}^*$ and $R = (R_0, \ldots, R_{n-1}) \in (\mathbb{R}_+^*)^n$. For $i = 0, 1, \ldots, n$, we denote by $\theta_i := \frac{2\pi}{n} i$ and $M_i := (R_i \cos(\theta_i), R_i \sin(\theta_i))$. Let $\Sigma := \Sigma_R$ be the interface defined as the union of the n following arcs, $i = 0, \ldots, n-1$

$$S_i := \left\{ M = \hat{M}_i(t) := (\hat{R}_i(t)\cos(\hat{\theta}_i(t)),\ \hat{R}_i(t)\sin(\hat{\theta}_i(t)),\ t \in [0,1] \right\}, \tag{1.28}$$

where $\hat{R}_i(t) := tR_{i+1} + (1-t)R_i$ and $\hat{\theta}_i(t) := t\theta_{i+1} + (1-t)\theta_i$ (see Figure 1.2 for an illustration) and where for the notation convenience we have set $R_n = R_0$. We also set $S_n = S_0$. We define the interface operator $\mathcal{T}_n$ by:

$$\begin{array}{rccl} \mathcal{T}_n : & (\mathbb{R}_+^*)^n & \longrightarrow & \mathcal{C} \\ & R & \longmapsto & \Sigma_R = \mathcal{T}_n(R) := \displaystyle\bigcup_{i=0}^{n-1} S_i. \end{array} \tag{1.29}$$

For $R \in (\mathbb{R}_+^*)^n$ sufficiently small, we denote by $\Omega_1 := \Omega_{1,R}$ the interior domain limited by the interface Σ_R and by $\Omega_2 := \Omega_{2,R} = \Omega \setminus \overline{\Omega_{1,R}}$. The unknown of the inverse problem is $\overline{R} \in (\mathbb{R}_+^*)^n$ that corresponds with $\overline{\Sigma} = \Sigma_{\overline{R}}$.

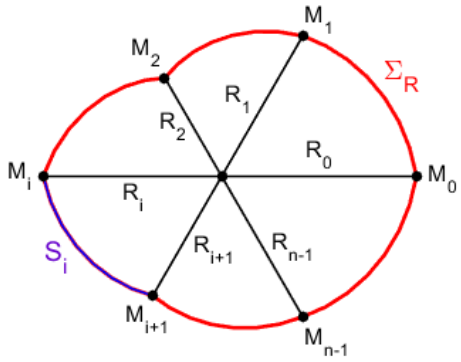

Figure 1.2: Description of the geometry in the case of a starlike geometry parameterized by (1.29), where the arc S_i is shown in blue, and the interface Σ_R is shown in red.

Let us set $\sigma(R) := \sigma_1 \chi_{\Omega_{1,R}} + \sigma_2 \chi_{\Omega_{2,R}}$ and define the function $\mathcal{J}$ by

$$\begin{array}{rccl} \mathcal{J}: & (\mathbb{R}_+^*)^n & \longrightarrow & \mathbb{R} \\ & R & \longmapsto & \mathcal{J}(R) = J(\sigma(R)). \end{array} \tag{1.30}$$

The partial derivative $\dfrac{\partial \mathcal{J}}{\partial R_i}$ can be evaluated by applying Theorem 1.6.5 to a deformation field $\zeta = \zeta_i \nu$ on Σ_R where ζ_i is hat function defined by, for $i = 0, \ldots, n-1$,

$$\zeta_i(M) = t \chi_{\{M = \hat{M}_{i-1}(t) \in S_{i-1}\}} + (1-t) \chi_{\{M = \hat{M}_i(t) \in S_i\}}$$

with $S_{-1} = S_{n-1}$, $\hat{M}_i(t)$ is defined in (1.28) and ν is the outward normal vector to Ω_1. We then get, by using Theorem 1.6.5 that the derivative of the cost function $\mathcal{J}$ with respect to R_i is given by the following formula:

$$\frac{\partial \mathcal{J}}{\partial R_i}(R) = [\sigma(R)] \int_{\Sigma_R} \left[\frac{1}{\sigma_1 \sigma_2} \left(\left| \sigma(R) \frac{\partial v_{\sigma(R)}}{\partial \nu} \right|^2 - \left| \sigma(R) \frac{\partial u_{\sigma(R)}}{\partial \nu} \right|^2 \right) + \left(|\nabla_\tau v_{\sigma(R)}|^2 - |\nabla_\tau u_{\sigma(R)}|^2 \right) \right] \zeta_i \, ds. \tag{1.31}$$

A gradient descent scheme to solve the inverse problem is summarized in Algorithm 1.

Algorithm 1: Gradient descent algorithm with exact direct solver

- Fix the number of parameters $n \in \mathbb{N}^*$ that serve to define the starlike interface.
- Consider an initial guess $R^0 \in (\mathbb{R}_+^*)^n$, the initial interface $\Sigma = \Sigma_{R^0} = \mathcal{T}_n(R^0)$ and the corresponding conductivity $\sigma(R^0) = \sigma_1 \chi_{\Omega_{1,R^0}} + \sigma_2 \chi_{\Omega_{2,R^0}}$ as defined above.
- $k = 0$.

repeat *until* $k \leq$ *maximum number of iterations*

- Use a direct solver to calculate $u_{\sigma(R^k)}$ and $v_{\sigma(R^k)}$, the respective solutions of $(N_{\sigma(R^k)})$ and $(D_{\sigma(R^k)})$.
- Calculate $\dfrac{\partial \mathcal{J}}{\partial R_i}(R^k)$, for $i = 0, \ldots, n-1$ using formula (1.31).
- Update $\Sigma = \mathcal{T}_n(R^{k+1})$ with

$$R_i^{k+1} := R_i^k - \tau \frac{\partial \mathcal{J}}{\partial R_i}(R^k),\ i = 0, \ldots, n-1,$$

  where $\tau > 0$ is chosen sufficiently small (a step adaptation can be incorporated here).
- $R^k = R^{k+1}$.
- $k = k + 1$.

end

The objective of the following three sections is to study the convergence of this algorithm in specific simplified domains Ω:

- The one-dimensional case in Section 1.7.1.
- The case of an annulus in Section 1.7.2.
- The case of an open disk in Section 1.7.3.

This study serves as a first step in the analysis of the combined inverse scheme introduced in Chapter 3.

1.7.1 The one dimensional case

In this part, we study the convergence of Algorithm 1 in the particular case where the domain $\Omega =]0, 1[$, the inner domain $\Omega_1 =]0, \delta[$ and $\Omega_2 =]\delta, 1[$ where $\delta \in]0, 1[$.

Let $(\phi, f) \in \mathbb{R}^* \times \mathbb{R}$, we will consider the following model problems:

$$(\widehat{N}_\sigma) \begin{cases} -(\sigma u')' = 0 \quad \text{in }]0,1[, \\ u(0) = 0, \\ \sigma_2 u'(1) = \phi. \end{cases} \quad ; \quad (\widehat{D}_\sigma) \begin{cases} -(\sigma v')' = 0 \quad \text{in }]0,1[, \\ v(0) = 0, \\ v(1) = f. \end{cases}$$

The solution of the direct problem $(\widehat{N}_\sigma)$ is calculated explicitly by the following proposition:

Proposition 1.7.1. *The solution u_σ of the direct problem $(\widehat{N}_\sigma)$ is given by the following expression*

$$u_\sigma(x) = \begin{cases} u_1(x) = \dfrac{\phi}{\sigma_1}\, x & \text{in } \Omega_1, \\ u_2(x) = \dfrac{\phi}{\sigma_2}\, x + \dfrac{\sigma_2 - \sigma_1}{\sigma_1 \sigma_2} \phi\, \delta & \text{in } \Omega_2. \end{cases} \tag{1.32}$$

Proof. The solution of the direct problem $(\widehat{N}_\sigma)$ can be explicitly expressed as

$$u_\sigma(x) = \begin{cases} u_1(x) = \alpha_N\, x & \text{in } \Omega_1, \\ u_2(x) = \beta_N\, x + \gamma_N & \text{in } \Omega_2, \end{cases}$$

Using the boundary condition $\sigma_2 u'(1) = \phi$ and the transmission conditions (1.11) and (1.12), we deduce that

$$\alpha_N := \frac{\phi}{\sigma_1} \quad ; \quad \beta_N := \frac{\phi}{\sigma_2} \quad ; \quad \gamma_N := \frac{\sigma_2 - \sigma_1}{\sigma_1 \sigma_2} \phi\, \delta. \tag{1.33}$$

□

In the sequel, we denote by $\overline{\delta}$ the solution of the inverse problem. Then the measurement f is given by:

$$f = \frac{\phi}{\sigma_1 \sigma_2} \left[\sigma_1 (1 - \overline{\delta}) + \sigma_2 \overline{\delta} \right], \tag{1.34}$$

and similary to Proposition 1.7.1, we have the following proposition:

Proposition 1.7.2. *The solution v_σ of the Dirichlet problem $(\widehat{D}_\sigma)$ is given by the following expression*

$$v_{\sigma(\delta)}(x) = \begin{cases} v_1(x) = \dfrac{\sigma_2 f}{(\sigma_2 - \sigma_1)\delta + \sigma_1}\, x & \text{in } \Omega_1, \\ v_2(x) = \dfrac{\sigma_1 f}{(\sigma_2 - \sigma_1)\delta + \sigma_1}\, x + \dfrac{(\sigma_2 - \sigma_1)\delta f}{(\sigma_2 - \sigma_1)\delta + \sigma_1} & \text{in } \Omega_2. \end{cases} \tag{1.35}$$

The Kohn-Vogelius cost function J depends here only on the one variable δ and its

derivative is given by the following theorem

Theorem 1.7.3. *The Kohn-Vogelius cost function J is derivable with respect to δ and its derivative is given by:*

$$J'(\delta) = \frac{[\sigma]}{\sigma_1\sigma_2}\left[\frac{(\sigma_1\sigma_2 f)^2}{((\sigma_2-\sigma_1)\delta+\sigma_1)^2} - \phi^2\right], \tag{1.36}$$

where $[\sigma] = \sigma_1 - \sigma_2$.

Proof. We have

$$J(\delta) = J_N(\delta) + J_D(\delta) - 2J_{ND}(\sigma),$$

where

$$\begin{cases} J_N(\delta) &= \displaystyle\int_0^\delta \sigma_1|u'_\sigma|^2dx + \int_\delta^1 \sigma_2|u'_\sigma|^2dx, \\ J_D(\delta) &= \displaystyle\int_0^\delta \sigma_1|v'_\sigma|^2dx + \int_\delta^1 \sigma_2|v'_\sigma|^2dx, \\ J_{ND}(\delta) &= \displaystyle\int_0^\delta \sigma_1 u'_\sigma v'_\sigma dx + \int_\delta^1 \sigma_2 u'_\sigma v'_\sigma dx. \end{cases}$$

From equations (1.32) and (1.35), we obtain:

$$\begin{cases} J_N(\delta) = -\dfrac{[\sigma]\phi^2}{\sigma_1\sigma_2}\delta + \dfrac{\phi^2}{\sigma_2}, \\ J_D(\delta) = \dfrac{\sigma_1\sigma_2 f^2}{(\sigma_2-\sigma_1)\delta+\sigma_1}, \\ J_{ND}(\delta) = \phi f. \end{cases} \tag{1.37}$$

Consequently,

$$\begin{aligned} J'(\delta) &= J'_N(\delta) + J'_D(\delta) \\ &= -\frac{[\sigma]}{\sigma_1\sigma_2}\phi^2 + \frac{\sigma_1\sigma_2[\sigma]f^2}{((\sigma_2-\sigma_1)\delta+\sigma_1)^2}, \end{aligned}$$

where $[\sigma] = \sigma_1 - \sigma_2$. □

Let ϵ be a small enough positive real such that $\overline{\delta} \in C = [\epsilon, 1-\epsilon] \subset]0,1[$ and define the

projection mapping P_C by

$$\begin{array}{rccl} P_C: & [0,1] & \longrightarrow & C \\ & x & \longmapsto & P_C(x) = \left\{ \begin{array}{ll} \epsilon & \text{if } x \leq \epsilon, \\ x & \text{if } x \in C, \\ 1-\epsilon & \text{if } x \geq 1-\epsilon. \end{array} \right. \end{array}$$

Let us consider now the iterative sequence δ^k obtained by the gradient algorithm:

$$\left\{ \begin{array}{l} \delta^0 \in C, \\ \delta^{k+1} = P_C(\delta^k - \tau J'(\delta^k)) \end{array} \right.$$

where $\tau > 0$ denotes the descent step of the gradient algorithm. We then have the following proposition.

Proposition 1.7.1. *Assume that $\sigma_1 \neq \sigma_2$ and let $\phi \in \mathbb{R}^*$. Then, for every $\delta \in C$, $J''(\delta) > 0$ and the sequence δ^k is convergent for every $\tau \in]0, 2\alpha/M^2[$, where $\alpha = \min_{\delta \in C} J''(\delta)$ and $M = \max_{\delta \in C} J''(\delta)$.*

Proof. From (1.36), the Kohn-Vogelius cost function J is three differentiable on $]0,1[$ and we have

$$J''(\delta) = \frac{2[\sigma]^2(\sigma_1\sigma_2 f)^2}{\sigma_1\sigma_2 \left[\sigma_2\delta + \sigma_1(1-\delta)\right]^3} > 0, \text{ for all } \delta \in C \tag{1.38}$$

$$J^{(3)}(\delta) = \frac{6[\sigma]^3(\sigma_1\sigma_2 f)^2}{\sigma_1\sigma_2 \left[\sigma_2\delta + \sigma_1(1-\delta)\right]^4}. \tag{1.39}$$

Then, the sequence δ^k converges to $\overline{\delta}$ for every $\tau \in]0, 2\alpha/M^2[$ where:

$$\alpha = \min_{\delta \in C} J''(\delta) \;\; ; \;\; M = \max_{\delta \in C} J''(\delta).$$

. Then we have the two following cases:

- If $[\sigma] > 0$, then $\alpha = J''(\epsilon)$ and $M = J''(1-\epsilon)$.
- If $[\sigma] < 0$, then $\alpha = J''(1-\epsilon)$ and $M = J''(\epsilon)$.

□

1.7.2 The case of an annulus

We study here the convergence of Algorithm 1 in the case of the annulus domain:

$$\Omega = \{(x,y) \in \mathbb{R}^2 \text{ such that } \ R_1^2 < x^2 + y^2 < R_2^2\},$$

bounded by the circles

$$\Gamma_1 = \{(x,y) \in \mathbb{R}^2 \text{ such that } \ x^2 + y^2 = R_1^2\} \ ; \ \Gamma_2 = \{(x,y) \in \mathbb{R}^2 \text{ such that } \ x^2 + y^2 = R_1^2\}.$$

Let $R \in]R_1, R_2[$ and $\Sigma = \Sigma_R = \{(x,y) \in \mathbb{R}^2 \text{ such that } \ x^2 + y^2 = R^2\}$

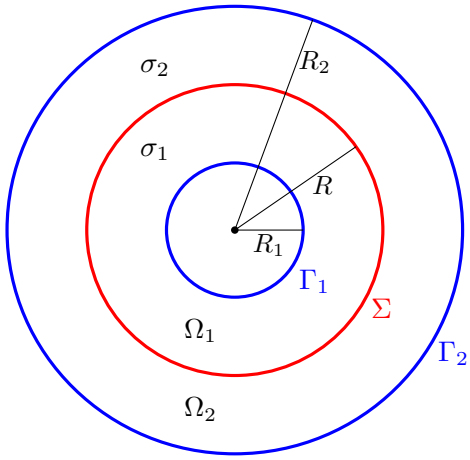

Figure 1.3: Description of the geometry in the case of an annulus domain. $\Omega_1 : R_1 < r < R$ and $\Omega_2 : R < r < R_2$.

Discription of the problem

Let $(\phi, f) \in \mathbb{R}^* \times \mathbb{R}$ and $\sigma = \sigma_1 \chi_{\Omega_1} + \sigma_2 \chi_{\Omega_2}$. We denote by $(\widetilde{N}_\sigma)$ and $(\widetilde{D}_\sigma)$ the two following problems:

$$(\widetilde{N}_\sigma) \begin{cases} -div(\sigma \nabla u) = 0 & \text{in } \Omega, \\ u = 0 & \text{on } \Gamma_1, \\ \sigma \dfrac{\partial u}{\partial \nu} = \phi & \text{on } \Gamma_2. \end{cases} \quad ; \quad (\widetilde{D}_\sigma) \begin{cases} -div(\sigma \nabla v) = 0 & \text{in } \Omega, \\ v = 0 & \text{on } \Gamma_1, \\ v = f & \text{on } \Gamma_2. \end{cases}$$

Using the polar coordinates (r, θ), the solution u_σ of $(\widetilde{N}_\sigma)$ is given by:

$$u_{\sigma(R)}(r,\theta) = \begin{cases} u_1(r,\theta) = \widetilde{\alpha}_N \ \log\left(\dfrac{r}{R_1}\right) & \text{if } (r,\theta) \in [R_1, R] \times [0, 2\pi], \\ u_2(r,\theta) = \widetilde{\beta}_N \ \log\left(\dfrac{r}{R_1}\right) + \widetilde{\gamma_N} & \text{if } (r,\theta) \in [R, R_2] \times [0, 2\pi], \end{cases}$$

where:

$$\begin{cases} \widetilde{\alpha}_N := \widetilde{\alpha}_N(R) = \dfrac{R_2\phi}{\sigma_1}, \\ \widetilde{\beta}_N := \widetilde{\beta}_N(R) = \dfrac{R_2\phi}{\sigma_2}, \\ \widetilde{\gamma}_N := \widetilde{\gamma}_N(R) = \dfrac{(\sigma_2 - \sigma_1)R_2\phi}{\sigma_1\sigma_2} \log\left(\dfrac{R}{R_1}\right), \end{cases} \tag{1.40}$$

and the solution v_σ of the Dirichlet problem $(\widetilde{D}_\sigma)$ is given by

$$v_{\sigma(R)}(r,\theta) = \begin{cases} v_1(r,\theta) = \widetilde{\alpha}_D \ \log\left(\dfrac{r}{R_1}\right) & \text{if } (r,\theta) \in [R_1, R] \times [0, 2\pi], \\ v_2(r,\theta) = \widetilde{\beta}_D \ \log\left(\dfrac{r}{R_2}\right) + \widetilde{\gamma_D} & \text{if } (r,\theta) \in [R, R_2] \times [0, 2\pi], \end{cases}$$

where:

$$\begin{cases} \widetilde{\alpha}_D := \widetilde{\alpha}_D(R) = \dfrac{\sigma_2 f}{\sigma_2 \log\left(\dfrac{R}{R_1}\right) + \sigma_1 \log\left(\dfrac{R_2}{R}\right)}, \\ \widetilde{\beta}_D := \widetilde{\beta}_D(R) = \dfrac{\sigma_1 f}{\sigma_2 \log\left(\dfrac{R}{R_1}\right) + \sigma_1 \log\left(\dfrac{R_2}{R}\right)}, \\ \widetilde{\gamma}_D := \widetilde{\gamma}_D(R) = f. \end{cases} \tag{1.41}$$

In the sequel, we denote by $\overline{R}$ the solution of the inverse problem, we then have:

$$f := u_2(R_2,\theta) = \frac{R_2\phi}{\sigma_2} \ \log\left(\frac{R_2}{R_1}\right) + \frac{(\sigma_2 - \sigma_1)R_2\phi}{\sigma_1\sigma_2} \log\left(\frac{\overline{R}}{R_1}\right). \tag{1.42}$$

The function $\mathcal{J}$ depends here only on the one variable $R \in]R_1, R_2[$ and its derivative is given by (1.31) for $i = 0$ with $\zeta_0 = 1$, namely,

$$\begin{aligned} \mathcal{J}'(R) &= [\sigma(R)] \int_0^{2\pi} \left[\frac{1}{\sigma_1\sigma_2} \left(\left| \sigma(R) \frac{\partial v_{\sigma(R)}}{\partial \nu} \right|^2 - \left| \sigma(R) \frac{\partial u_{\sigma(R)}}{\partial \nu} \right|^2 \right) + \left(|\nabla_\tau v_{\sigma(R)}|^2 - |\nabla_\tau u_{\sigma(R)}|^2 \right) \right] R \, d\theta \\ &= \frac{2\pi\sigma_1(\sigma_1 - \sigma_2)}{\sigma_2 R} (\widetilde{\alpha}_D^2(R) - \widetilde{\alpha}_N^2(R)). \end{aligned} \tag{1.43}$$

Let us consider now the iterative sequence R^k obtained by the gradient algorithm:

$$\begin{cases} R^0 \in]R_1, R_2[, \\ R^{k+1} = R^k - \tau \mathcal{J}'(R^k), \end{cases}$$

where $\tau > 0$ denotes the descent step of the gradient algorithm. We say that the sequence R^k is locally convergent, if there exists $\varepsilon > 0$, such that, for every $R^0 \in]\overline{R} - \varepsilon, \overline{R} + \varepsilon[$, the sequence R^k converges. We then have the following proposition.

Proposition 1.7.2. *Assume that $\sigma_1 \neq \sigma_2$ and let $\phi \in \mathbb{R}^*$. Then, $\mathcal{J}''(\overline{R}) > 0$ and the sequence R^k is locally convergent if and only if the descent step $\tau \in]0, 2/\mathcal{J}''(\overline{R})[$.*

Proof. The function $\mathcal{J}$ is twice differentiable on $]R_1, R_2[$ and we have

$$\mathcal{J}''(R) = F_1'(R)F_2(R) + F_1(R)F_2'(R)$$

where

$$F_1(R) := \frac{2\pi\sigma_1(\sigma_1 - \sigma_2)}{\sigma_2 R} \text{ and } F_2(R) := \widetilde{\alpha}_D^2(R) - \widetilde{\alpha}_N^2(R).$$

From the fact $\widetilde{\alpha}_D(\overline{R}) = \widetilde{\alpha}_N(\overline{R})$, we deduce that

$$\mathcal{J}''(\overline{R}) = F_1(\overline{R})F_2'(\overline{R}) = 2F_1(\overline{R})\widetilde{\alpha}_D(\overline{R})\left(\widetilde{\alpha}_D'(\overline{R}) - \widetilde{\alpha}_N'(\overline{R})\right),$$

where:

$$\widetilde{\alpha}_N'(\overline{R}) = 0, \ ; \ \widetilde{\alpha}_D'(\overline{R}) = \frac{\sigma_2 f(\sigma_1 - \sigma_2)}{\overline{R}\left[\sigma_2 \log\left(\frac{\overline{R}}{R_1}\right) + \sigma_1 \log\left(\frac{R_2}{\overline{R}}\right)\right]^2},$$

then

$$\mathcal{J}''(\overline{R}) \ = \ \frac{4\pi\sigma_1\sigma_2(\sigma_1 - \sigma_2)^2 f^2}{\overline{R}^2\left[\sigma_2 \log\left(\frac{\overline{R}}{R_1}\right) + \sigma_1 \log\left(\frac{R_2}{\overline{R}}\right)\right]^3}.$$

By using (1.42), we obtain

$$\mathcal{J}''(\overline{R}) \ = \ \frac{4\pi\phi^2 R_2^2(\sigma_1 - \sigma_2)^2}{\sigma_1\sigma_2\overline{R}^2\left[\sigma_2 \log\left(\frac{\overline{R}}{R_1}\right) + \sigma_1 \log\left(\frac{R_2}{\overline{R}}\right)\right]}. \tag{1.44}$$

Moreover, the recurrent sequence R^k can be written as $R^{k+1} = g(R^k)$, where

$$g(R) = R - \tau \mathcal{J}'(R).$$

Then, the sequence R^k converges locally if and only if $|g'(\overline{R})| = |1 - \mathcal{J}''(\overline{R})| < 1$. From the condition: $\sigma_1 \neq \sigma_2$, we deduce from (1.44) that $\mathcal{J}''(\overline{R}) > 0$, and then the sequence R^k converges locally if and only if $\tau \in]0, 2/\mathcal{J}''(\overline{R})[$.

□

1.7.3 The case of an open disk

We study here the convergence of Algorithm 1 in the case $n = 1$, i.e Ω_1 is an open disk of center $(0, 0)$ and radius $R > 0$. We also choose the domain Ω to be the open disk of center $(0, 0)$ and radius $R_2 > 0$. In this case the interface $\Sigma = \Sigma_R$ coincides with the circle of center $(0, 0)$ and radius R (note that $S_{-1} = S_0 = S_1$) as shown in the following figure

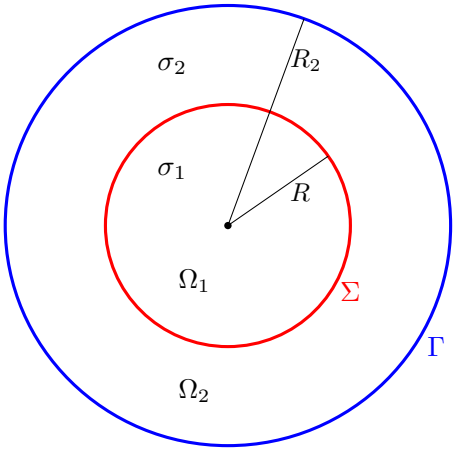

Figure 1.4: Description of the geometry in the case of an open disk domain of center $(0, 0)$ and radius R_2. Ω_1 is an open disk of center $(0, 0)$ and radius R.

The unknown of the inverse problem is $\overline{R}$ that corresponds with $\overline{\Sigma} = \Sigma_{\overline{R}}$. We impose the current flux $\phi(\theta) = m\cos(m\theta)$ or $\phi(\theta) = m\sin(m\theta)$, $\theta \in [0, 2\pi]$ and $m \in \mathbb{N}^*$. The solution of the direct problem $(N_{\sigma(R)})$ with the additional condition $\int_\Sigma u \; ds = 0$ can be explicitly expressed as

$$u_{\sigma(R)}(r, \theta) = \begin{cases} u_1(r, \theta) = \alpha_N \; r^m \dfrac{\phi(\theta)}{m} & \text{in } \Omega_1, \\ u_2(r, \theta) = \left(\beta_N \; r^m + \dfrac{\gamma_N}{r^m}\right) \dfrac{\phi(\theta)}{m} & \text{in } \Omega_2, \end{cases}$$

where:

$$\begin{cases} \alpha_N := \alpha_N(R) = \dfrac{2R_2^{m+1}}{\sigma_1(R_2^{2m}+R^{2m})+\sigma_2(R_2^{2m}-R^{2m})}, \\ \beta_N := \beta_N(R) = \dfrac{(\sigma_2+\sigma_1)R_2^{m+1}}{\sigma_2\left[\sigma_1(R_2^{2m}+R^{2m})+\sigma_2(R_2^{2m}-R^{2m})\right]}, \\ \gamma_N := \gamma_N(R) = \dfrac{(\sigma_2-\sigma_1)R_2^{m+1}R^{2m}}{\sigma_2\left[\sigma_1(R_2^{2m}+R^{2m})+\sigma_2(R_2^{2m}-R^{2m})\right]}. \end{cases} \tag{1.45}$$

The measurement f is then given by:

$$f(\theta) = C_f \frac{\phi(\theta)}{m},$$

where

$$C_f := \beta_N(\overline{R})\ R_2^m + \frac{\gamma_N(\overline{R})}{R_2^m} = \frac{R_2}{\sigma_2}\frac{[\sigma_1(R_2^{2m}-\overline{R}^{2m})+\sigma_2(R_2^{2m}+\overline{R}^{2m})]}{[\sigma_1(R_2^{2m}+\overline{R}^{2m})+\sigma_2(R_2^{2m}-\overline{R}^{2m})]}. \tag{1.46}$$

Consequently, the solution of the Dirichlet problem $(D_{\sigma(R)})$ is

$$v_{\sigma(R)}(r,\theta) = \begin{cases} v_1(r,\theta) = \alpha_D\ r^m \dfrac{\phi(\theta)}{m} & \text{in } \Omega_1, \\ v_2(r,\theta) = \left(\beta_D\ r^m + \dfrac{\gamma_D}{r^m}\right)\dfrac{\phi(\theta)}{m} & \text{in } \Omega_2, \end{cases}$$

where:

$$\begin{cases} \alpha_D := \alpha_D(R) = \dfrac{2\sigma_2 R_2^m C_f}{\sigma_1(R_2^{2m}-R^{2m})+\sigma_2(R_2^{2m}+R^{2m})}, \\ \beta_D := \beta_D(R) = \dfrac{(\sigma_2+\sigma_1)R_2^m C_f}{\sigma_1(R_2^{2m}-R^{2m})+\sigma_2(R_2^{2m}+R^{2m})}, \\ \gamma_D := \gamma_D(R) = \dfrac{(\sigma_2-\sigma_1)R_2^m R^{2m} C_f}{\sigma_1(R_2^{2m}-R^{2m})+\sigma_2(R_2^{2m}+R^{2m})}. \end{cases} \tag{1.47}$$

The function $\mathcal{J}$ depends here only on the one variable R and its derivative is given by (1.31) for $i=0$ with $\zeta_0 = 1$, namely,

$$\begin{aligned} \mathcal{J}'(R) &= [\sigma(R)]\int_0^{2\pi}\left[\frac{1}{\sigma_1\sigma_2}\left(\left|\sigma(R)\frac{\partial v_{\sigma(R)}}{\partial \nu}\right|^2 - \left|\sigma(R)\frac{\partial u_{\sigma(R)}}{\partial \nu}\right|^2\right) + \left(|\nabla_\tau v_{\sigma(R)}|^2 - |\nabla_\tau u_{\sigma(R)}|^2\right)\right] R\, d\theta \\ &= \frac{\pi m^2(\sigma_1^2-\sigma_2^2)}{\sigma_2} R^{2m-1}(\alpha_D^2(R)-\alpha_N^2(R)). \end{aligned} \tag{1.48}$$

Let us consider now the iterative sequence R^k obtained by the gradient algorithm:

$$R^{k+1} = R^k - \tau \mathcal{J}'(R^k).$$

We then have the following proposition.

Proposition 1.7.3. *Assume that $\sigma_1 \neq \sigma_2$ and let $\phi(\theta) = m\cos(m\theta)$ or $\phi(\theta) = m\sin(m\theta)$, $m \in \mathbb{N}^*$. Then $\mathcal{J}''(\overline{R}) > 0$ and the sequence R^k is locally convergent if and only if the descent step $\tau < 2/\mathcal{J}''(\overline{R})$.*

Proof. The function $\mathcal{J}$ is twice differentiable on $]0, R_2[$ and we have

$$\mathcal{J}''(R) = F_1'(R)F_2(R) + F_1(R)F_2'(R)$$

where

$$F_1(R) := \frac{\pi m^2(\sigma_1^2 - \sigma_2^2)}{\sigma_2} R^{2m-1} \text{ and } F_2(R) := \alpha_D^2(R) - \alpha_N^2(R).$$

From the fact $\alpha_N(\overline{R}) = \alpha_D(\overline{R})$, we deduce that

$$\mathcal{J}''(\overline{R}) = F_1(\overline{R})F_2'(\overline{R}) = 2F_1(\overline{R})\alpha_N(\overline{R})\left(\alpha_D'(\overline{R}) - \alpha_N'(\overline{R})\right),$$

where:

$$\alpha_N'(\overline{R}) = \frac{4(\sigma_2 - \sigma_1)mR_2^{m+1}\overline{R}^{2m-1}}{\left[\sigma_1(R_2^{2m} + \overline{R}^{2m}) + \sigma_2(R_2^{2m} - \overline{R}^{2m})\right]^2},$$

and

$$\alpha_D'(\overline{R}) = \frac{4(\sigma_1 - \sigma_2)m\sigma_2 C_f R_2^m \overline{R}^{2m-1}}{\left[\sigma_1(R_2^{2m} - \overline{R}^{2m}) + \sigma_2(R_2^{2m} + \overline{R}^{2m})\right]^2}.$$

By using (1.46), we obtain

$$\alpha_D'(\overline{R}) = \frac{4(\sigma_1 - \sigma_2)mR_2^{m+1}\overline{R}^{2m-1}}{\left[\sigma_1(R_2^{2m} - \overline{R}^{2m}) + \sigma_2(R_2^{2m} + \overline{R}^{2m})\right]\left[\sigma_1(R_2^{2m} + \overline{R}^{2m}) + \sigma_2(R_2^{2m} - \overline{R}^{2m})\right]}.$$

Consequently

$$\begin{aligned} F_2'(\overline{R}) &= 2\,\alpha_N(\overline{R})\left(\alpha_D'(\overline{R}) - \alpha_N'(\overline{R})\right) \\ &= \frac{32m(\sigma_1^2 - \sigma_2^2)R_2^{4m+2}\overline{R}^{2m-1}}{\left[\sigma_1(R_2^{2m} - \overline{R}^{2m}) + \sigma_2(R_2^{2m} + \overline{R}^{2m})\right]\left[\sigma_1(R_2^{2m} + \overline{R}^{2m}) + \sigma_2(R_2^{2m} - \overline{R}^{2m})\right]^3}, \end{aligned}$$

and then

$$\mathcal{J}''(\overline{R}) = \frac{32\pi m^3(\sigma_1^2-\sigma_2^2)^2 R_2^{4m+2}\overline{R}^{4m-2}}{\sigma_2\left[\sigma_1(R_2^{2m}-\overline{R}^{2m})+\sigma_2(R_2^{2m}+\overline{R}^{2m})\right]\left[\sigma_1(R_2^{2m}+\overline{R}^{2m})+\sigma_2(R_2^{2m}-\overline{R}^{2m})\right]^3}. \tag{1.49}$$

The iterations for R^k can be written as $R^{k+1} = g(R^k)$, where

$$g(R) = R - \tau\mathcal{J}'(R).$$

Then, the sequence R^k converges locally if and only if $|g'(\overline{R})| = |1 - \mathcal{J}''(\overline{R})| < 1$. From the condition: $\sigma_1 \neq \sigma_2$, we deduce from (1.49) that $\mathcal{J}''(\overline{R}) > 0$, and then the sequence R^k converges locally if and only if $\tau \in]0, 2/\mathcal{J}''(\overline{R})[$.

□

1.8 Numerical experiments and validation

In this section, we present some numerical results obtained by using a minimization algorithm of gradient type. The numerical examples are based on synthetic data numerically simulated using the FreeFem++ software [35]. Indeed, our algorithm on σ_i can be written as:

$$\sigma_i^{k+1} = \sigma_i^k - \tau\frac{\partial J}{\partial\sigma_i}(\sigma^k), i = 1, 2.$$

where $\tau > 0$ is chosen sufficiently small (a step adaptation can be incorporated here i.e. τ is determined so that the functional J decreases) and $\dfrac{\partial J}{\partial\sigma_i}$, $i = 1, 2$ are given by Corollary 1.6.4. In addition, our gradient descent algorithm for the identification of the interface Σ is described in Algorithm 1.

For our numerical validation, we choose for example the domain Ω an open disk of center $(0, 0)$ and radius $R_2 = 2$. Moreover, in most of the experiments below the exact interface $\overline{\Sigma} := \Sigma_{\overline{R}}$ is represented by the parametrization (1.29) used in the inversion algorithms. Indeed, we choose for example the case of $n = 9$ and $\overline{R}$ given by

$$\overline{R} = (1, 0.8, 0.7, 0.9, 1, 1.7, 1.6, 1.5, 1.4),$$

the conductivity values $\overline{\sigma_1} = 1$, $\overline{\sigma_2} = 2$, the current flux $\phi(\theta) = \cos(\theta)$, $\theta \in [0, 2\pi]$ and the gradient descent step $\tau = 0.05$. The synthetic data f is represented by the values f_i, $i = 1, \ldots, N_\Gamma$ of the numerical solution at the nodes belonging to Γ. In order to simulate noise in the data f we artificially corrupt the computed values f_i with random noise as follows:

$$f_i^\epsilon := f_i + \epsilon(1 - 2r_i)f_i, \; i = 1, \ldots, N_\Gamma,$$

where r_i are randomly chosen between 0 and 1 and ϵ denotes the noise level.

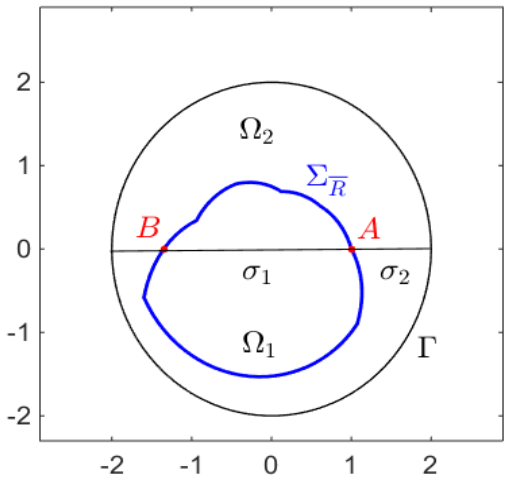

Figure 1.5: Description of the geometry for the numerical experiments.

To gain insight into the behavior of the Kohn-Vogelius cost functional J with respect to various parameters of the inverse problem, $\overline{\sigma_1}$, $\overline{\sigma_2}$, and $\Sigma_{\overline{R}}$, we consider the following scenarios:

- Scenario 1: Only $\overline{\sigma_1}$ is unknown ($\overline{\sigma_2}$ and $\Sigma_{\overline{R}}$ are known).
- Scenario 2: Only $\overline{\sigma_2}$ is unknown ($\overline{\sigma_1}$ and $\Sigma_{\overline{R}}$ are known).
- Scenario 3: Both $\overline{\sigma_1}$ and $\overline{\sigma_2}$ are unknown (only $\Sigma_{\overline{R}}$ is known).
- Scenario 4: Only $\Sigma_{\overline{R}}$ is unknown (both $\overline{\sigma_1}$ and $\overline{\sigma_2}$ are known).

In Figures 1.6 and 1.7, we show the convexity of the function J with respect to σ_1 and σ_2, respectively. Additionally, Figures 1.8 and 1.9 respectively illustrate the scenario where only $\overline{\sigma_1}$ is unknown and the scenario where only $\overline{\sigma_2}$ is unknown.

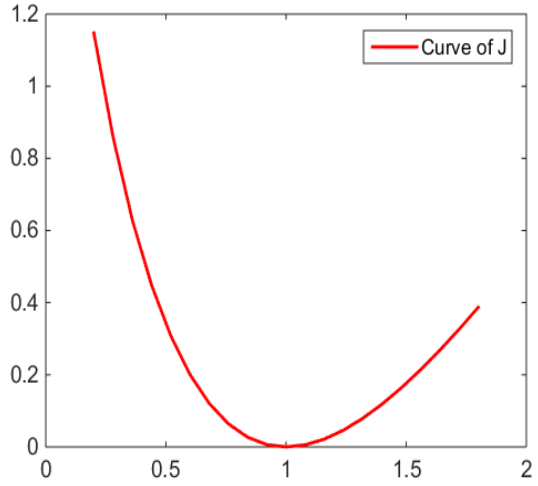

J versus the values of σ_1.

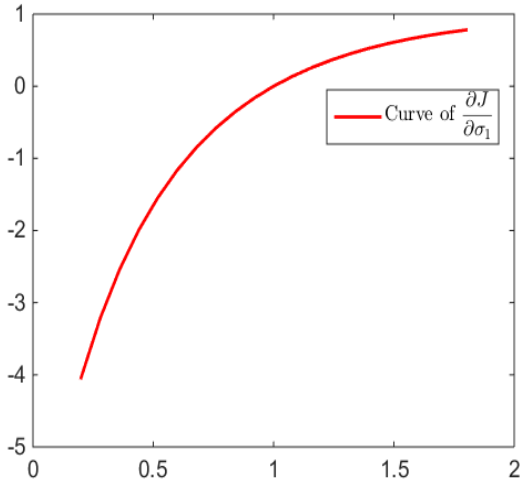

$\dfrac{\partial J}{\partial \sigma_1}$ versus the values of σ_1.

Figure 1.6: Convexity of the function J with respect to σ_1.

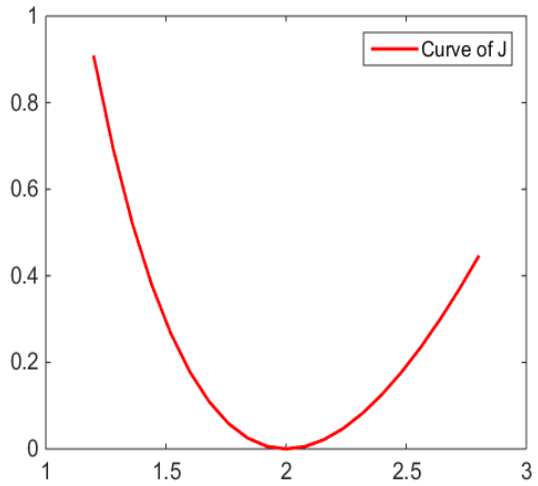

J versus the values of σ_2.

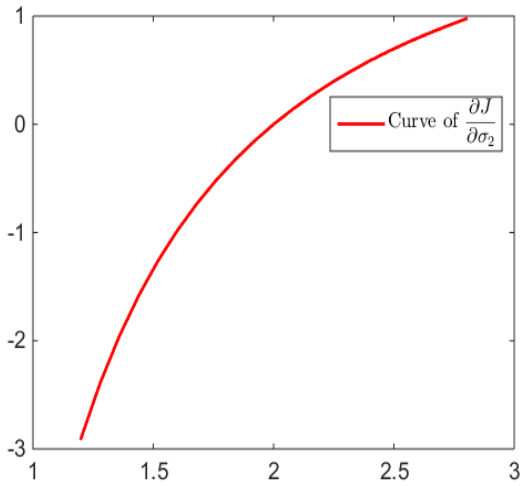

$\dfrac{\partial J}{\partial \sigma_2}$ versus the values of σ_2.

Figure 1.7: Convexity of the function J with respect to σ_2

1.8.1 Scenario 1: only $\overline{\sigma_1}$ is unknown

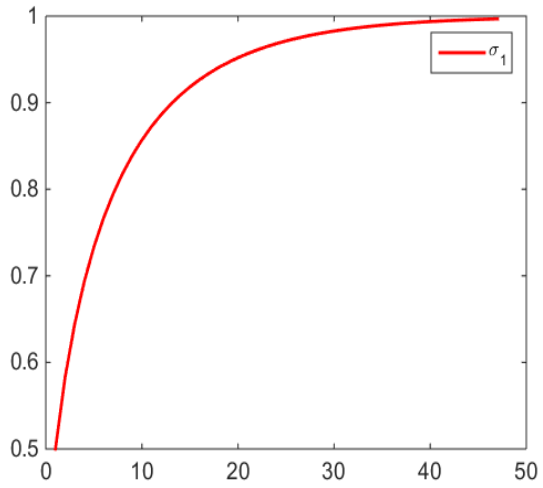

Values of σ_1.

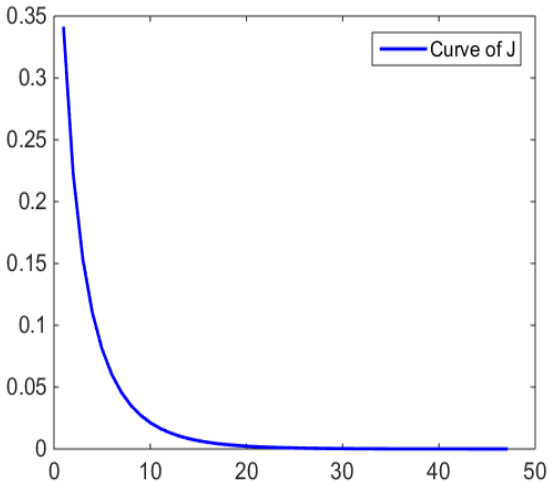

J versus the number of iterations.

Figure 1.8: Identification of $\overline{\sigma_1}$ is shown on the left, and the evolution of J versus the number of iterations is shown on the right.

1.8.2 Scenario 2: only $\overline{\sigma_2}$ is unknown

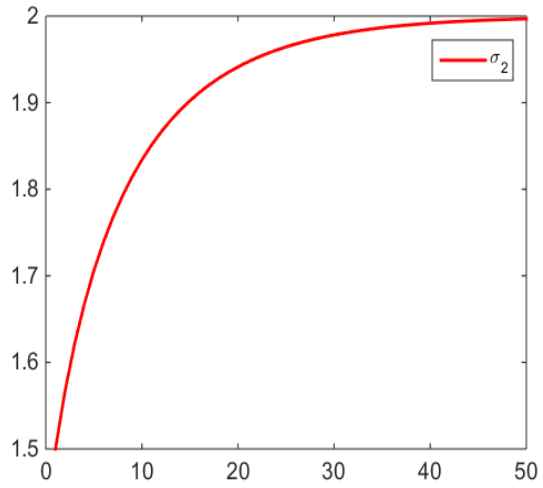

Values of σ_2.

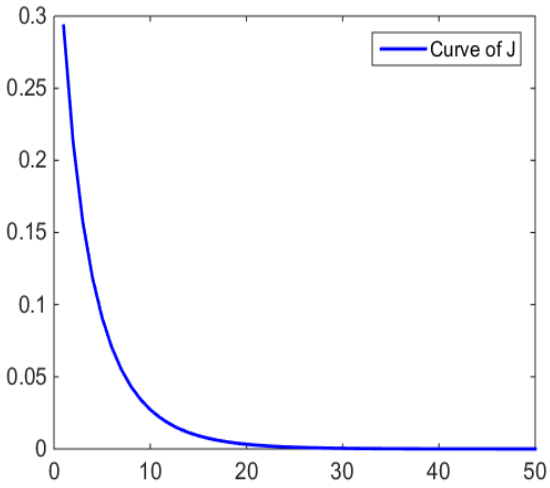

J versus the number of iterations.

Figure 1.9: Identification of $\overline{\sigma_2}$ is shown on the left, and the evolution of J versus the number of iterations is shown on the right.

1.8.3 Scenario 3: both $\overline{\sigma_1}$ and $\overline{\sigma_2}$ are unknown

We assume that the singularity support $\Sigma_{\overline{R}}$ of $\overline{\sigma}$ is known, and we are interested in identifying the conductivity values $\overline{\sigma_1}$ and $\overline{\sigma_2}$ from the knowledge of ϕ and f. In the numerical identification experiments, we illustrate the identification process in Figure 1.10 where the geometry $\Sigma_{\overline{R}}$ is parameterized by (1.29), intersecting the x-axis at the two singularity points A and B (see Figure 1.5 for an illustration). Additionally, different noisy data are considered.

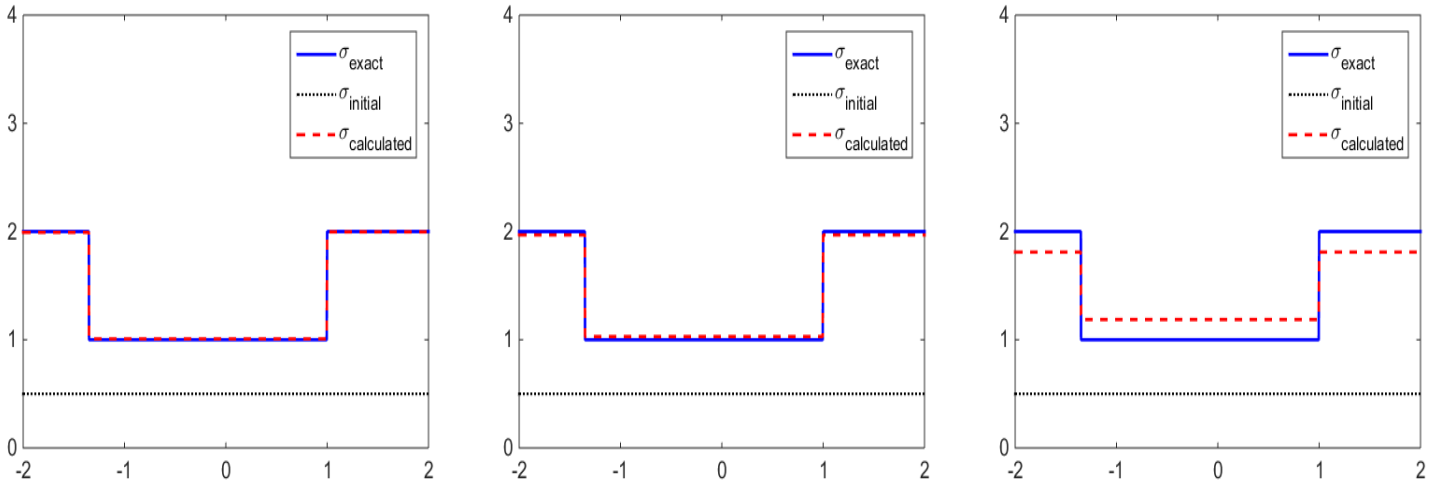

Figure 1.10: Values of σ at the location where $\Sigma_{\overline{R}}$ intersects the x-axis at the two singularity points A and B with different noisy data: noise-free data (left), noise level $\epsilon = 1\%$ (middle), and $\epsilon = 3\%$ (right).

1.8.4 Scenario 4: only $\Sigma_{\overline{R}}$ is unknown

Here, we assume that both of the conductivity values $\overline{\sigma_1}$ and $\overline{\sigma_2}$ are known, and we are interested in identifying the singularity support $\Sigma_{\overline{R}}$ of $\overline{\sigma}$ from the knowledge of ϕ and f.
As an initial guess, we choose $R^0 = (1.7, 1.6, 1.55, 1.4, 1.3, 1.3, 1.2, 1.4, 1.5)$.

In Figure 1.11, we show the reconstruction of $\Sigma_{\overline{R}}$ obtained by Algorithm 1 for different noisy data: free noisy data Figure 1.11(b), noise level $\epsilon = 3\%$ Figure 1.11(c), and $\epsilon = 5\%$ Figure 1.11(d). The exact shape and initial guess are depicted in Figure1.11(a).

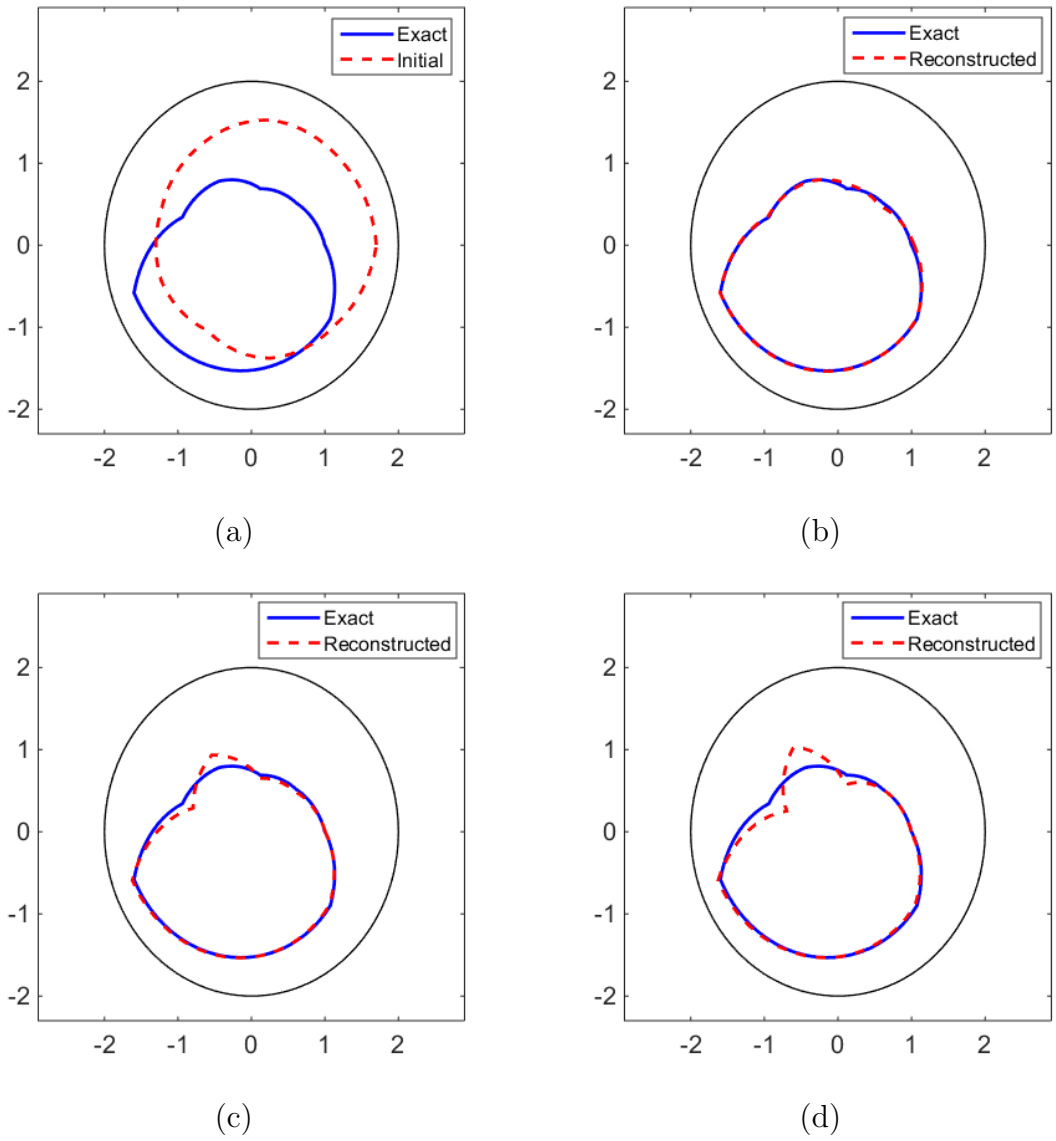

(a) (b)

(c) (d)

Figure 1.11: Reconstruction of $\Sigma_{\overline{R}}$ by Algorithm 1 for different noisy data: free noisy data (b), noise level $\epsilon = 3\%$ (c) and $\epsilon = 5\%$ (d). The exact shape and initial guess are shown in Figure (a).

1.9 Conclusion

In this chapter, we have introduced the direct problem together with the Kohn-Vogelius method as an inversion method for solving the inverse problem. First, we investigated the existence and uniqueness of the solution of the direct problem (N_σ). Subsequently, we presented the Kohn-Vogelius method, which consists of transforming the inverse problem $(\mathcal{I}.\mathcal{P})$ into

an optimization one by constructing the Kohn-Vogelius cost function J. We proved that $\overline{\sigma}$ is a minimum of J and subsequently calculated its derivative with respect to the conductivity values σ_1 and σ_2. The existence and expression of the shape derivative of the Kohn-Vogelius cost function with respect to the singularity interface Σ of σ have been studied by Afraites et al. in [2].

Furthermore, as a preparatory step for the combined inversion algorithm introduced in Chapter 3 for a geometrical inverse conductivity problem, we explicitly present the gradient descent algorithm tailored to starlike interfaces. We developed a gradient descent scheme, summarized in Algorithm 1, to effectively identify the singularity curve $\Sigma_{\overline{R}}$ of $\overline{\sigma}$. Additionally, we analyzed the convergence of this algorithm in some simplified geometries. This study serves as an essential step in the convergence analysis of the combined inverse scheme.

To conclude the chapter, we provided some numerical experiments obtained using this inversion method. These experiments illustrated the effectiveness and applicability of the proposed method.

CHAPTER 2

A non-overlapping Domain Decomposition Method

2.1 Introduction

In order to evaluate the solutions of the direct problems (N_σ) and (D_σ) studied in Chapter 1, this chapter employs a non-overlapping Domain Decomposition Method (DDM) known as the Optimized Schwarz Method (OSM). The OSM enforces communications at the interfaces of the domains through Robin-type boundary conditions [48, 39, 40, 25, 21]. The chapter begins with a brief introduction to Domain Decomposition Methods (DDMs) and then presents the OSM as the chosen non-overlapping DDM. Next, we reformulate the direct problems (N_σ) and (D_σ) as an equivalent multi-domain problem using Robin transmission conditions. The convergence rate of OSM is investigated in one dimension and in the case of circular interfaces. These findings are valuable for analyzing the convergence of the combined inversion algorithm. Finally, we present some numerical illustrations on the convergence of OSM.

2.2 On the domain decomposition methods

Domain Decomposition Methods (DDMs) were introduced as techniques for solving partial differential equations based on a decomposition of the partial domain of the problem into several subdomains. The problems on the subdomains are independent, which makes DDMs suitable for parallel computing. Indeed, DDMs were originally introduced for prob-

lems on "complex" geometries, and they are now widely used as parallel algebraic solvers and preconditioners for solutions of various problems. Moreover, DDMs are typically used as preconditioners for Krylov space iterative methods, such as the conjugate gradient method, GMRES, and LOBPCG.

The concept of domain decomposition methods was first introduced in 1869–1870 by Hermann Schwarz [54] to prove the uniqueness of the solution to the Dirichlet problem (2.1) in a domain with complex geometric shapes.

In overlapping DDMs, the subdomains overlap by more than the interface. The example in Figure 2.1(left) shows such a situation, which include the Schwarz alternating method introduced in Definition 2.2.1 and the additive Schwarz method. Many DDMs can be written and analyzed as a special case of the abstract additive Schwarz method. Intuitively, the existence of an overlap region allows more information to be exchanged at each iteration, and therefore suggests better convergence of the method.

In non-overlapping DDMs, the subdomains intersect only on their interface. The example in Figure 2.1(right) shows such a situation. In primal methods, such as Balancing domain decomposition and BDDC, the continuity of the solution across subdomain interface is enforced by representing the value of the solution on all neighboring subdomains by the same unknown. In dual methods, such as FETI, the continuity of the solution across the subdomain interface is enforced by Lagrange multipliers. The FETI-DP method is hybrid between a dual and a primal method. The two figures below show a typical example of DDMs, where the first domain decomposition method was introduced by Schwarz for a complicated domain, composed of two simple ones, namely a disk and a rectangle.

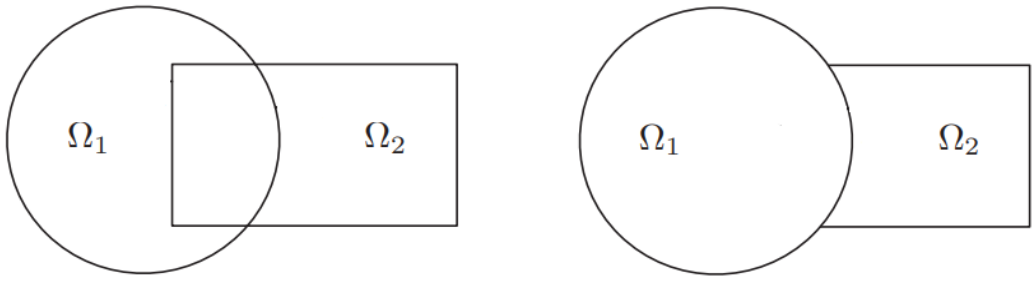

Figure 2.1: Typical example of domain decomposition method with overlap (left), as it appears in Schwarz's article in 1870, and without overlap (right).

Let the domain Ω be the union of a disk and a rectangle, see the figure above, which is

on the left. Consider the Dirichlet problem which consists in finding $u : \Omega \longrightarrow \mathbb{R}$ such that

$$\begin{cases} -\Delta u = 0 & \text{in } \Omega, \\ u = g & \text{on } \partial\Omega. \end{cases} \tag{2.1}$$

Definition 2.2.1. *(Original Schwarz algorithm) The Schwarz algorithm is an iterative method based on solving subproblems alternatively in domains Ω_1 and Ω_2. It updates $(u_1^n, u_2^n) \to (u_1^{n+1}, u_2^{n+1})$ by*

$$\begin{cases} -\Delta u_1^{n+1} = 0 & \text{in } \Omega_1, \\ u_1^{n+1} = g & \text{on } \partial\Omega_1 \cap \partial\Omega, \\ u_1^{n+1} = u_2^n & \text{on } \partial\Omega_1 \cap \overline{\Omega_2}. \end{cases}$$

$$\begin{cases} -\Delta u_2^{n+1} = 0 & \text{in } \Omega_2, \\ u_2^{n+1} = g & \text{on } \partial\Omega_2 \cap \partial\Omega, \\ u_2^{n+1} = u_1^{n+1} & \text{on } \partial\Omega_2 \cap \overline{\Omega_1}. \end{cases}$$

Schwarz proved the convergence of the algorithm and thus the well-posedness of the Poisson problem in complex geometries. For a more detailed history of Schwarz methods, one may consult Martin Gander's article [26], which explains the similarities and differences of the methods presented here through numerous citations from major contributors in the field.

During the past few decades, a new class of nonoverlapping and overlapping Schwarz methods has been developed for PDEs, known as Optimized Schwarz Methods (OSMs). These methods, which were introduced by P. L. Lions in [48] for elliptic problems and by B. Després in [20] for propagative wave phenomena, have gained significant popularity. They are based on classical domain decomposition techniques but employ more effective transmission conditions at the interfaces between subdomains compared to the traditional Dirichlet conditions. In the case of elliptic problems, the original Schwarz method [54] only applies to overlapping domain decompositions, and its performance in terms of iteration counts relies on the width of the overlap. However, the algorithm introduced by P. L. Lions [48] can be applied to both overlapping and nonoverlapping subdomains. It is based on improving Schwarz methods by replacing the Dirichlet interface conditions by Robin interface conditions. Let $\alpha > 0$, the optimized Schwarz algorithm reads as

$$\begin{cases} -\Delta u_1^{n+1} & = 0 & \text{in } \Omega_1, \\ u_1^{n+1} & = g & \text{on } \partial\Omega_1 \cap \partial\Omega, \\ \dfrac{\partial u_1^{n+1}}{\partial n_1} + \alpha u_1^{n+1} & = \dfrac{\partial u_2^n}{\partial n_2} + \alpha u_2^n & \text{on } \partial\Omega_1 \cap \overline{\Omega_2}. \end{cases}$$

$$\begin{cases} -\Delta u_2^{n+1} & = 0 & \text{in } \Omega_2, \\ u_2^{n+1} & = g & \text{on } \partial\Omega_2 \cap \partial\Omega, \\ \dfrac{\partial u_2^{n+1}}{\partial n_2} + \alpha u_2^{n+1} & = \dfrac{\partial u_1^n}{\partial n_1} + \alpha u_1^n & \text{on } \partial\Omega_2 \cap \overline{\Omega_1}, \end{cases}$$

where n_1 and n_2 denote the outward normals which are shown in Figure 2.2.

Moreover, Robin interface conditions can be replaced by more general interface conditions that can be optimized for a better convergence, see for instance [39, 40, 25]. Furthermore, the convergence of the domain decomposition method remains slow in certain cases, which is why higher-order transmission conditions have been developed.

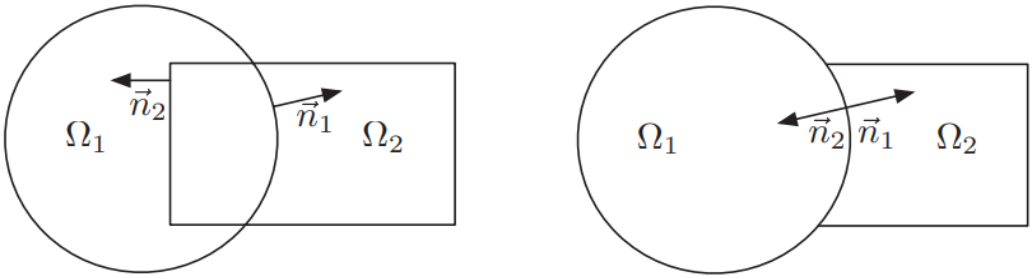

Figure 2.2: Outward normals for overlapping (left) and nonoverlapping (right) subdomains for Optimized Schwarz Method. Image from the book of V. Dolean et al. [21].

2.3 Multidomain formulation using OSM

Let us present here the OSM for solving the direct problems (N_σ) and (D_σ) in the case of non-overlapping subdomains. To ensure uniqueness of the solution to problem (N_σ), we impose that

$$\int_\Sigma u \, ds = 0. \tag{2.2}$$

However, the advantage of using (2.2) is that it can be naturally encoded in the domain decomposition scheme introduced later (see Lemma 2.3.2).

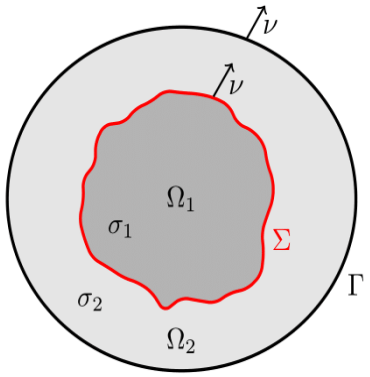

Figure 2.3: Outward normals for nonoverlapping subdomains Ω_1 and Ω_2 for OSM.

2.3.1 The case of the direct problem (N_σ)

Lemma 2.3.1. *Let $u_i := u_{|\Omega_i}$ be the restriction of u to Ω_i, $i = 1, 2$. Then, problem (N_σ) can be reformulated as an equivalent multidomain problem consisting of the following subdomain problems*

$$-\sigma_i \Delta u_i = 0 \quad \text{in } \Omega_i,$$
$$\sigma_2 \frac{\partial u_2}{\partial \nu} = \phi \quad \text{on } \Gamma,$$

together with the transmission conditions on the interface Σ,

$$u_1 = u_2 \quad \text{on } \Sigma,$$
$$\sigma_1 \frac{\partial u_1}{\partial \nu} = \sigma_2 \frac{\partial u_2}{\partial \nu} \quad \text{on } \Sigma.$$

Alternatively and equivalently, one may impose the Robin transmission conditions,

$$\sigma_i \frac{\partial u_i}{\partial \nu} \pm \alpha u_i = \sigma_j \frac{\partial u_j}{\partial \nu} \pm \alpha u_j \quad \text{on } \Sigma \text{ for all } i = 1, 2 \text{ and } j \neq i, \tag{2.3}$$

where $\alpha > 0$ is a fixed parameter that may be optimized to improve the convergence rate of the iterative domain decomposition method (see [48, 39, 40, 25, 21]). The resulting method is referred to as the Optimized Schwarz Method, which can be described as follows. Given arbitrary initial guesses $(u_i^0)_{1 \leq i \leq 2} \in \mathcal{H}^2(\Omega_i)$, we inductively build the sequences

$u_i^\ell \in \mathcal{H}^1(\Omega_i), i = 1, 2$, by solving (in parallel) for all $\ell \geq 0$

$$\begin{cases} -\sigma_i \Delta u_i^{\ell+1} & = 0 & \text{in } \Omega_i, \\ \sigma_2 \dfrac{\partial u_2^{\ell+1}}{\partial \nu} & = \phi & \text{on } \Gamma, \\ \sigma_1 \dfrac{\partial u_1^{\ell+1}}{\partial \nu} + \alpha u_1^{\ell+1} & = \sigma_2 \dfrac{\partial u_2^{\ell}}{\partial \nu} + \alpha u_2^{\ell} & \text{on } \Sigma, \\ \sigma_2 \dfrac{\partial u_2^{\ell+1}}{\partial \nu} - \alpha u_2^{\ell+1} & = \sigma_1 \dfrac{\partial u_1^{\ell}}{\partial \nu} - \alpha u_1^{\ell} & \text{on } \Sigma. \end{cases} \tag{2.4}$$

A direct use of (2.3) would require a numerical evaluation of the normal derivatives along the interfaces Σ in order to compute the right-hand sides in the transmission conditions of (2.4). This can be avoided by renaming the problematic quantities

$$\lambda_{i,N}^\ell := \sigma_j \frac{\partial u_j^\ell}{\partial \nu} \pm \alpha u_j^\ell \quad \text{respectively for } \ i = 1, 2 \text{ and } j = 1, 2, \ j \neq i. \tag{2.5}$$

where $\lambda_{i,N}^\ell$ is the information coming from the neighboring subdomain Ω_j $(j \neq i)$ at step ℓ of the algorithm. One can easily verify that

$$\begin{cases} \lambda_{1,N}^{\ell+1} = \sigma_2 \dfrac{\partial u_2^{\ell+1}}{\partial \nu} + \alpha u_2^{\ell+1} = \sigma_2 \dfrac{\partial u_2^{\ell+1}}{\partial \nu} - \alpha u_2^{\ell+1} + 2\alpha\, u_2^{\ell+1}, \\ \lambda_{2,N}^{\ell+1} = \sigma_1 \dfrac{\partial u_1^{\ell+1}}{\partial \nu} - \alpha u_1^{\ell+1} = \sigma_1 \dfrac{\partial u_1^{\ell+1}}{\partial \nu} + \alpha u_1^{\ell+1} - 2\alpha u_1^{\ell+1}. \end{cases}$$

Therefore, the parameters $\lambda_{i,N}^\ell$ satisfy the induction

$$\begin{cases} \lambda_{1,N}^{\ell+1} & = \lambda_{2,N}^{\ell} + 2\alpha\, u_2^{\ell+1}, \\ \lambda_{2,N}^{\ell+1} & = \lambda_{1,N}^{\ell} - 2\alpha\, u_1^{\ell+1}, \end{cases} \tag{2.6}$$

which can replace (2.5). We can now rewrite the iterative algorithm as follows. Given an

initial guess $(\lambda_{i,N}^0)_{1\leq i\leq 2} \in L^2(\Sigma)$ solve for each iteration $\ell \in \mathbb{N}$ the two following problems:

$$\begin{cases} -\sigma_i \Delta u_i^{\ell+1} & = 0 \qquad \text{in } \Omega_i, \\ \sigma_2 \dfrac{\partial u_2^{\ell+1}}{\partial \nu} & = \phi \qquad \text{on } \Gamma, \\ \sigma_1 \dfrac{\partial u_1^{\ell+1}}{\partial \nu} + \alpha u_1^{\ell+1} & = \lambda_{1,N}^{\ell} \quad \text{on } \Sigma, \\ \sigma_2 \dfrac{\partial u_2^{\ell+1}}{\partial \nu} - \alpha u_2^{\ell+1} & = \lambda_{2,N}^{\ell} \quad \text{on } \Sigma, \end{cases} \tag{2.7}$$

where the boundary values $\lambda_{i,N}^{\ell}$, $i = 1, 2$ are updated using (2.6). For the convergence analysis of this algorithm, we refer to [48, 28, 22]. Let us observe that condition (2.2) is ensured at convergence as soon as it is verified by the initial guess $(\lambda_{i,N}^0)_{1\leq i\leq 2}$. This is what we summarize in the following lemma.

Lemma 2.3.2. *Let $(\lambda_{i,N}^0)_{1\leq i\leq 2} \in L^2(\Sigma)$, such that $\int_\Sigma \lambda_{i,N}^0 \, ds = 0$; $i = 1, 2$, then for $\ell \in \mathbb{N}^*$, we have: $\int_\Sigma \lambda_{i,N}^{\ell} \, ds = 0$, and $\int_\Sigma u_i^{\ell} \, ds = 0$.*

Proof. We prove this Lemma by induction. By integrating equations (2.7) for $\ell = 0$ in Ω_i against a constant function in Ω_i we obtain

$$\begin{cases} \displaystyle\int_\Sigma u_1^1 \, ds = -\frac{1}{\alpha}\left[\int_\Sigma \lambda_{1,N}^0 \, ds\right] = 0, \\ \displaystyle\int_\Sigma u_2^1 \, ds = \frac{1}{\alpha}\left[-\int_\Sigma \lambda_{2,N}^0 \, ds + \int_\Gamma \phi \, ds\right] = 0, \end{cases}$$

which proves the statement for $\ell = 1$. Assume that

$$\int_\Sigma \lambda_{i,N}^{\ell} \, ds = \int_\Sigma u_i^{\ell} \, ds = 0, \text{ for } i = 1, 2.$$

By integrating equations (2.7) in Ω_i against a constant function in Ω_i we obtain

$$\begin{cases} \displaystyle\int_\Sigma u_1^{\ell+1} \, ds = -\frac{1}{\alpha}\left[\int_\Sigma \lambda_{1,N}^{\ell} \, ds\right] = 0, \\ \displaystyle\int_\Sigma u_2^{\ell+1} \, ds = \frac{1}{\alpha}\left[-\int_\Sigma \lambda_{2,N}^{\ell} \, ds + \int_\Gamma \phi \, ds\right] = 0, \end{cases}$$

and by using (2.6), we obtain

$$\int_\Sigma \lambda_{1,N}^{\ell+1} \, ds = \int_\Sigma \lambda_{2,N}^{\ell+1} \, ds = 0,$$

which prove the lemma.

□

The weak formulation of the relevant subdomain problems (2.7) is given by:

$$(V_{1,N})\begin{cases} \text{Find } u_1^{\ell+1} \in \mathcal{H}^1(\Omega_1) \text{ such that :} \\ \displaystyle\int_{\Omega_1} \sigma_1 \nabla u_1^{\ell+1}.\nabla v\, dx + \int_\Sigma \alpha u_1^{\ell+1} v\, ds = \int_\Sigma \lambda_{1,N}^{\ell}\, v\, ds \qquad \text{for all } v \in \mathcal{H}^1(\Omega_1). \end{cases}$$

$$(V_{2,N})\begin{cases} \text{Find } u_2^{\ell+1} \in \mathcal{H}^1(\Omega_2) \text{ such that :} \\ \displaystyle\int_{\Omega_2} \sigma_2 \nabla u_2^{\ell+1}.\nabla v\, dx + \int_\Sigma \alpha u_2^{\ell+1} v\, ds = -\int_\Sigma \lambda_{2,N}^{\ell}\, v\, ds + \int_\Gamma \phi\, v\, ds \quad \text{for all } v \in \mathcal{H}^1(\Omega_2). \end{cases}$$

2.3.2 The case of the Dirichlet problem (D_σ)

Similarly to above, we also apply the OSM for solving the Dirichlet problem (D_σ). Let $v_i := v_{|\Omega_i}$ be the restriction of v to Ω_i, $i = 1, 2$. Then problem (D_σ) can be reformulated as an equivalent multidomain problem consisting of the following subdomain problems

$$\begin{aligned} -\sigma_i \Delta v_i = 0 \quad &\text{in } \Omega_i, \\ v_2 = f \quad &\text{on } \Gamma, \end{aligned}$$

together with the Robin transmission conditions:

$$\sigma_i \frac{\partial v_i}{\partial \nu} \pm \alpha v_i = \sigma_j \frac{\partial v_j}{\partial \nu} \pm \alpha v_j \quad \text{on } \Sigma \ \text{ for all } i = 1, 2 \text{ and } j \neq i. \tag{2.8}$$

The OSM for this problem can be then formulated as: Given an initial guess $(\lambda_{i,D}^0)_{1\leq i\leq 2} \in L^2(\Sigma)$ solve for each iteration $\ell \in \mathbb{N}$ the two following problems:

$$\begin{cases} -\sigma_i \Delta v_i^{\ell+1} = 0 & \text{in } \Omega_i, \\ v_2^{\ell+1} = f & \text{on } \Gamma, \\ \sigma_1 \dfrac{\partial v_1^{\ell+1}}{\partial \nu} + \alpha v_1^{\ell+1} = \lambda_{1,D}^{\ell} & \text{on } \Sigma, \\ \sigma_2 \dfrac{\partial v_2^{\ell+1}}{\partial \nu} - \alpha v_2^{\ell+1} = \lambda_{2,D}^{\ell} & \text{on } \Sigma, \end{cases} \tag{2.9}$$

where the parameters $\lambda_{i,D}^{\ell+1}$, $i = 1, 2$, verify the induction

$$\left\{ \begin{array}{rcl} \lambda_{1,D}^{\ell+1} & = & \lambda_{2,D}^{\ell} + 2\alpha\ v_2^{\ell+1}, \\ \lambda_{2,D}^{\ell+1} & = & \lambda_{1,D}^{\ell} - 2\alpha\ v_1^{\ell+1}. \end{array} \right. \tag{2.10}$$

Let $K = \{w \in \mathcal{H}^1(\Omega_2)/w_{|\Gamma} = f\}$ and $K_0 = \{w \in \mathcal{H}^1(\Omega_2)/w_{|\Gamma} = 0\}$, then, the weak formulation of the relevant subdomain problems is given by:

$$(V_{1,D}) \left\{ \begin{array}{l} \text{Find } v_1^{\ell+1} \in \mathcal{H}^1(\Omega_1), \text{ such that :} \\ \displaystyle\int_{\Omega_1} \sigma_1 \nabla v_1^{\ell+1}.\nabla w\ dx + \int_{\Sigma} \alpha v_1^{\ell+1} w\ ds = \int_{\Sigma} \lambda_{1,D}^{\ell}\ w\ ds \qquad \forall\ w \in \mathcal{H}^1(\Omega_1). \end{array} \right.$$

$$(V_{2,D}) \left\{ \begin{array}{l} \text{Find } v_2^{\ell+1} \in K, \text{ such that :} \\ \displaystyle\int_{\Omega_2} \sigma_2 \nabla v_2^{\ell+1}.\nabla w\ dx + \int_{\Sigma} \alpha v_2^{\ell+1}\ w\ ds = -\int_{\Sigma} \lambda_{2,D}^{\ell}\ w\ ds \qquad \forall\ w \in K_0. \end{array} \right.$$

2.4 Convergence rate for OSM in some particular domains

As a second step in the analysis of the combined inverse scheme introduced in Chapter 3, we study the convergence rate of the OSM in some simplified cases of the domain Ω. We begin with the one dimensional case.

2.4.1 The one dimensional case

We consider the particular case where the domain $\Omega =]0, 1[$, $\Omega_1 =]0, \delta[$ and $\Omega_2 =]\delta, 1[$ where δ denotes the discontinuity point separating the two subdomains Ω_1 and Ω_2. Let $(\phi, f) \in \mathbb{R}^* \times \mathbb{R}$, we will consider the following model problems:

$$(\widehat{N}_\sigma) \left\{ \begin{array}{ll} -(\sigma u')' = 0 & \text{in }]0, 1[, \\ u(0) = 0, & \\ \sigma_2 u'(1) = \phi. & \end{array} \right. \quad ; \quad (\widehat{D}_\sigma) \left\{ \begin{array}{ll} -(\sigma v')' = 0 & \text{in }]0, 1[, \\ v(0) = 0, & \\ v(1) = f. & \end{array} \right.$$

The OSM for the Neumann problem $(\widehat{N_\sigma})$ can be then formulated as: Given an initial guess $(\lambda_{i,N}^0)_{1\leq i\leq 2}$ solve for each iteration $\ell \in \mathbb{N}$ the two following problems:

$$\begin{cases} -\sigma_i (u_i^{\ell+1})'' & = 0 \qquad \text{in } \Omega_i, i=1,2, \\ u_1^{\ell+1}(0) & = 0, \\ \sigma_2 (u_2^{\ell+1})'(1) & = \phi, \\ \sigma_1 (u_1^{\ell+1})'(\delta) + \alpha u_1^{\ell+1}(\delta) & = \lambda_{1,N}^{\ell}(\delta), \\ \sigma_2 (u_2^{\ell+1})'(\delta) - \alpha u_2^{\ell+1}(\delta) & = \lambda_{2,N}^{\ell}(\delta), \end{cases} \tag{2.11}$$

where the parameters $\lambda_{i,N}^{\ell+1}(\delta)$, $i=1,2$, verify the induction

$$\begin{cases} \lambda_{1,N}^{\ell+1}(\delta) & = \lambda_{2,N}^{\ell}(\delta) + 2\alpha\ u_2^{\ell+1}(\delta), \\ \lambda_{2,N}^{\ell+1}(\delta) & = \lambda_{1,N}^{\ell}(\delta) - 2\alpha\ u_1^{\ell+1}(\delta). \end{cases} \tag{2.12}$$

Similarly to above, the OSM for the Dirichlet problem $(\widehat{D_\sigma})$ can be then formulated as: Given an initial guess $(\lambda_{i,D}^0)_{1\leq i\leq 2}$ solve for each iteration $\ell \in \mathbb{N}$ the two following problems:

$$\begin{cases} -\sigma_i (v_i^{\ell+1})'' & = 0 \qquad \text{in } \Omega_i, i=1,2, \\ v_1^{\ell+1}(0) & = 0, \\ v_2^{\ell+1}(1) & = f, \\ \sigma_1 (v_1^{\ell+1})'(\delta) + \alpha v_1^{\ell+1}(\delta) & = \lambda_{1,D}^{\ell}(\delta), \\ \sigma_2 (v_2^{\ell+1})'(\delta) - \alpha v_2^{\ell+1}(\delta) & = \lambda_{2,D}^{\ell}(\delta), \end{cases} \tag{2.13}$$

where the parameters $\lambda_{i,D}^{\ell+1}(\delta)$, $i=1,2$, verify the induction

$$\begin{cases} \lambda_{1,D}^{\ell+1}(\delta) & = \lambda_{2,D}^{\ell}(\delta) + 2\alpha\ v_2^{\ell+1}(\delta), \\ \lambda_{2,D}^{\ell+1}(\delta) & = \lambda_{1,D}^{\ell}(\delta) - 2\alpha\ v_1^{\ell+1}(\delta). \end{cases} \tag{2.14}$$

In the sequel, we set

$$k^\alpha(\delta) := \frac{\sigma_1 - \alpha\delta}{\sigma_1 + \alpha\delta}, \tag{2.15}$$

$$p^\alpha(\delta) := -1. \tag{2.16}$$

$$q^{\alpha}(\delta) := \frac{\sigma_2 - \alpha(1-\delta)}{\sigma_2 + \alpha(1-\delta)}. \tag{2.17}$$

Then, we have the following two propositions:

Proposition 2.4.1. *For $\phi \in \mathbb{R}^*$, the OSM (2.11)-(2.12), initialized with $\lambda_{i,N}^0 = 0$, $i = 1, 2$, geometrically converges for all $\alpha > 0$ and the convergence rate is given by the spectral radius*

$$\rho^{\alpha}(\delta) := \sqrt{|\ k^{\alpha}(\delta) p^{\alpha}(\delta)\ |} < 1.$$

Proof. The solutions of the problem (2.11) can be written as:

$$u^{\ell+1}(x) = \begin{cases} u_1^{\ell+1}(x) = \alpha_N^{\ell+1} x & \text{in } \Omega_1, \\ u_2^{\ell+1}(x) = \beta_N^{\ell+1} x + \gamma_N^{\ell+1} & \text{in } \Omega_2, \end{cases}$$

where the constants $\alpha_N^{\ell+1}$, $\beta_N^{\ell+1}$ and $\gamma_N^{\ell+1}$ are determined by the following equations:

$$\begin{cases} \sigma_2 (u_2^{\ell+1})'(1) & = \phi, \\ \sigma_1 (u_1^{\ell+1})'(\delta) + \alpha u_1^{\ell+1}(\delta) & = \lambda_{1,N}^{\ell}(\delta), \\ \sigma_2 (u_2^{\ell+1})'(\delta) - \alpha u_2^{\ell+1}(\delta) & = \lambda_{2,N}^{\ell}(\delta). \end{cases} \tag{2.18}$$

From the second equation of (2.18), we obtain:

$$u_1^{\ell+1}(x) = \frac{\lambda_{1,N}^{\ell}}{(\sigma_1 + \alpha\delta)} x \tag{2.19}$$

and from the first and the third equations of (2.18), we obtain:

$$u_2^{\ell+1}(x) = \frac{\phi}{\sigma_2}(x - \delta) + \frac{\phi - \lambda_{2,N}^{\ell}}{\alpha}.$$

From the second equation of (2.12), we obtain:

$$\lambda_{2,N}^{\ell+1} = k^{\alpha}(\delta)\ \lambda_{1,N}^{\ell}.$$

In the same way we get:

$$\lambda_{1,N}^{\ell+1} = p^{\alpha}(\delta)\ \lambda_{2,N}^{\ell} + \eta^{\alpha}(\delta),$$

where

$$\eta^{\alpha}(\delta) := 2\phi. \tag{2.20}$$

Therefore, the DDM iterations can be written as:

$$\begin{pmatrix} \lambda_{1,N}^{\ell+1} \\ \\ \lambda_{2,N}^{\ell+1} \end{pmatrix} = \begin{pmatrix} 0 & p^{\alpha}(\delta) \\ \\ k^{\alpha}(\delta) & 0 \end{pmatrix} \begin{pmatrix} \lambda_{1,N}^{\ell} \\ \\ \lambda_{2,N}^{\ell} \end{pmatrix} + \begin{pmatrix} \eta^{\alpha}(\delta) \\ \\ 0 \end{pmatrix}. \tag{2.21}$$

Then, this induction converges if and only if $\rho^{\alpha}(\delta) = \sqrt{\mid k^{\alpha}(\delta)p^{\alpha}(\delta) \mid} < 1$, which is always true for every $\alpha > 0$ and $\delta \in]0,1[$. □

Proposition 2.4.2. *For $f \in \mathbb{R}^*$, the OSM* (2.13)-(2.14)*, geometrically converges for all $\alpha > 0$ and the convergence rate is given by the spectral radius*

$$\hat{\rho}^{\alpha}(\delta) := \sqrt{\mid k^{\alpha}(\delta)q^{\alpha}(\delta) \mid} < 1.$$

Proof. The solutions of the problem (2.13) can be written as:

$$v^{\ell+1}(x) = \begin{cases} v_1^{\ell+1}(x) = \alpha_D^{\ell+1} x & \text{in } \Omega_1, \\ v_2^{\ell+1}(x) = \beta_D^{\ell+1} x + \gamma_D^{\ell+1} & \text{in } \Omega_2, \end{cases}$$

where the constants $\alpha_D^{\ell+1}$, $\beta_D^{\ell+1}$ and $\gamma_D^{\ell+1}$ are determined by the following equations:

$$\begin{cases} v_2^{\ell+1}(1) & = f, \\ \sigma_1 (v_1^{\ell+1})'(\delta) + \alpha v_1^{\ell+1}(\delta) & = \lambda_{1,D}^{\ell}(\delta), \\ \sigma_2 (v_2^{\ell+1})'(\delta) - \alpha v_2^{\ell+1}(\delta) & = \lambda_{2,D}^{\ell}(\delta). \end{cases} \tag{2.22}$$

From the second equation of (2.22), we obtain:

$$v_1^{\ell+1}(x) = \frac{\lambda_{1,D}^{\ell}}{(\sigma_1 + \alpha\delta)} x \tag{2.23}$$

and from the first and the third equations of (2.22), we obtain:

$$v_2^{\ell+1}(x) = \frac{\lambda_{2,D}^{\ell} + \alpha f}{\sigma_2 + \alpha(1-\delta)}(x-1) + f.$$

From the second equation of (2.14), we obtain:

$$\lambda_{2,D}^{\ell+1} = k^{\alpha}(\delta)\ \lambda_{1,D}^{\ell}.$$

In the same way we get:

$$\lambda_{1,D}^{\ell+1} = q^{\alpha}(\delta)\ \lambda_{2,D}^{\ell} + \omega^{\alpha}(\delta),$$

where

$$\omega^{\alpha}(\delta) := \frac{2\alpha\sigma_2 f}{\sigma_2 + \alpha(1-\delta)}. \tag{2.24}$$

Therefore, the DDM iterations can be written as:

$$\begin{pmatrix} \lambda_{1,D}^{\ell+1} \\ \\ \lambda_{2,D}^{\ell+1} \end{pmatrix} = \begin{pmatrix} 0 & q^{\alpha}(\delta) \\ \\ k^{\alpha}(\delta) & 0 \end{pmatrix} \begin{pmatrix} \lambda_{1,D}^{\ell} \\ \\ \lambda_{2,D}^{\ell} \end{pmatrix} + \begin{pmatrix} \omega^{\alpha}(\delta) \\ \\ 0 \end{pmatrix}. \tag{2.25}$$

This induction converges if and only if $\hat{\rho}^{\alpha}(\delta) = \sqrt{\mid k^{\alpha}(\delta) q^{\alpha}(\delta) \mid} < 1$, which is always true for $\alpha > 0$ and $0 < \delta < 1$.

□

Remark 2.4.3. *Equations* (2.15) *and* (2.17) *deserve a few remarks.*

1. *For* $\alpha = \dfrac{\sigma_1}{\delta}$, *the DDM iterations matrix of* (2.21) *is nilpotent and therefore the method converges in maximum* 2 *iterations.*
2. *For* $\alpha = \dfrac{\sigma_1}{\delta}$ *or* $\alpha = \dfrac{\sigma_2}{1-\delta}$, *the DDM iterations matrix of* (2.25) *is nilpotent and therefore the method converges in maximum* 2 *iterations.*

2.4.2 The case of an annulus

We study in this part the convergence rate of OSM in the particular case where the domain Ω is an annulus given by

$$\Omega = \{(x, y) \in \mathbb{R}^2, \text{ such that } R_1^2 < x^2 + y^2 < R_2^2\},$$

and where the subdomains Ω_1 and Ω_2 are defined by:

$$\Omega_1 = \{(x, y) \in \mathbb{R}^2, \text{ such that } R_1^2 < x^2 + y^2 < R^2\},$$

$$\Omega_2 = \{(x, y) \in \mathbb{R}^2, \text{ such that } R^2 < x^2 + y^2 < R_2^2\},$$

let Γ_1 and Γ_2 respectively the interior and exterior boundary of Ω and $\Gamma := \partial\Omega = \Gamma_1 \cup \Gamma_2$(see Figure 1.3 for an illustration). In this case the interface $\Sigma = \Sigma_R$ coincides with the circle of

center $(0,0)$ and radius R. Let $(\phi, f) \in \mathbb{R}^* \times \mathbb{R}$ and $(\widetilde{N}_\sigma)$, $(\widetilde{D}_\sigma)$ the two following problems

$$(\widetilde{N}_\sigma)\begin{cases} -div(\sigma\nabla u) = 0 & \text{in } \Omega, \\ u = 0 & \text{on } \Gamma_1, \\ \sigma\dfrac{\partial u}{\partial \nu} = \phi & \text{on } \Gamma_2. \end{cases} \quad ; \quad (\widetilde{D}_\sigma)\begin{cases} -div(\sigma\nabla v) = 0 & \text{in } \Omega, \\ v = 0 & \text{on } \Gamma_1, \\ v = f & \text{on } \Gamma_2. \end{cases}$$

The OSM for the Neumann problem $(\widetilde{N}_\sigma)$ can be then formulated as: Given an initial guess $(\lambda^0_{i,N})_{1\leq i\leq 2} \in L^2(\Sigma)$, solve for each iteration $\ell \in \mathbb{N}$ the two following problems:

$$\begin{cases} -\sigma_i \Delta u_i^{\ell+1} & = 0 & \text{in } \Omega_i, i = 1,2, \\ u_1^{\ell+1} & = 0 & \text{on } \Gamma_1, \\ \sigma_2 \dfrac{u_2^{\ell+1}}{\partial \nu} & = \phi & \text{on } \Gamma_2, \\ \sigma_1 \dfrac{\partial u_1^{\ell+1}}{\partial \nu} + \alpha u_1^{\ell+1} & = \lambda^\ell_{1,N} & \text{on } \Sigma, \\ \sigma_2 \dfrac{\partial u_2^{\ell+1}}{\partial \nu} - \alpha u_2^{\ell+1} & = \lambda^\ell_{2,N} & \text{on } \Sigma, \end{cases} \tag{2.26}$$

where the parameters $\lambda^{\ell+1}_{i,N}$, $i = 1,2$, verify the induction

$$\begin{cases} \lambda^{\ell+1}_{1,N} & = & \lambda^\ell_{2,N} + 2\alpha\, u_2^{\ell+1}, \\ \lambda^{\ell+1}_{2,N} & = & \lambda^\ell_{1,N} - 2\alpha\, u_1^{\ell+1}. \end{cases} \tag{2.27}$$

Similarly to above, the OSM for the Dirichlet problem $(\widetilde{D}_\sigma)$ can be then formulated as: Given an initial guess $(\lambda^0_{i,D})_{1\leq i\leq 2} \in L^2(\Sigma)$, solve for each iteration $\ell \in \mathbb{N}$ the two following problems:

$$\begin{cases} -\sigma_i \Delta v_i^{\ell+1} & = 0 & \text{in } \Omega_i, i = 1,2, \\ v_1^{\ell+1} & = 0 & \text{on } \Gamma_1, \\ v_2^{\ell+1} & = f & \text{on } \Gamma_2, \\ \sigma_1 \dfrac{\partial v_1^{\ell+1}}{\partial \nu} + \alpha v_1^{\ell+1} & = \lambda^\ell_{1,D} & \text{on } \Sigma, \\ \sigma_2 \dfrac{\partial v_2^{\ell+1}}{\partial \nu} - \alpha v_2^{\ell+1} & = \lambda^\ell_{2,D} & \text{on } \Sigma, \end{cases} \tag{2.28}$$

where the parameters $\lambda_{i,D}^{\ell+1}$, $i = 1, 2$, verify the induction

$$\left\{ \begin{array}{rcl} \lambda_{1,D}^{\ell+1} & = & \lambda_{2,D}^{\ell} + 2\alpha\, v_2^{\ell+1}, \\ \lambda_{2,D}^{\ell+1} & = & \lambda_{1,D}^{\ell} - 2\alpha\, v_1^{\ell+1}. \end{array} \right. \tag{2.29}$$

In the sequel, we set

$$k^{\alpha}(R) := \frac{\sigma_1 - \alpha R \log\left(\frac{R}{R_1}\right)}{\sigma_1 + \alpha R \log\left(\frac{R}{R_1}\right)}, \tag{2.30}$$

$$p^{\alpha}(R) := -1, \tag{2.31}$$

$$q^{\alpha}(R) := \frac{\sigma_2 - \alpha R \log\left(\frac{R_2}{R}\right)}{\sigma_2 + \alpha R \log\left(\frac{R_2}{R}\right)}. \tag{2.32}$$

Then, we have the following two propositions:

Proposition 2.4.4. *For $\phi \in \mathbb{R}^*$, the OSM (2.26)-(2.27), initialized with $\lambda_{i,N}^0 = 0$, $i = 1, 2$, geometrically converges for all $\alpha > 0$ and the convergence rate is given by the spectral radius*

$$\rho^{\alpha}(R) := \sqrt{\mid k^{\alpha}(R) p^{\alpha}(R) \mid} < 1.$$

Proof. The solutions of the problem (2.26) can be written as:

$$u^{\ell+1}(r,\theta) = \left\{ \begin{array}{ll} u_1^{\ell+1}(r,\theta) = \alpha_N^{\ell+1} \log\left(\frac{r}{R_1}\right) & \text{in } \Omega_1, \\ u_2^{\ell+1}(r,\theta) = \beta_N^{\ell+1} \log\left(\frac{r}{R_1}\right) + \gamma_N^{\ell+1} & \text{in } \Omega_2, \end{array} \right.$$

where the constants $\alpha_N^{\ell+1}$, $\beta_N^{\ell+1}$ and $\gamma_N^{\ell+1}$ are determined by the following equations:

$$\left\{ \begin{array}{lll} \sigma_2 \dfrac{u_2^{\ell+1}}{\partial \nu} & = \phi & \text{on } \Gamma_2, \\ \sigma_1 \dfrac{\partial u_1^{\ell+1}}{\partial \nu} + \alpha u_1^{\ell+1} & = \lambda_{1,N}^{\ell} & \text{on } \Sigma, \\ \sigma_2 \dfrac{\partial u_2^{\ell+1}}{\partial \nu} - \alpha u_2^{\ell+1} & = \lambda_{2,N}^{\ell} & \text{on } \Sigma. \end{array} \right. \tag{2.33}$$

From the second equation of (2.33), we obtain:

$$u_1^{\ell+1}(r,\theta) = \frac{R\lambda_{1,N}^{\ell}}{\left(\sigma_1 + \alpha R \log\left(\frac{R}{R_1}\right)\right)} \log\left(\frac{r}{R_1}\right), \tag{2.34}$$

and from the first and the third equations of (2.33), we obtain:

$$u_2^{\ell+1}(r,\theta) = \frac{R_2\phi}{\sigma_2} \log\left(\frac{r}{R_1}\right) + \frac{R_2\phi}{\alpha\sigma_2 R}\left(\sigma_2 - \alpha R \log\left(\frac{R}{R_1}\right)\right) - \frac{\lambda_{2,N}^{\ell}}{\alpha}.$$

From the second equation of (2.12), we obtain:

$$\lambda_{2,N}^{\ell+1} = k^{\alpha}(R)\ \lambda_{1,N}^{\ell}.$$

In the same way we get:

$$\lambda_{1,N}^{\ell+1} = p^{\alpha}(R)\ \lambda_{2,N}^{\ell} + \eta^{\alpha}(R),$$

where

$$\eta^{\alpha}(R) := 2\phi\frac{R_2}{R}. \tag{2.35}$$

Therefore, the DDM iterations can be written as:

$$\begin{pmatrix} \lambda_{1,N}^{\ell+1} \\ \\ \lambda_{2,N}^{\ell+1} \end{pmatrix} = \begin{pmatrix} 0 & p^{\alpha}(R) \\ \\ k^{\alpha}(R) & 0 \end{pmatrix} \begin{pmatrix} \lambda_{1,N}^{\ell} \\ \\ \lambda_{2,N}^{\ell} \end{pmatrix} + \begin{pmatrix} \eta^{\alpha}(R) \\ \\ 0 \end{pmatrix}. \tag{2.36}$$

This induction converges if and only if $\rho^{\alpha}(R) = \sqrt{\mid k^{\alpha}(R)p^{\alpha}(R) \mid} < 1$, which is always true for $\alpha > 0$ and $R_1 < R < R_2$.

□

Proposition 2.4.5. *For $f \in \mathbb{R}^*$, the OSM (2.28)-(2.29), initialized with $\lambda_{i,D}^0 = 0$, $i = 1, 2$, geometrically converges for all $\alpha > 0$ and the convergence rate is given by the spectral radius*

$$\hat{\rho}^{\alpha}(R) := \sqrt{\mid k^{\alpha}(R)q^{\alpha}(R) \mid} < 1.$$

Proof. The solutions of the problem (2.28) can be written as:

$$v^{\ell+1}(r,\theta) = \begin{cases} v_1^{\ell+1}(r,\theta) = \alpha_D^{\ell+1} \log\left(\dfrac{r}{R_1}\right) & \text{in } \Omega_1, \\ v_2^{\ell+1}(r,\theta) = \beta_D^{\ell+1} \log\left(\dfrac{r}{R_2}\right) + \gamma_D^{\ell+1} & \text{in } \Omega_2, \end{cases}$$

where the constants $\alpha_D^{\ell+1}$, $\beta_D^{\ell+1}$ and $\gamma_D^{\ell+1}$ are determined by the following equations:

$$\begin{cases} v_2^{\ell+1} & = f & \text{on } \Gamma_2, \\ \sigma_1 \dfrac{\partial v_1^{\ell+1}}{\partial \nu} + \alpha v_1^{\ell+1} & = \lambda_{1,D}^{\ell} & \text{on } \Sigma, \\ \sigma_2 \dfrac{\partial v_2^{\ell+1}}{\partial \nu} - \alpha v_2^{\ell+1} & = \lambda_{2,D}^{\ell} & \text{on } \Sigma. \end{cases} \tag{2.37}$$

From the second equation of (2.37), we obtain:

$$v_1^{\ell+1}(r,\theta) = \frac{R\lambda_{1,D}^{\ell}}{\left(\sigma_1 + \alpha R \log\left(\dfrac{R}{R_1}\right)\right)} \log\left(\frac{r}{R_1}\right), \tag{2.38}$$

and from the first and the third equations of (2.37), we obtain:

$$v_2^{\ell+1}(r,\theta) = \frac{\alpha R f + R\lambda_{2,D}^{\ell}}{\sigma_2 - \alpha R \log\left(\dfrac{R}{R_2}\right)} \log\left(\frac{r}{R_2}\right) + f.$$

From the second equation of (2.29), we obtain:

$$\lambda_{2,D}^{\ell+1} = k^{\alpha}(R)\ \lambda_{1,D}^{\ell}.$$

In the same way we get:

$$\lambda_{1,D}^{\ell+1} = q^{\alpha}(R)\ \lambda_{2,D}^{\ell} + \omega^{\alpha}(R),$$

where

$$\omega^{\alpha}(R) := \frac{2\alpha\ \sigma_2\ f}{\sigma_2 + \alpha R \log\left(\dfrac{R_2}{R}\right)}. \tag{2.39}$$

Therefore, the DDM iterations can be written as:

$$\begin{pmatrix} \lambda_{1,D}^{\ell+1} \\ \\ \lambda_{2,D}^{\ell+1} \end{pmatrix} = \begin{pmatrix} 0 & q^{\alpha}(R) \\ \\ k^{\alpha}(R) & 0 \end{pmatrix} \begin{pmatrix} \lambda_{1,D}^{\ell} \\ \\ \lambda_{2,D}^{\ell} \end{pmatrix} + \begin{pmatrix} \omega^{\alpha}(R) \\ \\ 0 \end{pmatrix}. \tag{2.40}$$

This induction converges if and only if $\hat{\rho}^{\alpha}(R) = \sqrt{\mid k^{\alpha}(R)q^{\alpha}(R) \mid} < 1$, which is always true for $\alpha > 0$ and $R_1 < R < R_2$.

□

Remark 2.4.6. *Equations* (2.30) *and* (2.32) *deserve a few remarks.*

1. *For* $\alpha = \dfrac{\sigma_1}{R\log\left(\dfrac{R}{R_1}\right)}$, *the DDM iterations matrix of* (2.36) *is nilpotent and therefore the method converges in maximum* 2 *iterations.*
2. *For* $\alpha = \dfrac{\sigma_1}{R\log\left(\dfrac{R}{R_1}\right)}$ *or* $\alpha = \dfrac{\sigma_2}{R\log\left(\dfrac{R_2}{R}\right)}$, *the DDM iterations matrix of* (2.40) *is nilpotent and therefore the method converges in maximum* 2 *iterations.*

2.4.3 The case of an open disk

We consider in this part the case where the domain Ω_1 is the open disk of center $(0,0)$ and radius $R > 0$ of $\mathbb{R}^2$ and Ω_2 is the annulus domain $R < |x| < R_2$ (see Figure 1.4 for an illustration). The interface Σ coincides with the circle of center $(0,0)$ and radius R. We set for $m > 0$,

$$k_m^{\alpha}(R) := \frac{\sigma_1 m - \alpha R}{\sigma_1 m + \alpha R}, \tag{2.41}$$

$$p_m^{\alpha}(R) := \frac{\sigma_2 m(R_2^{2m} - R^{2m}) - \alpha R(R_2^{2m} + R^{2m})}{\sigma_2 m(R_2^{2m} - R^{2m}) + \alpha R(R_2^{2m} + R^{2m})}. \tag{2.42}$$

$$q_m^{\alpha}(R) := \frac{\sigma_2 m(R_2^{2m} + R^{2m}) - \alpha R(R_2^{2m} - R^{2m})}{\sigma_2 m(R_2^{2m} + R^{2m}) + \alpha R(R_2^{2m} - R^{2m})}. \tag{2.43}$$

Then, we have the two following propositions:

Proposition 2.4.7. *For* $\phi(\theta) = m\cos(m\theta)$ *or* $\phi(\theta) = m\sin(m\theta)$, $\theta \in [0, 2\pi]$ *and* $m \in \mathbb{N}^*$, *the OSM* (2.6)-(2.7), *initialized with* $\lambda_{i,N}^0 = 0$, $i = 1, 2$, *geometrically converges for all* $\alpha > 0$

and the convergence rate is given by the spectral radius

$$\rho_m^\alpha(R) := \sqrt{\mid k_m^\alpha(R) p_m^\alpha(R) \mid} < 1. \tag{2.44}$$

Proof. For $\phi(\theta) = m\cos(m\theta)$ or $\phi(\theta) = m\sin(m\theta)$, $\theta \in [0, 2\pi]$ and $m \in \mathbb{N}^*$, the solutions of the problem (2.7) can be written as:

$$u^{\ell+1}(r,\theta) = \begin{cases} u_1^{\ell+1}(r,\theta) = \alpha_N^{\ell+1}\, r^m \dfrac{\phi(\theta)}{m} & \text{in } \Omega_1, \\ u_2^{\ell+1}(r,\theta) = \left(\beta_N^{\ell+1}\, r^m + \dfrac{\gamma_N^{\ell+1}}{r^m}\right) \dfrac{\phi(\theta)}{m} & \text{in } \Omega_2, \end{cases}$$

where the constants $\alpha_N^{\ell+1}$, $\beta_N^{\ell+1}$ and $\gamma_N^{\ell+1}$ are determined by the following equations:

$$\begin{cases} \sigma_2 \dfrac{\partial u_2^{\ell+1}}{\partial \nu} & = \phi(\theta) \quad \text{on } \Gamma, \\ \sigma_1 \dfrac{\partial u_1^{\ell+1}}{\partial \nu} + \alpha u_1^{\ell+1} & = \lambda_{1,N}^\ell \quad \text{on } \Sigma, \\ \sigma_2 \dfrac{\partial u_2^{\ell+1}}{\partial \nu} - \alpha u_2^{\ell+1} & = \lambda_{2,N}^\ell \quad \text{on } \Sigma. \end{cases} \tag{2.45}$$

For $i = 1, 2$, we denote by $\hat{\lambda}_{i,N}^\ell = \lambda_{i,N}^\ell \dfrac{m}{\phi(\theta)}$. Then, from the second equation of (2.45), we obtain:

$$u_1^{\ell+1}(r,\theta) = \frac{\hat{\lambda}_{1,N}^\ell}{R^{m-1}(m\sigma_1 + \alpha R)} r^m \frac{\phi(\theta)}{m}, \tag{2.46}$$

and from the first and the third equations of (2.45), we obtain:

$$u_2^{\ell+1}(r,\theta) = \left[\frac{R_2^{m+1} R^{m+1} \left((\sigma_2 m - \alpha R) R^{m-1} - \sigma_2 \hat{\lambda}_{2,N}^\ell R_2^{m-1} \right)}{\sigma_2 \left(\sigma_2 m (R_2^{2m} - R^{2m}) + \alpha R (R_2^{2m} + R^{2m}) \right)} \left(\frac{r^m}{R_2^{2m}} + \frac{1}{r^m} \right) + \frac{r^m}{\sigma_2 R_2^{m-1}} \right] \frac{\phi(\theta)}{m}.$$

From (2.6) and using the fact that $\lambda_{i,N}^{\ell+1} = \hat{\lambda}_{i,N}^{\ell+1} \dfrac{\phi(\theta)}{m}$, we obtain:

$$\hat{\lambda}_{2,N}^{\ell+1} = k_m^\alpha(R)\ \hat{\lambda}_{1,N}^\ell.$$

In the same way we get:

$$\hat{\lambda}_{1,N}^{\ell+1} = p_m^\alpha(R)\ \hat{\lambda}_{2,N}^\ell + \eta_m^\alpha(R),$$

where

$$\eta_m^\alpha(R) := \frac{4m\alpha R^m R_2^{m+1}}{\sigma_2 m(R_2^{2m} - R^{2m}) + \alpha R(R_2^{2m} + R^{2m})}. \tag{2.47}$$

Therefore, the DDM iterations can be written as:

$$\begin{pmatrix} \hat{\lambda}_{1,N}^{\ell+1} \\ \\ \hat{\lambda}_{2,N}^{\ell+1} \end{pmatrix} = \begin{pmatrix} 0 & p_m^\alpha(R) \\ \\ k_m^\alpha(R) & 0 \end{pmatrix} \begin{pmatrix} \hat{\lambda}_{1,N}^{\ell} \\ \\ \hat{\lambda}_{2,N}^{\ell} \end{pmatrix} + \begin{pmatrix} \eta_m^\alpha(R) \\ \\ 0 \end{pmatrix}. \tag{2.48}$$

This induction converges if and only if $\rho_m^\alpha(R) = \sqrt{\mid k_m^\alpha(R) p_m^\alpha(R) \mid} < 1$, which is always true for $\alpha > 0$, $m > 0$ and $0 < R < R_2$.

□

We can state and prove similar convergence results as in Proposition 2.4.7.

Proposition 2.4.8. *For $f(\theta) = C_f \dfrac{\phi(\theta)}{m}$, $C_f \in \mathbb{R}$, $m \in \mathbb{N}^*$, the OSM (2.9)-(2.10) geometrically converges for all $\alpha > 0$ and the convergence rate is given by the spectral radius*

$$\hat{\rho}_m^\alpha(R) = \sqrt{\mid k_m^\alpha(R) q_m^\alpha(R) \mid} < 1. \tag{2.49}$$

Proof. For $f(\theta) = C_f \dfrac{\phi(\theta)}{m}$, $C_f \in \mathbb{R}$, the approximate solutions of the problem (2.9) can be written as:

$$v^{\ell+1}(r,\theta) = \begin{cases} v_1^{\ell+1}(r,\theta) = \alpha_D^{\ell+1}\, r^m \dfrac{\phi(\theta)}{m} & \text{in } \Omega_1, \\ v_2^{\ell+1}(r,\theta) = \left(\beta_D^{\ell+1}\, r^m + \dfrac{\gamma_D^{\ell+1}}{r^m}\right) \dfrac{\phi(\theta)}{m} & \text{in } \Omega_2. \end{cases}$$

where the constants $\alpha_D^{\ell+1}$, $\beta_D^{\ell+1}$ and $\gamma_D^{\ell+1}$ are calculated by the following equations:

$$\begin{cases} v_2^{\ell+1} = f(\theta) & \text{on } \Gamma, \\ \sigma_1 \dfrac{\partial v_1^{\ell+1}}{\partial \nu} + \alpha v_1^{\ell+1} = \lambda_{1,D}^{\ell} & \text{on } \Sigma, \\ \sigma_2 \dfrac{\partial v_2^{\ell+1}}{\partial \nu} - \alpha v_2^{\ell+1} = \lambda_{2,D}^{\ell} & \text{on } \Sigma. \end{cases} \tag{2.50}$$

For $i = 1, 2$, we denote by $\hat{\lambda}_{i,D}^{\ell} = \lambda_{i,D}^{\ell} \dfrac{m}{\phi(\theta)}$. Then, from the second equation of (2.50), we obtain:

$$v_1^{\ell+1}(r,\theta) = \frac{\hat{\lambda}_{1,D}^{\ell}}{R^{m-1}(m\sigma_1 + \alpha R)} r^m \frac{\phi(\theta)}{m}, \tag{2.51}$$

and from the first and the third equation of (2.50), we get

$$v_2^{\ell+1}(r,\theta) = \left[\frac{R_2^m R^{m+1}\left((\sigma_2 m - \alpha R)C_f R^{m-1} - \hat{\lambda}_{2,D}^{\ell} R_2^m\right)}{\sigma_2 m(R_2^{2m}+R^{2m}) + \alpha R(R_2^{2m}-R^{2m})}\left(\frac{1}{r^m} - \frac{r^m}{R_2^{2m}}\right) + \frac{C_f}{R_2^m} r^m\right]\frac{\phi(\theta)}{m}.$$

From (2.10) and using the fact that $\lambda_{i,D}^{\ell+1} = \hat{\lambda}_{i,D}^{\ell+1}\dfrac{\phi(\theta)}{m}$, we obtain

$$\hat{\lambda}_{2,D}^{\ell+1} = k_m^{\alpha}(R)\ \hat{\lambda}_{1,D}^{\ell}.$$

In the same way we get

$$\hat{\lambda}_{1,D}^{\ell+1} = q_m^{\alpha}(R)\ \hat{\lambda}_{2,D}^{\ell} + \omega_m^{\alpha}(R),$$

where

$$\omega_m^{\alpha}(R) = \frac{4\alpha\sigma_2 m C_f R^m R_2^m}{\sigma_2 m(R_2^{2m}+R^{2m}) + \alpha R(R_2^{2m}-R^{2m})}. \tag{2.52}$$

Therefore, the DDM iterations can be written as:

$$\begin{pmatrix} \hat{\lambda}_{1,D}^{\ell+1} \\ \\ \hat{\lambda}_{2,D}^{\ell+1} \end{pmatrix} = \begin{pmatrix} 0 & q_m^{\alpha}(R) \\ \\ k_m^{\alpha}(R) & 0 \end{pmatrix}\begin{pmatrix} \hat{\lambda}_{1,D}^{\ell} \\ \\ \hat{\lambda}_{2,D}^{\ell} \end{pmatrix} + \begin{pmatrix} \omega_m^{\alpha}(R) \\ \\ 0 \end{pmatrix}. \tag{2.53}$$

This induction converges if and only if $\hat{\rho}_m^{\alpha}(R) = \sqrt{\mid k_m^{\alpha}(R) q_m^{\alpha}(R) \mid} < 1$, which is always true for $\alpha > 0$, $m > 0$ and $0 < R < R_2$.

□

Remark 2.4.9. *Equations* (2.41), (2.42) *and* (2.43) *deserve a few remarks.*

1. *For* $\alpha = \dfrac{\sigma_1 m}{R}$ *or* $\alpha = \dfrac{\sigma_2 m}{R}\dfrac{(R_2^{2m}-R^{2m})}{(R_2^{2m}+R^{2m})}$, *the DDM iterations matrix of* (2.48) *is nilpotent and therefore the method converges in maximum* 2 *iterations.*

2. *For* $\alpha = \dfrac{\sigma_1 m}{R}$ *or* $\alpha = \dfrac{\sigma_2 m}{R}\dfrac{(R_2^{2m}+R^{2m})}{(R_2^{2m}-R^{2m})}$, *the DDM iterations matrix of* (2.53) *is nilpotent and therefore the method converges in maximum* 2 *iterations.*

3. *One can see that for all* $\alpha > 0$ *and from the equations* (2.44) *and* (2.49),

$$\lim_{m\to+\infty} \rho_m^{\alpha}(R) = 1 \quad \textit{and} \quad \lim_{m\to+\infty} \hat{\rho}_m^{\alpha}(R) = 1.$$

The following figures obtained by fixing: $R_2 = 2$, $R = 1.5$, *the conductivity parameters* $\sigma_1 = 1$, $\sigma_2 = 2$ *and the OSM parameter* $\alpha = 2$ *confirm clearly these observations.*

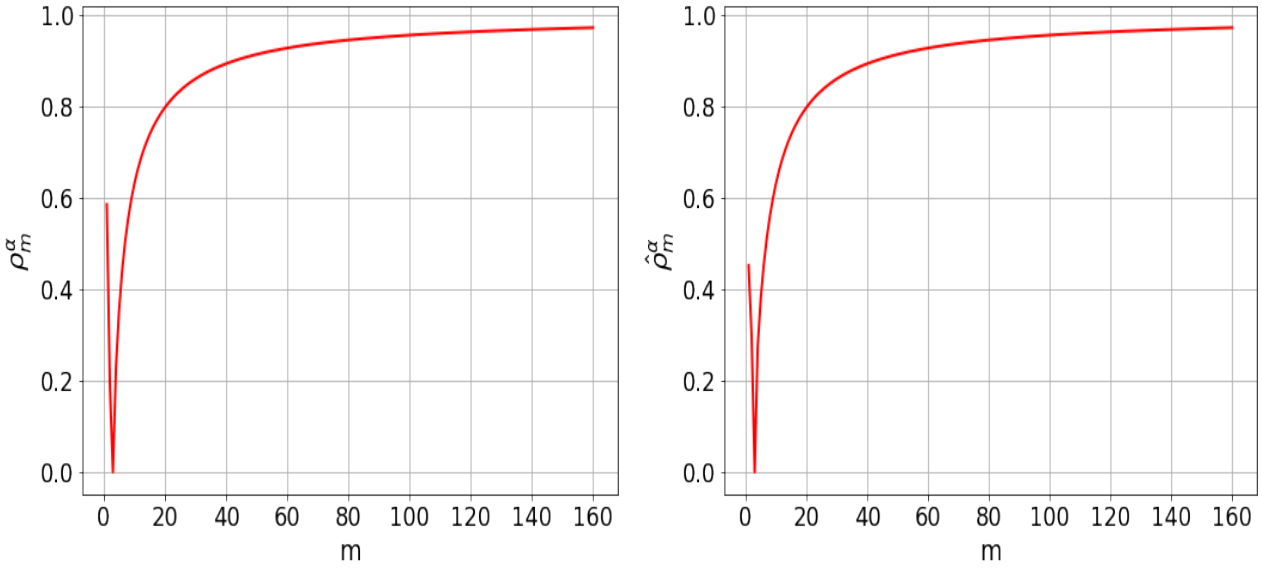

Figure 2.4: Evolution of the convergence rate ρ_m^α (left) and $\hat{\rho}_m^\alpha$ (right) as a function of $m \in \mathbb{N}^*$. The OSM parameter $\alpha = 2$.

We now discuss the influence of the OSM parameter on the convergence rate history factors ρ_m^α *and* $\hat{\rho}_m^\alpha$. *Let us fix, for example,* $m = 1$ *and vary* α *as shown in Figure 2.5 and Figure 2.6. For sufficiently small values of* α, *the convergence rate curves for both* ρ_m^α *and* $\hat{\rho}_m^\alpha$ *are smaller than 1 (see Figure 2.5). However, as* α *goes to infinity,* $\rho_m^\alpha \to 1$ *and* $\hat{\rho}_m^\alpha \to 1$ *(see Figure 2.6).*

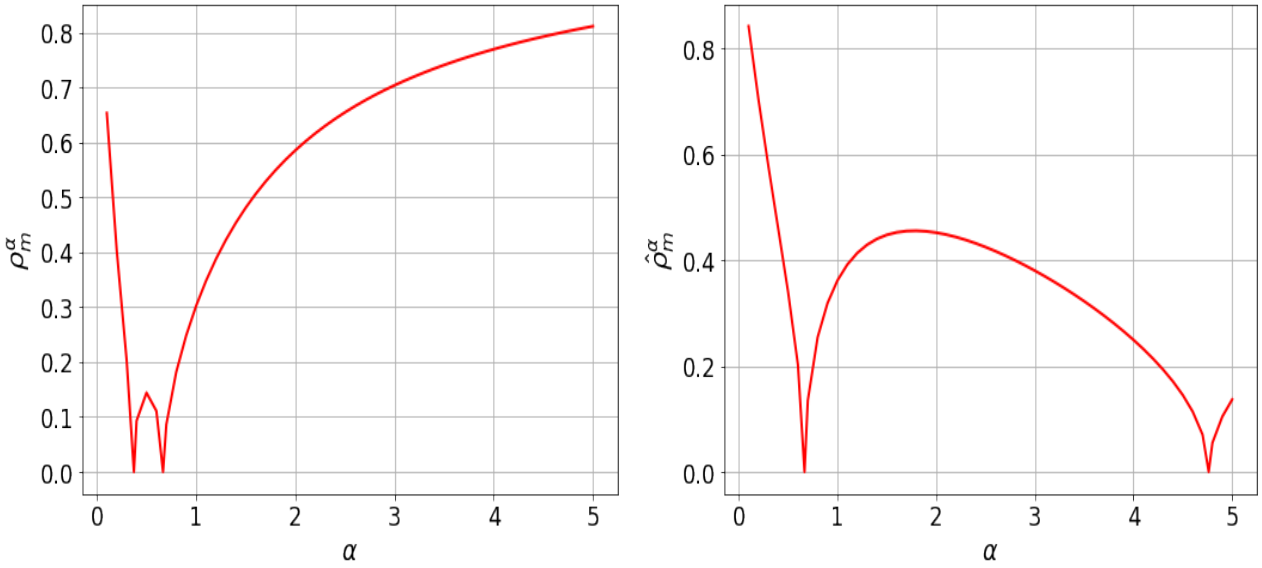

Figure 2.5: Evolution of the convergence rate ρ_m^α (left) and $\hat{\rho}_m^\alpha$ (right) as a function of $\alpha \in [0.1, 5]$.

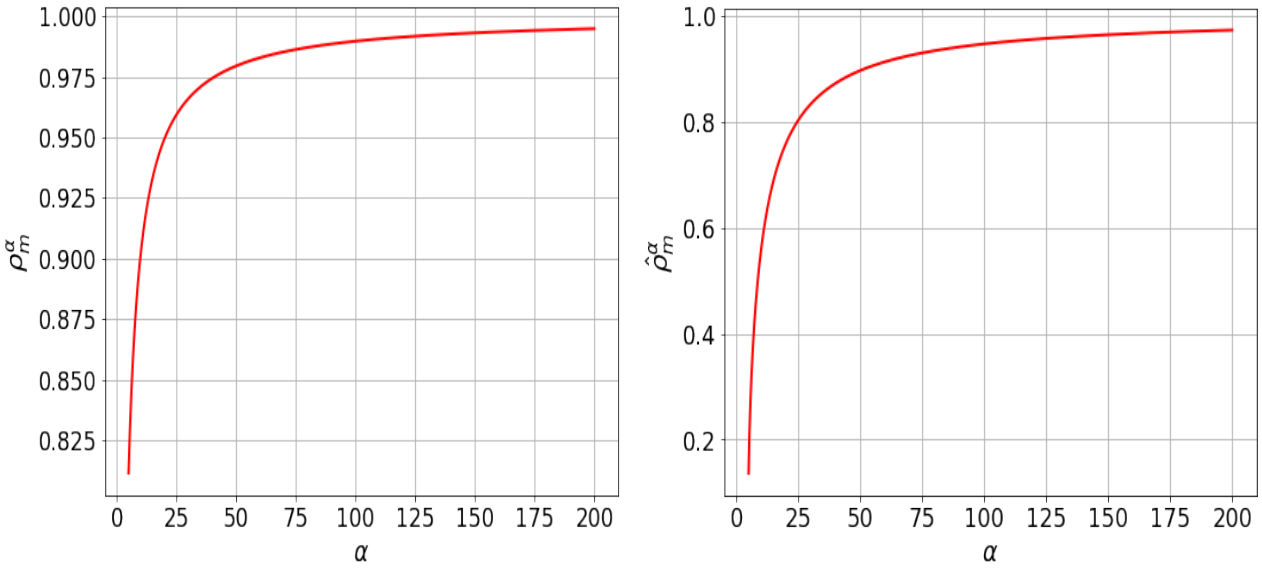

Figure 2.6: Evolution of the convergence rate ρ_m^α (left) and $\hat{\rho}_m^\alpha$ (right) as a function of $\alpha \in [5, 200]$.

2.5 Numerical illustrations

In this section, we give some numerical illustrations obtained by using OSM for solving the direct problem (N_σ). For our numerical validation, we choose for example the case where the

domain Ω is the open disk of center $(0,0)$ and radius $R_2 = 2$ shown in Figure 1.4. Numerically, we solve the variational problems $(V_{1,N})$ and $(V_{2,N})$ by using the finite element method $\mathbb{P}_1$. We then perform some numerical experiments in FreeFem++ [35] for the case of circular geometry and with the following setting:

- The conductivity parameters $\sigma_1 = 1$, $\sigma_2 = 2$.
- The OSM parameter $\alpha = 1$.
- The initial boundary values $\lambda_{i,N} = 0$ on Σ, $i = 1, 2$.

Let us denote by u_{OSM} the approximate solution obtained by solving the direct problem with OSM (2.6)-(2.7), and by u_σ the approximate solution obtained by solving the direct problem with a direct solver. We assume that the current flux $\phi(\theta) = m\cos(m\theta)$ or $\phi(\theta) = m\sin(m\theta)$, $\theta \in [0, 2\pi]$, $m \in \mathbb{N}^*$. The exact solution of the direct problem (N_σ) then can be explicitly expressed as

$$u_{\sigma,exact}(r,\theta) = \begin{cases} u_1(r,\theta) = \alpha_N\, r^m \dfrac{\phi(\theta)}{m} & \text{in } \Omega_1, \\ u_2(r,\theta) = \left(\beta_N\, r^m + \dfrac{\gamma_N}{r^m}\right)\dfrac{\phi(\theta)}{m} & \text{in } \Omega_2, \end{cases}$$

where:

$$\begin{cases} \alpha_N = \dfrac{2R_2^{m+1}}{\sigma_1(R_2^{2m} + R^{2m}) + \sigma_2(R_2^{2m} - R^{2m})}, \\ \beta_N = \dfrac{(\sigma_2 + \sigma_1)R_2^{m+1}}{\sigma_2\left[\sigma_1(R_2^{2m} + R^{2m}) + \sigma_2(R_2^{2m} - R^{2m})\right]}, \\ \gamma_N = \dfrac{(\sigma_2 - \sigma_1)R_2^{m+1}R^{2m}}{\sigma_2\left[\sigma_1(R_2^{2m} + R^{2m}) + \sigma_2(R_2^{2m} - R^{2m})\right]}. \end{cases} \tag{2.54}$$

In Figure 2.8, we present the isovalues of the solution obtained by OSM (2.6)-(2.7) at different iterations. For example, at iteration 0 Figure 2.8(a), iteration 1 Figure 2.8(b), and iteration 9 Figure 2.8(c). Additionally, we display the exact solution in Figure 2.8(d). The current flux is defined as $\phi(\theta) = \cos(\theta)$, $\theta \in [0, 2\pi]$. The mesh used for this numerical experiment is depicted in Figure 2.7. We observe that after 9 iterations, the OSM approximate solution converges to the exact solution.

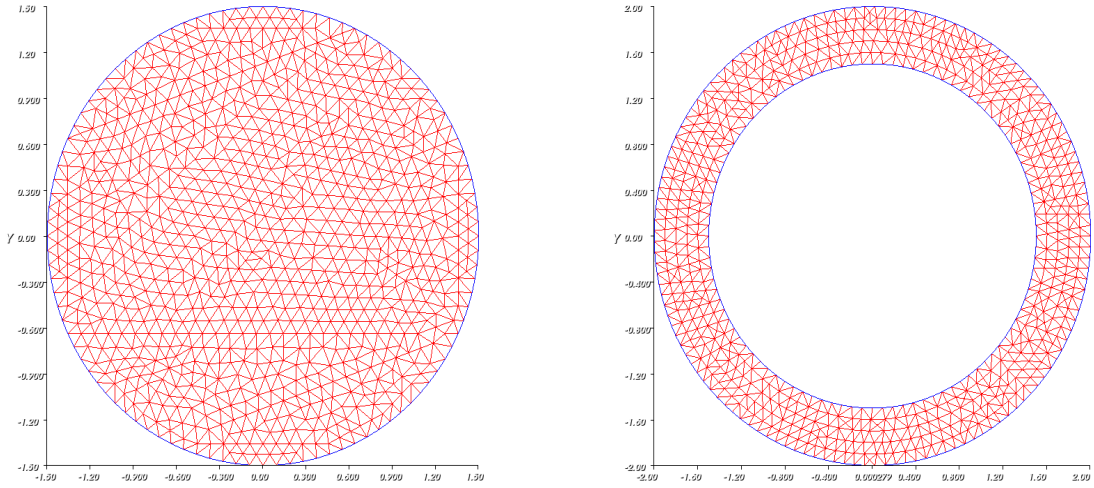

Figure 2.7: Example of meshes used for the circular geometry problem. Subdomain Ω_1 is on the left and subdomain Ω_2 is on the right.

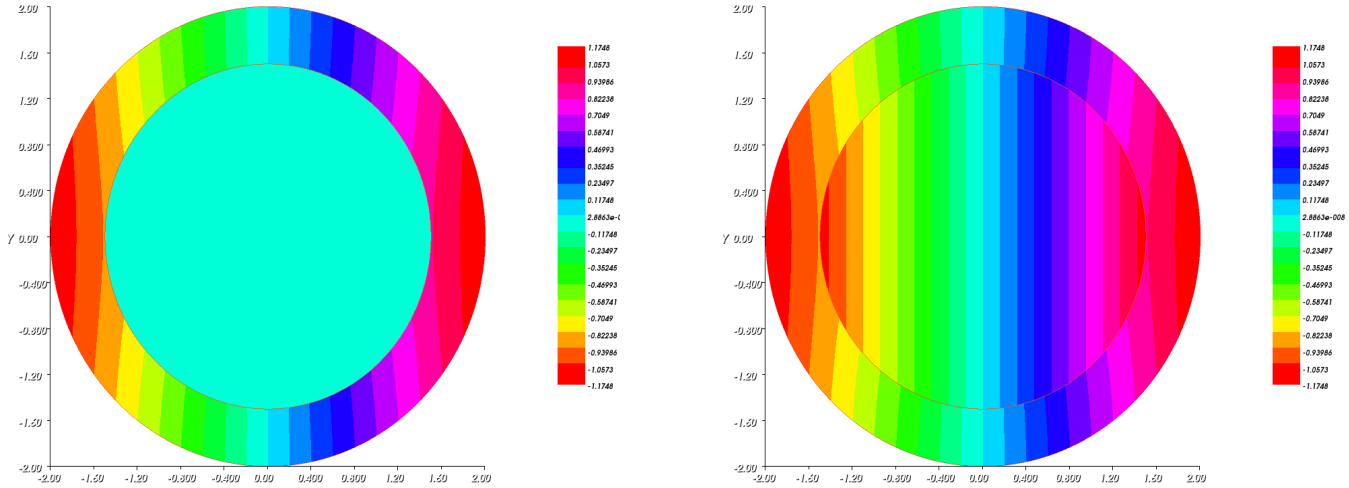

(a) (b)

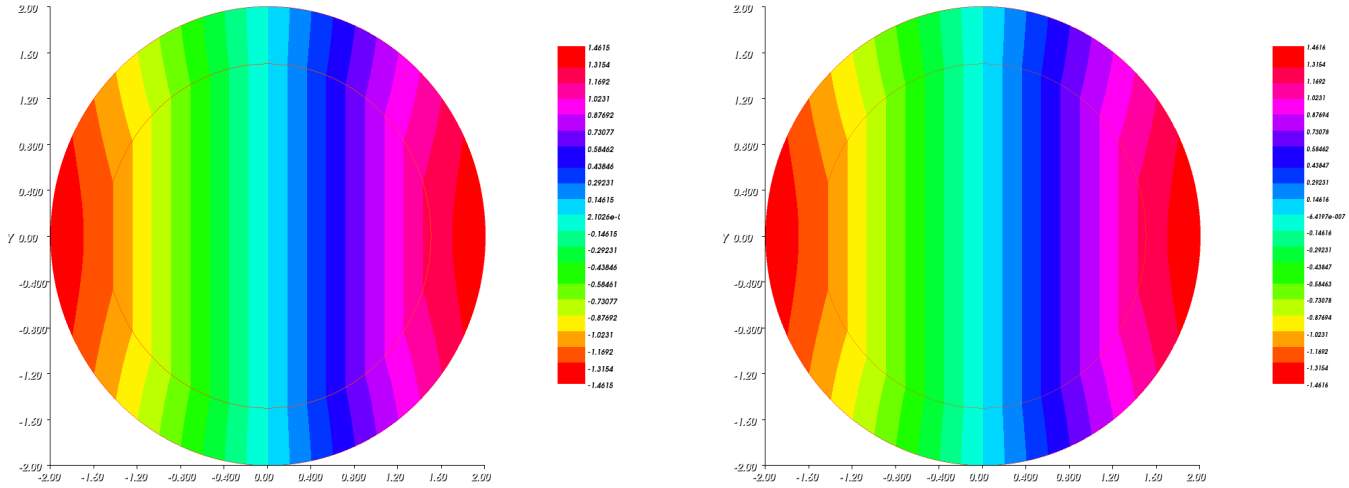

(c) (d)

Figure 2.8: Isovalues of the solution obtained by OSM (2.6)-(2.7) at different OSM iterations are displayed: at iteration 0 (a), at iteration 1 (b), and at iteration 9 (c). The exact solution is shown in Figure (d). The current flux is given by $\phi(\theta) = \cos(\theta)$, $\theta \in [0, 2\pi]$.

In Figure 2.9 we show a log-log plot illustrating the convergence of the error e^{ℓ} mentioned below as a function of the number of OSM iterations ℓ. The relative error between the exact

solution u_{exact} and the OSM approximate solution of (2.6)-(2.7) can be written as:

$$e^{\ell} = \frac{\|u^{\ell}_{OSM} - u_{exact}\|_{L^2(\Omega)}}{\|u_{exact}\|_{L^2(\Omega)}}, \quad \ell \in \mathbb{N}.$$

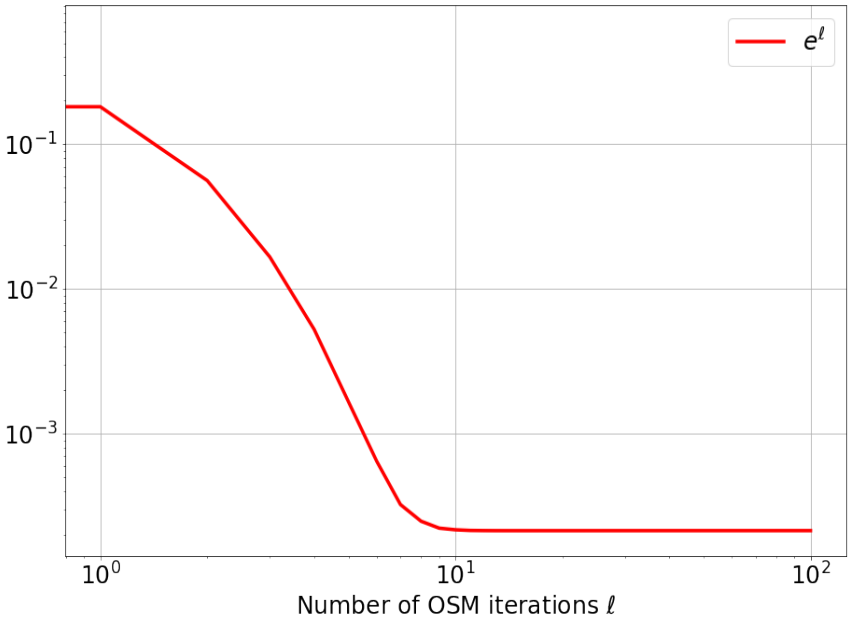

Figure 2.9: Convergence curve for the example depicted in Figure 2.8: Evolution of the relative error e^{ℓ} versus the number of OSM iterations ℓ.

In Figure 2.10 we show a log-log plot illustrating the convergence of the approximation errors e^{ℓ}_{Σ} and $\hat{e}^{\ell}_{\Sigma}$ mentioned below as a function of the number of OSM iterations.The errors, denoted by e^{ℓ}_{Σ} and $\hat{e}^{\ell}_{\Sigma}$, are defined as follows.

$$e^{\ell}_{\Sigma} = \frac{\|u^{\ell}_1 - u^{\ell}_2\|_{L^2(\Sigma)}}{\|U^{\ell}\|_{L^2(\Sigma)}}, \text{ where } U^{\ell} = \frac{u^{\ell}_1 + u^{\ell}_2}{2}.$$

$$\hat{e}^{\ell}_{\Sigma} = \frac{\left\|\sigma_1 \frac{\partial u^{\ell}_1}{\partial \nu} - \sigma_2 \frac{\partial u^{\ell}_2}{\partial \nu}\right\|_{L^2(\Sigma)}}{\|V^{\ell}\|_{L^2(\Sigma)}}, \text{ where } V^{\ell} = \frac{\sigma_1 \frac{\partial u^{\ell}_1}{\partial \nu} + \sigma_2 \frac{\partial u^{\ell}_2}{\partial \nu}}{2}.$$

We observe that the continuity of the trace and the normal trace of the electric potential u on Σ (i.e. $u_1 = u_2$ on Σ and $\sigma_1 \frac{\partial u_1}{\partial \nu} = \sigma_2 \frac{\partial u_2}{\partial \nu}$ on Σ) are satisfied only at convergence of the optimized Schwarz algorithm (2.6)-(2.7) as shown in Figure 2.10.

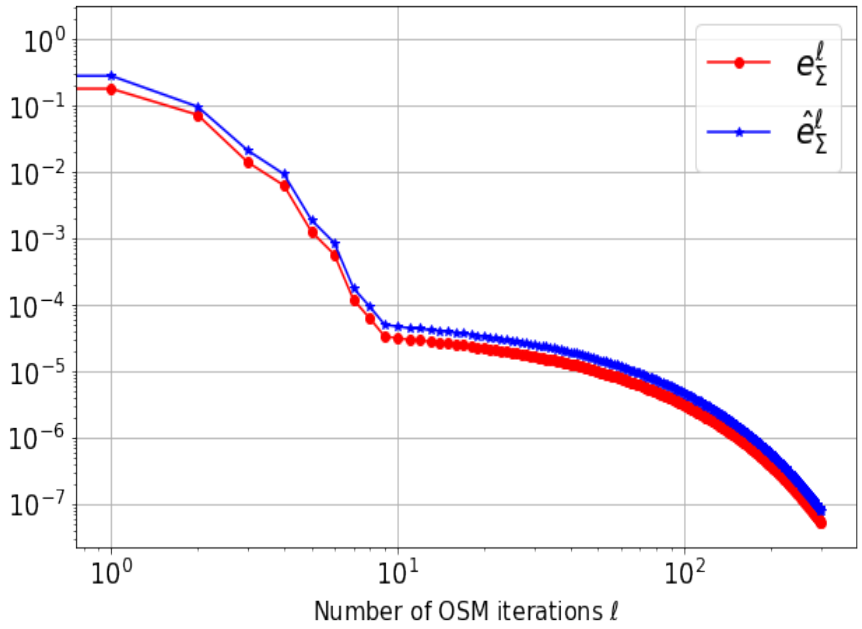

Figure 2.10: Convergence curves of the approximation errors e_Σ^ℓ and $\hat{e}_\Sigma^\ell$ versus the number of OSM iterations.

Numerically, to ensure better accuracy, it is preferable to have a sufficiently fine mesh. Additionally, for the numerical validation of the theoretical resolution of the direct problem using OSM, it is important to have a numerical solution that is sufficiently close to the exact solution. That's why we are studying the effect of refining the mesh by increasing the number of nodes, and then calculating the relative errors e^ℓ as a measure of accuracy.

We now discuss the influence of the numbers of points of discretization on the convergence history. Let us denote by $N_\Gamma := \dfrac{R_2}{R} N_\Sigma$, the number of the external boundary Γ and we discretize of the interior boundary Σ with N_Σ points uses for different refinements. In Figure 2.11, the convergence of the OSM for different refinements are shown with a logarithmic scale. We observe that the refinement effect is clearly visible on the final accuracy. However, the rate of convergence is not affected for the first iterations.

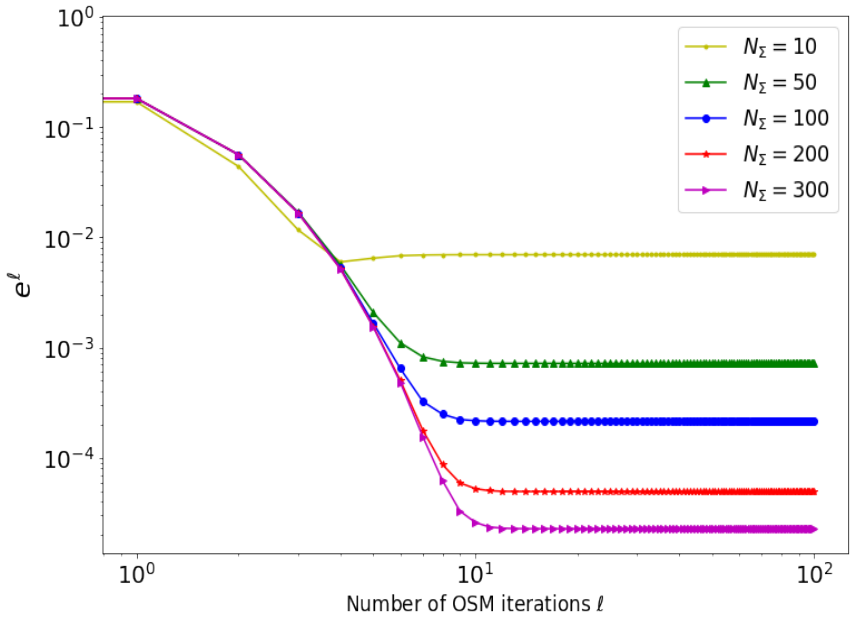

Figure 2.11: Convergence curves for different refinements: error e^ℓ versus the number of OSM iterations ℓ.

2.6 Conclusion

In conclusion, this chapter provided a brief introduction to Domain Decomposition Methods (DDMs) and presented the Optimized Schwarz Method (OSM) as the selected non-overlapping DDM. The direct problems (N_σ) and (D_σ) were then reformulated as an equivalent multi-domain problem using Robin transmission conditions. In addition, the convergence rate of OSM was studied in both one dimension and the case of circular interfaces of $\mathbb{R}^2$, providing valuable insights for analyzing the convergence of the combined inversion algorithm. The chapter is concluded with numerical illustrations demonstrating the effectiveness of OSM in solving the problem at hand.

CHAPTER 3

A combined inversion method for a geometrical inverse conductivity problem

The content of this chapter is partially extracted from [19], in collaboration with S. Chaabane and H. Haddar, published in Inverse Problems, 2023. It contains additional materials to those in [19] on the convergence analysis for simplified geometries.

3.1 Introduction

In this chapter, we assume that σ_1 and σ_2 are known bounded regular functions on Ω and are positive definite and we will study the shape inverse problem which consists in identifying the singularity support Σ of σ from the knowledge of the flux ϕ together with the potential $f = u_{\overline{\sigma}|\Gamma}$. For this, we develop in this chapter some inversion algorithms combining the previous gradient algorithm as defined by Algorithm 1 in Section 1.7 of Chapter 1 with a non-overlapping domain decomposition method (Optimized Schwarz Method) described in Chapter 2, that respects the partitioning of the domain Ω into $\Omega_1 \cup \Omega_2 \cup \Sigma$. The main idea consists in approximating the direct problems $(N_{\sigma(R^k)})$ and $(D_{\sigma(R^k)})$ (at each iteration k of Algorithm 1) using only one or a few OSM steps.

We shall present first the combined inversion algorithm in Section 3.2. We provide in particular a local convergence result for some simplified cases in Section 3.3. Section 3.4 is dedicated to some numerical experiments for testing the efficiency of the combined algorithm

and comparing with the classical one.

3.2 Combined inversion algorithm

We present in this section the combined inversion algorithm that couples Algorithm 1 with OSM. Given an integer $L > 0$, an interface Σ and an initial guess $\lambda_{i,N}^0 \in L^2(\Sigma)$, $i = 1, 2$ we denote by $N^L(\Sigma, \lambda_{1,N}, \lambda_{2,N})$ the L^{th} iterate of (2.7). More precisely, we set

$$\begin{cases} N^L(\Sigma, \lambda_{1,N}^0, \lambda_{2,N}^0) := u_1^L & \text{in } \Omega_1, \\ N^L(\Sigma, \lambda_{1,N}^0, \lambda_{2,N}^0) := u_2^L & \text{in } \Omega_2, \end{cases}$$

where (u_1^ℓ) and (u_2^ℓ), $\ell = 1, \ldots, L$ verify the induction (2.7). We also set

$$\Lambda_{i,N}^L(\Sigma, \lambda_{1,N}^0, \lambda_{2,N}^0) := \lambda_{i,N}^L \text{ on } \Sigma, \ i = 1, 2,$$

where $\lambda_{i,N}^L$ is the iterate number L of (2.7).

Similarly, for some initial guess $\lambda_{i,D}^0 \in L^2(\Sigma)$, $i = 1, 2$ we define:

$$\begin{cases} D^L(\Sigma, \lambda_{1,D}^0, \lambda_{2,D}^0) := v_1^L & \text{in } \Omega_1, \\ D^L(\Sigma, \lambda_{1,D}^0, \lambda_{2,D}^0) := v_2^L & \text{in } \Omega_2, \end{cases}$$

where (v_1^ℓ) and (v_2^ℓ), $\ell = 1, \ldots, L$ verify the induction (2.9) and by

$$\Lambda_{i,D}^L(\Sigma, \lambda_{1,D}^0, \lambda_{2,D}^0) := \lambda_{i,D}^L \text{ on } \Sigma, \ i = 1, 2,$$

where $\lambda_{i,D}^L$ is the iterate number L of (2.9).

Roughly speaking, the combined algorithm consists in replacing $u_{\sigma(R^k)}$ and $v_{\sigma(R^k)}$ respectively with $N^L(\Sigma, \lambda_{1,N}^0, \lambda_{2,N}^0)$ and $D^L(\Sigma, \lambda_{1,D}^0, \lambda_{2,D}^0)$ where $\Sigma = \mathcal{T}_n(R^k)$ as in Algorithm 1. The main ambiguity in the construction of the induction is the update for $\lambda_{i,N}$ and $\lambda_{i,D}$ on $\Sigma = \mathcal{T}_n(R^{k+1})$ using the boundary values of the solutions at previous iterate. We choose to transport these values using the same gradient flow that is used to update the interface. We choose to transport these values on the new update of the interface (i.e $\Sigma = \mathcal{T}_n(R^{k+1})$) using the same mapping that transforms $\mathcal{T}_n(R^k)$ into $\mathcal{T}_n(R^{k+1})$. We explicit this for starlike interfaces as in Algorithm 1 where we suppose that the number of subdivisions n of the interface is kept fixed during iterations. A function λ defined on $\Sigma = \Sigma_R$ can be parameterized on S_j,

$j = 0, \ldots, n-1$ as a function of the variable $t \in [0,1]$ as follows

$$\lambda(t) \equiv \lambda(\hat{M}_j(t)) \tag{3.1}$$

where $\hat{M}_j(t)$ is given by (1.28). The gradient flow as defined by Algorithm 1 preserves the parametrization of Σ in terms of S_j. Therefore the update for the boundary values on Σ can be written easily in terms of the variable $t \in [0,1]$ since the latter is independent from the iteration index.

There is also an ambiguity in defining the partial shape derivative given by (1.31) since the OSM iterates are not continuous across Σ_R nor are the fluxes in general. One can either evaluate the shape gradient with respect to $N^L(\Sigma, \lambda^0_{1,N}, \lambda^0_{2,N})$ and $D^L(\Sigma, \lambda^0_{1,D}, \lambda^0_{2,D})$ or approximate the gradient of the exact cost functional using these approximate solutions of the direct problems. The first option would require the introduction of two adjoint problems and therefore may render the method more costly. This is why we adopt the second approach, that indeed lead to an incorrect gradient at first iterations, but this gradient becomes close to the exact one as the iterations number increases. More precisely, the gradient expression given by (1.31) requires the trace and the normal trace values of the solutions to the Dirichlet and Neumann problems which are continuous for the exact solutions. However, these values are no longer the same if we use the restriction of solutions to Ω_1 or Ω_2 coming from incomplete OSM iterations. In the following algorithm, we choose to apply (1.31) using the traces and the normal traces of $u_{\sigma(R)|\Omega_1}$ and $v_{\sigma(R)|\Omega_1}$. With these notation the proposed combined algorithm can be summarized as follows.

Algorithm 2: A combined inversion algorithm for a geometrical inverse problem

- Fix the number of parameters $n \in \mathbb{N}^*$ that serve to define the starlike interface.
- Consider an initial guess $R^0 \in (\mathbb{R}_+^*)^n$, the initial interface $\Sigma = \Sigma_{R^0} = \mathcal{T}_n(R^0)$ and the corresponding conductivity $\sigma(R^0) = \sigma_1 \chi_{\Omega_{1,R^0}} + \sigma_2 \chi_{\Omega_{2,R^0}}$.
- Choose as initial boundary values: $\lambda_{i,N}(\Sigma) = 0,\ \lambda_{i,D}(\Sigma) = 0$ on $\Sigma,\ i = 1, 2$.
- k=0;

repeat *until* $k \leq$ *maximum number of iterations*

1. Set $\lambda_{i,N}^0 = \lambda_{i,N}(\Sigma),\ \lambda_{i,D}^0 = \lambda_{i,D}(\Sigma)$ on $\Sigma,\ i = 1, 2$.
2. Use L iterations of OSM to evaluate

$$u_{\sigma(R^k)} = N^L(\Sigma, \lambda_{1,N}^0, \lambda_{2,N}^0),\ \lambda_{i,N}^L(R^k) = \Lambda_{i,N}^L(\Sigma, \lambda_{1,N}^0, \lambda_{2,N}^0).$$

$$v_{\sigma(R^k)} = D^L(\Sigma, \lambda_{1,D}^0, \lambda_{2,D}^0),\ \lambda_{i,D}^L(R^k) = \Lambda_{i,D}^L(\Sigma, \lambda_{1,D}^0, \lambda_{2,D}^0).$$

3. Evaluate $\dfrac{\partial \mathcal{J}}{\partial R_j}(R^k)$, for $j = 0, \ldots, n-1$ using formula (1.31) where the boundary values are calculated using $u_{\sigma(R^k)_{|\Omega_1}}$ and $v_{\sigma(R^k)_{|\Omega_1}}$.
4. Update $\Sigma = \mathcal{T}_n(R^{k+1})$ with

$$R_j^{k+1} := R_j^k - \tau \frac{\partial \mathcal{J}}{\partial R_j}(R^k),\ j = 0, \ldots, n-1,$$

   where $\tau > 0$ is chosen sufficiently small. (A step adaptation can be incorporated here but only after a few iterations, when the gradient becomes sufficiently accurate and provides a descent direction).

5. Update the interface values on S_j as

$$\lambda_{i,N}(\Sigma)(\hat{M}_j(t)) = \lambda_{i,N}^L(R^k)(t),\ t \in [0, 1],$$

$$\lambda_{i,D}(\Sigma)(\hat{M}_j(t)) = \lambda_{i,D}^L(R^k)(t),\ t \in [0, 1],$$

   following the identification (3.1).

6. $R^k = R^{k+1}$.
7. $k = k + 1$.

end

Remark 3.2.1. *As indicated earlier, in step 3 of Algorithm 2, we could have made the choice to compute the derivative using* $u_{\sigma(R^k)_{|\Omega_2}}$ *and* $v_{\sigma(R^k)_{|\Omega_2}}$. *This would not affect the theoretical or numerical results below. We keep the choice made in Algorithm 2 for the remainder of this thesis for the sake of conciseness.*

3.3 Local convergence analysis in some particular cases

3.3.1 The one dimensional case

This section is dedicated to study the convergence analysis of Algorithm 2 in the one dimensional case and where the number of OSM iterations $L = 1$, i.e we perform only one DDM step per iteration. With the notation of Section 1.7.1 and Algorithm 2, the iterative scheme leads to the following.

From Theorem 1.6.5 and equation (1.36), we have

$$J'(\delta) = \frac{(\sigma_1 - \sigma_2)}{\sigma_1\sigma_2}\left(|\sigma_1 v'_{\sigma(\delta)}(\delta)|^2 - |\sigma_1 u'_{\sigma(\delta)}(\delta)|^2\right), \tag{3.2}$$

and the solutions after only one OSM step iterate are given in $]0, \delta[$ by

$$u_{\sigma(\delta^k)}(x) = \alpha_N^L(\delta^k)x,\ v_{\sigma(\delta^k)}(x) = \alpha_D^L(\delta^k)x,$$

where

$$\begin{cases} \alpha_N^L(\delta) := \dfrac{\lambda_{1,N}^L(\delta)}{(\sigma_1 + \alpha\delta)}, \\ \alpha_D^L(\delta) := \dfrac{\lambda_{1,D}^L(\delta)}{(\sigma_1 + \alpha\delta)}. \end{cases}$$

Hence, the gradient of the Kohn-Vogelius function with respect to $\delta \in]0, 1[$ is approximated by

$$J'(\delta^k) \simeq \frac{\sigma_1(\sigma_1 - \sigma_2)}{\sigma_2(\sigma_1 + \alpha\delta^k)^2}\left(|\lambda_{1,D}^L(\delta^k)|^2 - |\lambda_{1,N}^L(\delta^k)|^2\right).$$

The iterative scheme of Algorithm 2 now reads

$$\delta^{k+1} = \delta^k - \tau\frac{\sigma_1(\sigma_1 - \sigma_2)}{\sigma_2(\sigma_1 + \alpha\delta^k)^2}\left(|\lambda_{1,D}^L(\delta^k)|^2 - |\lambda_{1,N}^L(\delta^k)|^2\right) \tag{3.3}$$

and the updates for the boundary values are given by

$$\begin{aligned}
\lambda_{1,N}^{L}(\delta^{k+1}) &= p^{\alpha}(\delta^{k})\ \lambda_{2,N}^{L}(\sigma_1,\delta^{k}) + \eta^{\alpha}(\delta^{k}), && (3.4)\\
\lambda_{2,N}^{L}(\delta^{k+1}) &= k^{\alpha}(\delta^{k})\ \lambda_{1,N}^{L}(\delta^{k}), && (3.5)\\
\lambda_{1,D}^{L}(\delta^{k+1}) &= q^{\alpha}(\delta^{k})\ \lambda_{2,D}^{L}(R^{k}) + \omega^{\alpha}(\delta^{k}), && (3.6)\\
\lambda_{2,D}^{L}(\delta^{k+1}) &= k^{\alpha}(\delta^{k})\ \lambda_{1,D}^{L}(\delta^{k}). && (3.7)
\end{aligned}$$

where $p^{\alpha}(\delta^{k})$, $\eta^{\alpha}(\delta^{k})$, $k^{\alpha}(\delta^{k})$, $q^{\alpha}(\delta^{k})$ and $\omega^{\alpha}(\delta^{k})$ are respectively given by (2.16), (2.20), (2.15), (2.17) and (2.24).

If we set $X^{k} := (\delta^{k}, \lambda_{1,N}^{L}(\delta^{k}), \lambda_{2,N}^{L}(\delta^{k}), \lambda_{1,D}^{L}(\delta^{k}), \lambda_{2,D}^{L}(\delta^{k}))$, then the iterative scheme formed by (3.3)-(3.7) can be synthetically written as

$$X^{k+1} = G(X^{k}),$$

where the function G is given by

$$\begin{array}{rccl}
G: & \mathbb{R}^5 & \longrightarrow & \mathbb{R}^5 \\
& X=(x,y,z,t,h) & \longmapsto & G(X) = \left(g_1(X), g_2(X), g_3(X), g_4(X), g_5(X)\right),
\end{array}$$

such that:

$$\begin{aligned}
g_1(X) &:= x - \tau\frac{\sigma_1(\sigma_1-\sigma_2)}{\sigma_2(\sigma_1+\alpha x)^2}(t^2-y^2),\\
g_2(X) &:= p^{\alpha}(x)z + \eta^{\alpha}(x),\\
g_3(X) &:= k^{\alpha}(x)y,\\
g_4(X) &:= q^{\alpha}(x)h + \omega^{\alpha}(x),\\
g_5(X) &:= k^{\alpha}(x)t.
\end{aligned}$$

From the analysis of section 2.4.1 we observe that the sequence $\lambda_{i,N}^{\ell}(\overline{\delta})$, $i=1,2$ converges to $\lambda_{i,N}^{\infty}(\overline{\delta})$, $i=1,2$, where

$$\lambda_{i,N}^{\infty}(\overline{\delta}) = \frac{\phi}{\sigma_1}\psi_i,$$

with

$$\psi_1 = (\sigma_1 + \alpha\overline{\delta}) \quad \text{and} \quad \psi_2 = (\sigma_1 - \alpha\overline{\delta}).$$

Similarly, the sequence $\lambda_{i,D}^{\ell}(\overline{\delta})$, $i=1,2$ converges to $\lambda_{i,D}^{\infty}(\overline{\delta})$, $i=1,2$, where

$$\lambda_{i,D}^{\infty}(\overline{\delta})=\frac{\sigma_2 f}{\sigma_2\overline{\delta}+\sigma_1(1-\overline{\delta})}\psi_i.$$

Moreover, we have

$$\begin{cases}\lambda_{1,N}^{\infty}(\overline{\delta})=p^{\alpha}(\overline{\delta})\lambda_{2,N}^{\infty}(\overline{\delta})+\eta^{\alpha}(\overline{\delta}),\\ \lambda_{2,N}^{\infty}(\overline{\delta})=k^{\alpha}(\overline{\delta})\lambda_{1,N}^{\infty}(\overline{\delta}),\\ \lambda_{1,D}^{\infty}(\overline{\delta})=q^{\alpha}(\overline{\delta})\lambda_{2,D}^{\infty}(\overline{\delta})+w^{\alpha}(\overline{\delta}),\\ \lambda_{2,D}^{\infty}(\overline{\delta})=k^{\alpha}(\overline{\delta})\lambda_{1,D}^{\infty}(\overline{\delta}).\end{cases}$$

Using the expression of f given by (1.34) one can easily check that $\lambda_{i,N}^{\infty}(\overline{\delta})=\lambda_{i,D}^{\infty}(\overline{\delta})$ and then $\overline{X}=\left(\overline{\delta},\lambda_{1,N}^{\infty}(\overline{\delta}),\lambda_{2,N}^{\infty}(\overline{\delta}),\lambda_{1,D}^{\infty}(\overline{\delta}),\lambda_{2,D}^{\infty}(\overline{\delta})\right)=\left(\overline{\delta},\lambda_{1,N}^{\infty}(\overline{\delta}),\lambda_{2,N}^{\infty}(\overline{\delta}),\lambda_{1,N}^{\infty}(\overline{\delta}),\lambda_{2,N}^{\infty}(\overline{\delta})\right)$ is a fixed point of G. We first establish in the following lemma that $\overline{X}$ is the unique fixed point of G.

Lemma 3.3.1. *The point $\overline{X}$ defined above is the unique fixed point of G.*

Proof. Let $X=(x,y,z,t,h)$ a fixed point of G, then we have:

$$\begin{cases}t=y,\\ y=p^{\alpha}(x)z+\eta^{\alpha}(x),\\ z=k^{\alpha}(x)y,\\ t=q^{\alpha}(x)h+w^{\alpha}(x),\\ h=k^{\alpha}(x)t.\end{cases}$$

consequently

$$\begin{pmatrix}y\\ \\ z\end{pmatrix}=\begin{pmatrix}0 & p^{\alpha}(x)\\ \\ k^{\alpha}(x) & 0\end{pmatrix}\begin{pmatrix}y\\ \\ z\end{pmatrix}+\begin{pmatrix}\eta^{\alpha}(x)\\ \\ 0\end{pmatrix}.$$

and

$$\begin{pmatrix}t\\ \\ h\end{pmatrix}=\begin{pmatrix}0 & q^{\alpha}(x)\\ \\ k^{\alpha}(x) & 0\end{pmatrix}\begin{pmatrix}t\\ \\ h\end{pmatrix}+\begin{pmatrix}w^{\alpha}(x)\\ \\ 0\end{pmatrix}.$$

then we have:

$$\begin{cases}y=\dfrac{\phi(\sigma_1+\alpha x)}{\sigma_1},\\ t=\dfrac{\sigma_2 f(\sigma_1+\alpha x)}{\sigma_2 x+\sigma_1(1-x)}.\end{cases}$$

consequently,

$$f = \frac{\phi}{\sigma_1\sigma_2}\left[\sigma_2 x + \sigma_1(1-x)\right],$$

where the mapping defined on $]0,1[$ by :

$$g(x) = \frac{\phi}{\sigma_1\sigma_2}\left[\sigma_2 x + \sigma_1(1-x)\right]$$

is one to one. We deduce that, $x = \overline{\delta}$, and then

$$X = \left(\overline{\delta}, \lambda^{\infty}_{1,N}(\overline{\delta}), \lambda^{\infty}_{2,N}(\overline{\delta}), \lambda^{\infty}_{1,D}(\overline{\delta}), \lambda^{\infty}_{2,D}(\overline{\delta})\right) = \overline{X}.$$

□

Theorem 3.3.1. *There exists $\kappa > 0$ such that Algorithm 2 with $L = 1$ is locally convergent for all $\tau \in]0, \kappa[$.*

Proof. For short notation, let us set $\overline{x} = \overline{\delta}$, $\overline{y} = \lambda^{\infty}_{1,N}(\overline{\delta})$, and

$$k := k^{\alpha}(\overline{x}) = \frac{\sigma_1 - \alpha\overline{x}}{\sigma_1 + \alpha\overline{x}} = \frac{\psi_2}{\psi_1}. \tag{3.8}$$

Then from the previous Lemma, $\overline{X} = (\overline{x}, \overline{y}, k\overline{y}, \overline{y}, k\overline{y})$ is the unique fixed point of G. In order to prove the local convergence we shall establish that G is a contraction in a neighborhood of $\overline{X}$. This requires the study of the Jacobian matrix $DG(\overline{X})$. The latter is given by

$$DG(\overline{X}) = \begin{pmatrix} 1 & d\tau & 0 & -d\tau & 0 \\ 0 & 0 & -1 & 0 & 0 \\ b & k & 0 & 0 & 0 \\ c & 0 & 0 & 0 & q \\ b & 0 & 0 & k & 0 \end{pmatrix},$$

where we have set for short notation

$$d := \frac{1}{\tau}\frac{\partial g_1}{\partial y}(\overline{X}) = \frac{2\phi(\sigma_1-\sigma_2)}{\sigma_2(\sigma_1+\alpha x)}, \tag{3.9}$$

$$b := \frac{\partial g_3}{\partial x}(\overline{X}) = \frac{-2\alpha\phi}{(\sigma_1+\alpha\overline{x})}, \tag{3.10}$$

$$c := \frac{\partial g_4}{\partial x}(\overline{X}) = \frac{2\alpha\phi}{(\sigma_2+\alpha(1-\overline{x}))}, \tag{3.11}$$

$$q := \frac{\partial g_4}{\partial h}(\overline{X}) = q^{\alpha}(\overline{x}). \tag{3.12}$$

For every $(\lambda,\tau)\in\mathbb{R}\times\mathbb{R}$, we define the characteristic polynomial of $DG(\overline{X})$

$$P(\lambda,\tau) := det(DG(\overline{X})-\lambda I_5) = \begin{vmatrix} 1-\lambda & d\tau & 0 & -d\tau & 0 \\ a & -\lambda & -1 & 0 & 0 \\ b & k & -\lambda & 0 & 0 \\ c & 0 & 0 & -\lambda & q \\ b & 0 & 0 & k & -\lambda \end{vmatrix}$$

and we denote by $\lambda_j(\tau)\in\mathbb{C}$, $j=1,\ldots,5$, the eigenvalues of $DG(\overline{X})$. Then, we have

$$P(\lambda,\tau) = (1-\lambda)(\lambda^2+k)(\lambda^2-kq) - \tau\, d\left[c\lambda^3+(bq+b)\lambda^2+ck\lambda\right],$$

and $P(\lambda_j(\tau),\tau)=0$ for $j=1,\ldots,5$.

Let $\overline{\rho}(\tau) := \max\left\{|\lambda_j(\tau)|;\ j=1,\ldots,5\right\}$ be the spectral radius of $DG(\overline{X})$. We remark that for $\tau=0$, we have

$$P(\lambda,0) = (1-\lambda)(\lambda^2+k)(\lambda^2-kq),$$

where $|k|<1$ and $|kq|<1$. Then, for $\tau=0$, the eigenvalues of $DG(\overline{X})$ verifies:

$$|\lambda_1(0)|=1, \text{ and } |\lambda_j(0)|<1 \quad \forall j\in\{2,3,4,5\}.$$

Thus, one can choose $\kappa>0$ sufficiently small, such that

$$|\lambda_j(\tau)|<1\ \forall\ j\in\{2,3,4,5\}, \text{ and } \overline{\rho}(\tau)=|\lambda_0(\tau)| \quad \text{for all } \tau\in]0,\kappa[.$$

To show that if $\overline{\rho}(\tau)<1$ for small enough $\tau>0$, we use a first order Taylor expansion of

$(\lambda,\tau) \mapsto P(\lambda,\tau)$ in a neighborhood of the point $(1,0)$. Indeed

$$\begin{aligned} P(\lambda,\tau) &= P(1,0) + \frac{\partial P}{\partial \lambda}(1,0)\,(\lambda-1) + \frac{\partial P}{\partial \tau}(1,0)\,\tau + \epsilon(\lambda,\tau), \\ &= C_1(1-\lambda) - C_2\tau + \epsilon(\lambda,\tau), \end{aligned}$$

where $\lim\limits_{(\lambda,\tau)\to(1,0)} \dfrac{|\epsilon(\lambda,\tau)|}{\sqrt{(1-\lambda)^2+\tau^2}} = 0$, and

$$\left\{ \begin{array}{l} C_1 := (1+k)(1-kq), \\ C_2 := d\left[c(1+k) + b(1+q)\right]. \end{array} \right. \tag{3.13}$$

This shows that for τ sufficiently small

$$\lambda_0(\tau) = 1 - \frac{C_2}{C_1}\tau + o(\tau). \tag{3.14}$$

Clearly $C_1 > 0$ from the conditions $|k| < 1$ and $|kq| < 1$. Indeed, we also have

$$\begin{aligned} 1+k &= \frac{2\sigma_1}{(\sigma_1 + \alpha\overline{x})}, \\ 1+q &= \frac{2\sigma_2}{\sigma_2 + \alpha(1-\overline{x})}, \end{aligned}$$

then,

$$c(1+k) + b(1+q) = \frac{4\alpha\phi(\sigma_1-\sigma_2)}{(\sigma_1+\alpha\overline{x})(\sigma_2+\alpha(1-\overline{x}))},$$

where k, b, c and q are respectively given by (3.8), (3.10), (3.11) and (3.12).

Hence, according to (3.9), we get

$$\begin{aligned} C_2 &= d\left[c(1+k) + b(1+q)\right], \\ &= \frac{8\alpha\phi^2(\sigma_1-\sigma_2)^2}{\sigma_2(\sigma_1+\alpha\overline{x})^2(\sigma_2+\alpha(1-\overline{x}))} > 0. \end{aligned}$$

Then $C_2 > 0$ and from (3.14) there exists $\kappa > 0$ such that $\overline{\rho}(\tau) = |\lambda_0(\tau)| < 1$ for all $\tau \in]0,\kappa[$. This proves that G is a contraction for $\tau \in]0,\kappa[$, which gives the desired result.

□

Remark 3.3.2. *Using equations (3.8) and (3.12), we obtain*

$$\begin{aligned} C_1 &= (1+k)(1-kq), \\ &= \frac{4\alpha\sigma_1\Big[\sigma_2\overline{x}+\sigma_1(1-\overline{x})\Big]}{(\sigma_1+\alpha\overline{x})\,(\sigma_2+\alpha(1-\overline{x}))}. \end{aligned}$$

Therefore,

$$\frac{C_2}{C_1} = J''(\overline{\delta}) \;\; \textit{for all}\; \alpha > 0, \tag{3.15}$$

where $J''(\overline{x})$ is given by (1.38).
This shows that for this specific case, the local convergence of Algorithm 2 is equivalent to the local convergence of Algorithm 1 described in Section 1.7.1 of Chapter 1.

3.3.2 The case of an annulus

This section is dedicated to the study of the convergence analysis of Algorithm 2 in the case of an annulus domain of $\mathbb{R}^2$ where the number of OSM iterations $L = 1$. Using the same notation as in Section 1.7.2 and Algorithm 2, the iterative scheme leads to the following.

From (1.43), we have

$$\mathcal{J}'(R) = [\sigma(R)]\int_0^{2\pi}\left[\frac{1}{\sigma_1\sigma_2}\left(\left|\sigma(R)\frac{\partial v_{\sigma(R)}}{\partial\nu}\right|^2 - \left|\sigma(R)\frac{\partial u_{\sigma(R)}}{\partial\nu}\right|^2\right) + \left(|\nabla_\tau v_{\sigma(R)}|^2 - |\nabla_\tau u_{\sigma(R)}|^2\right)\right] R\,d\theta$$

and the solutions after only one OSM step iterate are given in $]R_1, R_2[$ by

$$u_{\sigma(R^k)}(r,\theta) = \alpha_N^L(R^k)\log\left(\frac{r}{R_1}\right), \quad v_{\sigma(R^k)}(r,\theta) = \alpha_D^L(R^k)\log\left(\frac{r}{R_1}\right),$$

where

$$\begin{cases} \alpha_N^L(R) := \dfrac{R\lambda_{1,N}^L}{\left(\sigma_1 + \alpha R\log\left(\dfrac{R}{R_1}\right)\right)}, \\ \alpha_D^L(R) := \dfrac{R\lambda_{1,D}^L}{\left(\sigma_1 + \alpha R\log\left(\dfrac{R}{R_1}\right)\right)}. \end{cases}$$

Then the gradient of the Kohn-Vogelius function with respect to $R \in]R_1, R_2[$ is approxi-

mated by

$$\frac{\partial \mathcal{J}}{\partial R}(R^k) \simeq \frac{2\pi\sigma_1(\sigma_1-\sigma_2)R^k}{\sigma_2\left(\sigma_1+\alpha R^k \log\left(\frac{R^k}{R_1}\right)\right)^2}\left(|\lambda^L_{1,D}(R^k)|^2-|\lambda^L_{1,N}(R^k)|^2\right).$$

The iterative scheme of Algorithm 2 now reads

$$R^{k+1} = R^k - \tau\frac{2\pi\sigma_1(\sigma_1-\sigma_2)R^k}{\sigma_2\left(\sigma_1+\alpha R^k \log\left(\frac{R^k}{R_1}\right)\right)^2}\left(|\lambda^L_{1,D}(R^k)|^2-|\lambda^L_{1,N}(R^k)|^2\right) \tag{3.16}$$

and the updates for the boundary values are given by

$$\begin{aligned}
\lambda^L_{1,N}(R^{k+1}) &= p^\alpha(R^k)\,\lambda^L_{2,N}(R^k)+\eta^\alpha(R^k), &(3.17)\\
\lambda^L_{2,N}(R^{k+1}) &= k^\alpha(R^k)\,\lambda^L_{1,N}(R^k), &(3.18)\\
\lambda^L_{1,D}(R^{k+1}) &= q^\alpha(R^k)\,\lambda^L_{2,D}(R^k)+\omega^\alpha(R^k), &(3.19)\\
\lambda^L_{2,D}(R^{k+1}) &= k^\alpha(R^k)\,\lambda^L_{1,D}(R^k). &(3.20)
\end{aligned}$$

where $p^\alpha(R^k)$, $\eta^\alpha(R^k)$, $k^\alpha(R^k)$, $q^\alpha(R^k)$ and $\omega^\alpha(R^k)$ are respectively given by (2.31), (2.35), (2.30), (2.32) and (2.39).
If we set $X^k := \left(R^k, \lambda^L_{1,N}(R^k), \lambda^L_{2,N}(R^k), \lambda^L_{1,D}(R^k), \lambda^L_{2,D}(R^k)\right)$, then the iterative scheme given by equations (3.16)-(3.20) can be synthetically written as

$$X^{k+1} = G(X^k),$$

where the function G is given by

$$\begin{array}{rccl}
G: & \mathbb{R}^5 & \longrightarrow & \mathbb{R}^5\\
& X=(x,y,z,t,h) & \longmapsto & G(X)=(g_1(X),g_2(X),g_3(X),g_4(X),g_5(X)),
\end{array}$$

such that:

$$\begin{aligned} g_1(X) &:= x - \tau \frac{2\pi\sigma_1(\sigma_1-\sigma_2)x}{\sigma_2\left(\sigma_1+\alpha x\log\left(\frac{x}{R_1}\right)\right)^2}\left(t^2-y^2\right), \\ g_2(X) &:= p^\alpha(x)z+\eta^\alpha(x), \\ g_3(X) &:= k^\alpha(x)y, \\ g_4(X) &:= q^\alpha(x)h+\omega^\alpha(x), \\ g_5(X) &:= k^\alpha(x)t. \end{aligned}$$

From the analysis of Section 2.4.2 we observe that the sequence $\lambda_{i,N}^{\ell}(\overline{R})$, $i=1,2$ converges to $\lambda_{i,N}^{\infty}(\overline{R})$, $i=1,2$, where

$$\lambda_{i,N}^{\infty}(\overline{R}) = \frac{\phi R_2}{\sigma_1\overline{R}}\psi_i$$

with

$$\psi_1 = \left[\sigma_1+\alpha\overline{R}\log\left(\frac{\overline{R}}{R_1}\right)\right] \text{ and } \psi_2 = \left[\sigma_1-\alpha\overline{R}\log\left(\frac{\overline{R}}{R_1}\right)\right].$$

Similarly, the sequence $\lambda_{i,D}^{\ell}(\overline{R})$, $i=1,2$ converges to $\lambda_{i,D}^{\infty}(\overline{R})$, $i=1,2$, where

$$\lambda_{i,D}^{\infty}(\overline{R}) = \frac{\sigma_2 f}{\overline{R}\left[\sigma_2\log\left(\frac{\overline{R}}{R_1}\right)+\sigma_1\log\left(\frac{R_2}{\overline{R}}\right)\right]}\psi_i.$$

Moreover, we have

$$\begin{cases} \lambda_{1,N}^{\infty} = p^\alpha(\overline{R})\lambda_{2,N}^{\infty}(\overline{R})+\eta^\alpha(\overline{R}), \\ \lambda_{2,N}^{\infty} = k^\alpha(\overline{R})\lambda_{1,N}^{\infty}(\overline{R}), \\ \lambda_{1,D}^{\infty} = q^\alpha(\overline{R})\lambda_{2,D}^{\infty}(\overline{R})+w^\alpha(\overline{R}), \\ \lambda_{2,D}^{\infty} = k^\alpha(\overline{R})\lambda_{1,D}^{\infty}(\overline{R}). \end{cases}$$

Using the expression of f given by (1.42) one can easily check that $\lambda_{i,N}^{\infty}(\overline{R}) = \lambda_{i,D}^{\infty}(\overline{R})$ and then $\overline{X} = \left(\overline{R}, \lambda_{1,N}^{\infty}(\overline{R}), \lambda_{2,N}^{\infty}(\overline{R}), \lambda_{1,D}^{\infty}(\overline{R}), \lambda_{2,D}^{\infty}(\overline{R})\right) = \left(\overline{R}, \lambda_{1,N}^{\infty}(\overline{R}), \lambda_{2,N}^{\infty}(\overline{R}), \lambda_{1,N}^{\infty}(\overline{R}), \lambda_{2,N}^{\infty}(\overline{R})\right)$ is a fixed point of G. We first establish in the following lemma that $\overline{X}$ is the unique fixed point of G.

Lemma 3.3.2. *The point $\overline{X}$ defined above is the unique fixed point of G.*

Proof. Let $X = (x, y, z, t, h)$ a fixed point of G, then we have:

$$\begin{cases} t = y, \\ y = p^{\alpha}(x)z + \eta^{\alpha}(x), \\ z = k^{\alpha}(x)y, \\ t = q^{\alpha}(x)h + w^{\alpha}(x), \\ h = k^{\alpha}(x)t. \end{cases}$$

Consequently

$$\begin{pmatrix} y \\ \\ z \end{pmatrix} = \begin{pmatrix} 0 & p^{\alpha}(x) \\ \\ k^{\alpha}(x) & 0 \end{pmatrix} \begin{pmatrix} y \\ \\ z \end{pmatrix} + \begin{pmatrix} \eta^{\alpha}(x) \\ \\ 0 \end{pmatrix}.$$

and

$$\begin{pmatrix} t \\ \\ h \end{pmatrix} = \begin{pmatrix} 0 & q^{\alpha}(x) \\ \\ k^{\alpha}(x) & 0 \end{pmatrix} \begin{pmatrix} t \\ \\ h \end{pmatrix} + \begin{pmatrix} w^{\alpha}(x) \\ \\ 0 \end{pmatrix},$$

then we have:

$$\begin{cases} y = \dfrac{\phi R_2 \left[\sigma_1 + \alpha x \log\left(\dfrac{x}{R_1}\right)\right]}{\sigma_1 x}, \\ t = \dfrac{\sigma_2 f \left[\sigma_1 + \alpha x \log\left(\dfrac{x}{R_1}\right)\right]}{x\left[\sigma_2 \log\left(\dfrac{x}{R_1}\right) + \sigma_1 \log\left(\dfrac{R_2}{x}\right)\right]}. \end{cases}$$

Consequently,

$$f = \frac{R_2\phi}{\sigma_1\sigma_2}\left[\sigma_2 \log\left(\frac{x}{R_1}\right) + \sigma_1 \log\left(\frac{R_2}{x}\right)\right],$$

where the mapping defined on $]R_1, R_2[$ by :

$$g(x) = \frac{R_2\phi}{\sigma_1\sigma_2}\left[\sigma_2 \log\left(\frac{x}{R_1}\right) + \sigma_1 \log\left(\frac{R_2}{x}\right)\right]$$

is one to one. We deduce that, $x = \overline{R}$, and then

$$X = \left(\overline{R}, \lambda_{1,N}^{\infty}(\overline{R}), \lambda_{2,N}^{\infty}(\overline{R}), \lambda_{1,D}^{\infty}(\overline{R}), \lambda_{2,D}^{\infty}(\overline{R})\right) = \overline{X}.$$

□

Theorem 3.3.3. *There exists $\kappa > 0$ such that Algorithm 2 with $L = 1$ is locally convergent*

for all $\tau \in]0, \kappa[$.

Proof. For short notation, let us set $\overline{x} = \overline{R}$, $\overline{y} = \lambda_{1,N}^{\infty}(\overline{R})$, and

$$k := k^{\alpha}(\overline{x}) = \frac{\left[\sigma_1 - \alpha \overline{R} \log\left(\frac{\overline{R}}{R_1}\right)\right]}{\left[\sigma_1 + \alpha \overline{R} \log\left(\frac{\overline{R}}{R_1}\right)\right]} = \frac{\psi_2}{\psi_1}. \tag{3.21}$$

Then from the previous Lemma, $\overline{X} = (\overline{x}, \overline{y}, k\overline{y}, \overline{y}, k\overline{y})$ is the unique fixed point of G. In order to prove the local convergence we shall establish that G is a contraction in a neighborhood of $\overline{X}$. This requires the study of the Jacobian matrix $DG(\overline{X})$. The latter is given by

$$DG(\overline{X}) = \begin{pmatrix} 1 & d\tau & 0 & -d\tau & 0 \\ a & 0 & -1 & 0 & 0 \\ b & k & 0 & 0 & 0 \\ c & 0 & 0 & 0 & q \\ b & 0 & 0 & k & 0 \end{pmatrix},$$

where we have set for short notation

$$d := \frac{1}{\tau}\frac{\partial g_1}{\partial y}(\overline{X}) = \frac{4\pi\phi R_2 (\sigma_1 - \sigma_2)}{\sigma_2 \left[\sigma_1 + \alpha \overline{R} \log\left(\frac{\overline{R}}{R_1}\right)\right]}, \tag{3.22}$$

$$a := \frac{\partial g_2}{\partial x}(\overline{X}) = \frac{-2R_2\phi}{\overline{R}^2}, \tag{3.23}$$

$$b := \frac{\partial g_3}{\partial x}(\overline{X}) = -\frac{2\alpha\phi R_2 \left(1 + \log\left(\frac{\overline{R}}{R_1}\right)\right)}{\overline{R}\left[\sigma_1 + \alpha \overline{R} \log\left(\frac{\overline{R}}{R_1}\right)\right]}, \tag{3.24}$$

$$c := \frac{\partial g_4}{\partial x}(\overline{X}) = -\frac{2\alpha\phi R_2 \left(\log\left(\frac{R_2}{\overline{R}}\right) - 1\right)}{\overline{R}\left[\sigma_2 + \alpha \overline{R} \log\left(\frac{R_2}{\overline{R}}\right)\right]}, \tag{3.25}$$

$$q := \frac{\partial g_4}{\partial h}(\overline{X}) = q^{\alpha}(\overline{x}). \tag{3.26}$$

For every $(\lambda,\tau)\in\mathbb{R}\times\mathbb{R}$, we define the characteristic polynomial of $DG(\overline{X})$

$$P(\lambda,\tau) \;:=\; det(DG(\overline{X})-\lambda I_5)=\begin{vmatrix} 1-\lambda & d\tau & 0 & -d\tau & 0\\ a & -\lambda & -1 & 0 & 0\\ b & k & -\lambda & 0 & 0\\ c & 0 & 0 & -\lambda & q\\ b & 0 & 0 & k & -\lambda \end{vmatrix}$$

and we denote by $\lambda_i(\tau)\in\mathbb{C}$, $i=1,\ldots,5$, the eigenvalues of $DG(\overline{X})$. Then, we have

$$P(\lambda,\tau) \;=\; (1-\lambda)(\lambda^2+k)(\lambda^2-kq)-\tau\, d\Big[(c-a)\lambda^3+(bq+b)\lambda^2+k(aq+c)\lambda\Big],$$

and $P(\lambda_i(\tau),\tau)=0$ for $i=1,\ldots,5$. Let $\overline{\rho}(\tau):=\max\Big\{|\lambda_i(\tau)|,\ i=1,\ldots,5\Big\}$ be the spectral radius of $DG(\overline{X})$. We remark that for $\tau=0$, we have

$$P(\lambda,0)=(1-\lambda)(\lambda^2+k)(\lambda^2-kq),$$

where $|k|<1$ and $|kq|<1$. Then, for $\tau=0$, the eigenvalues of $DG(\overline{X})$ verifies:

$$|\lambda_1(0)|=1,\ \text{and}\ |\lambda_i(0)|<1\ \forall\, i\in\{2,3,4,5\}.$$

Thus, one can choose $\kappa>0$ sufficiently small, such that

$$|\lambda_i(\tau)|<1\ \ \forall\, i\in\{2,3,4,5\},\ \text{and}\ \overline{\rho}(\tau)=|\lambda_0(\tau)|\ \text{for all}\ \tau\in]0,\kappa[.$$

To show that if $\overline{\rho}(\tau)<1$ for small enough $\tau>0$, we use a first order Taylor expansion of $(\lambda,\tau)\mapsto P(\lambda,\tau)$ in a neighborhood of the point $(1,0)$. Indeed

$$\begin{aligned} P(\lambda,\tau) &= P(1,0)+\frac{\partial P}{\partial\lambda}(1,0)\,(\lambda-1)+\frac{\partial P}{\partial\tau}(1,0)\,\tau+\epsilon(\lambda,\tau),\\ &= C_1(1-\lambda)-C_2\tau+\epsilon(\lambda,\tau), \end{aligned}$$

where $\lim\limits_{(\lambda,\tau)\to(1,0)}\dfrac{|\epsilon(\lambda,\tau)|}{\sqrt{(1-\lambda)^2+\tau^2}}=0$, and

$$\begin{cases} C_1:=(1+k)(1-kq),\\ C_2:=d\Big[(c-a)(1+k)+(b+ak)(1+q)\Big]. \end{cases} \tag{3.27}$$

This shows that for τ sufficiently small

$$\lambda_0(\tau) = 1 - \frac{C_2}{C_1}\tau + o(\tau). \tag{3.28}$$

Clearly $C_1 > 0$ from the conditions $|k| < 1$ and $|kq| < 1$. Indeed, we also have

$$\begin{aligned}
1 + k &= \frac{2\sigma_1}{\left[\sigma_1 + \alpha\overline{R}\log\left(\frac{\overline{R}}{R_1}\right)\right]}, && (3.29)\\
1 - kq &= \frac{2\alpha\overline{R}\left[\sigma_1\log\left(\frac{R_2}{\overline{R}}\right) + \sigma_2\log\left(\frac{\overline{R}}{R_1}\right)\right]}{\left[\sigma_1 + \alpha\overline{R}\log\left(\frac{\overline{R}}{R_1}\right)\right]\left[\sigma_2 + \alpha\overline{R}\log\left(\frac{R_2}{\overline{R}}\right)\right]}, && (3.30)\\
c - a &= \frac{2\phi R_2\left(\sigma_2 + \alpha\overline{R}\right)}{\overline{R}^2\left[\sigma_2 + \alpha\overline{R}\log\left(\frac{R_2}{\overline{R}}\right)\right]}, && (3.31)\\
b + ak &= \frac{-2\phi R_2\left(\sigma_1 + \alpha\overline{R}\right)}{\overline{R}^2\left[\sigma_2 + \alpha\overline{R}\log\left(\frac{R_2}{\overline{R}}\right)\right]}, && (3.32)\\
1 + q &= \frac{2\sigma_2}{\left[\sigma_2 + \alpha\overline{R}\log\left(\frac{R_2}{\overline{R}}\right)\right]}, && (3.33)
\end{aligned}$$

then

$$(c-a)(1+k) + (b+ak)(1+q) = \frac{4\alpha R_2\phi(\sigma_1 - \sigma_2)}{\overline{R}\left[\sigma_1 + \alpha\overline{R}\log\left(\frac{\overline{R}}{R_1}\right)\right]\left[\sigma_2 + \alpha\overline{R}\log\left(\frac{R_2}{\overline{R}}\right)\right]} \tag{3.34}$$

where k, q, c, a and b are respectively given by (3.21), (3.26), (3.25), (3.23) and (3.24). Hence, according to (3.22), we also get

$$\begin{aligned}
C_2 &= d\Big[(c-a)(1+k) + (b+ak)(1+q)\Big],\\
&= \frac{16\alpha\pi R_2^2\phi^2(\sigma_1 - \sigma_2)^2}{\sigma_2\overline{R}\left[\sigma_1 + \alpha\overline{R}\log\left(\frac{\overline{R}}{R_1}\right)\right]^2\left[\sigma_2 + \alpha\overline{R}\log\left(\frac{R_2}{\overline{R}}\right)\right]} > 0.
\end{aligned}$$

Then $C_2 > 0$ and from equation (3.28) there exists $\kappa > 0$ such that $\overline{\rho}(\tau) = |\lambda_0(\tau)| < 1$ for all $\tau \in]0, \kappa[$. This proves that G is a contraction for $\tau \in]0, \kappa[$, which gives the desired result.

□

Remark 3.3.4. *Using equations (3.29) and (3.30), we obtain*

$$\begin{aligned} C_1 &= (1+k)(1-kq), \\ &= \frac{4\sigma_1\alpha\overline{R}\left[\sigma_1\log\left(\frac{R_2}{\overline{R}}\right)+\sigma_2\log\left(\frac{\overline{R}}{R_1}\right)\right]}{\left[\sigma_1+\alpha\overline{R}\log\left(\frac{\overline{R}}{R_1}\right)\right]^2\left[\sigma_2+\alpha\overline{R}\log\left(\frac{R_2}{\overline{R}}\right)\right]}. \end{aligned}$$

Therefore,

$$\frac{C_2}{C_1} = \mathcal{J}''(\overline{R}) \ \textit{for all}\ \alpha > 0, \tag{3.35}$$

where $\mathcal{J}''(\overline{R})$ is given by (1.44).
This shows that for this specific case, the local convergence of Algorithm 2 is equivalent to the local convergence of Algorithm 1 described in Section 1.7.2 of Chapter 1.

3.3.3 The case of an open disk

This section is dedicated to the convergence analysis of Algorithm 2 in the case of an open disk domain of $\mathbb{R}^2$ and where the number of OSM iterations $L = 1$, i.e., we perform only one OSM step per iteration. Using the notation of Section 1.7.3 and Algorithm 2, the iterative scheme leads to the following. The boundary values at iteration k are of the form

$$\lambda_{i,N}^L(R^k) = \hat{\lambda}_{i,N}^L(R^k)\frac{\phi(\theta)}{m}, \quad \lambda_{i,D}^L(R^k) = \hat{\lambda}_{i,D}^L(R^k)\frac{\phi(\theta)}{m},$$

for some constants $\hat{\lambda}_{i,N}^L(R^k)$ and $\hat{\lambda}_{i,D}^L(R^k)$ and for $i = 1, 2$.
From (1.48), we have

$$\mathcal{J}'(R) = [\sigma(R)]\int_0^{2\pi}\left[\frac{1}{\sigma_1\sigma_2}\left(\left|\sigma(R)\frac{\partial v_{\sigma(R)}}{\partial\nu}\right|^2 - \left|\sigma(R)\frac{\partial u_{\sigma(R)}}{\partial\nu}\right|^2\right) + \left(|\nabla_\tau v_{\sigma(R)}|^2 - |\nabla_\tau u_{\sigma(R)}|^2\right)\right] R\, d\theta.$$

Therefore according to equations (2.46) and (2.51), the solutions after only one OSM step iterate are given in Ω_1 by

$$u_{\sigma(R^k)}(r,\theta) = \alpha_N^L(R^k)r^m\frac{\phi(\theta)}{m}, \quad v_{\sigma(R^k)}(r,\theta) = \alpha_D^L(R^k)r^m\frac{\phi(\theta)}{m},$$

for $R^k < r < R_2$ with

$$\begin{cases} \alpha_N^L(R) := \dfrac{\hat{\lambda}_{1,N}^L(R)}{R^{m-1}(m\sigma_1 + \alpha R)}, \\ \alpha_D^L(R) := \dfrac{\hat{\lambda}_{1,D}^L(R)}{R^{m-1}(m\sigma_1 + \alpha R)}. \end{cases}$$

Consequently, by step 3 of Algorithm 2, the gradient is approximated by

$$\frac{\partial \mathcal{J}}{\partial R}(R^k) \simeq \frac{\pi m^2(\sigma_1^2 - \sigma_2^2)R^k}{\sigma_2(\sigma_1 m + \alpha R^k)^2}(|\hat{\lambda}_{1,D}^L(R^k)|^2 - |\hat{\lambda}_{1,N}^L(R^k)|^2).$$

The iterative scheme of Algorithm 2 now reads

$$R^{k+1} = R^k - \tau \frac{\pi m^2(\sigma_1^2 - \sigma_2^2)R^k}{\sigma_2(\sigma_1 m + \alpha R^k)^2}(|\hat{\lambda}_{1,D}^L(R^k)|^2 - |\hat{\lambda}_{1,N}^L(R^k)|^2), \tag{3.36}$$

and the updates for the boundary values are given by

$$\begin{aligned} \hat{\lambda}_{1,N}^L(R^{k+1}) &= p_m^\alpha(R^k)\ \hat{\lambda}_{2,N}^L(R^k) + \eta_m^\alpha(R^k), && (3.37)\\ \hat{\lambda}_{2,N}^L(R^{k+1}) &= k_m^\alpha(R^k)\ \hat{\lambda}_{1,N}^L(R^k), && (3.38)\\ \hat{\lambda}_{1,D}^L(R^{k+1}) &= q_m^\alpha(R^k)\ \hat{\lambda}_{2,D}^L(R^k) + \omega_m^\alpha(R^k), && (3.39)\\ \hat{\lambda}_{2,D}^L(R^{k+1}) &= k_m^\alpha(R^k)\ \hat{\lambda}_{1,D}^L(R^k), && (3.40) \end{aligned}$$

where $p_m^\alpha(R^k)$, $\eta_m^\alpha(R^k)$, $k_m^\alpha(R^k)$, $q_m^\alpha(R^k)$ and $\omega_m^\alpha(R^k)$ are respectively given by (2.42), (2.47), (2.41), (2.43) and (2.52).

If we set $X^k := (R^k, \hat{\lambda}_{1,N}^L(R^k), \hat{\lambda}_{2,N}^L(R^k), \hat{\lambda}_{1,D}^L(R^k), \hat{\lambda}_{2,D}^L(R^k))$, then the iterative scheme formed by (3.36)-(3.40) can be synthetically written as

$$X^{k+1} = G(X^k),$$

where $G : \mathbb{R}^5 \longrightarrow \mathbb{R}^5$, $X = (x, y, z, t, h) \mapsto (g_1(X), g_2(X), g_3(X), g_4(X), g_5(X))$ are given by

$$\begin{aligned} g_1(X) &:= x - \tau \frac{\pi m^2(\sigma_1^2 - \sigma_2^2)x}{\sigma_2(\sigma_1 m + \alpha x)^2}(t^2 - y^2),\\ g_2(X) &:= p_m^\alpha(x)z + \eta_m^\alpha(x),\\ g_3(X) &:= k_m^\alpha(x)y,\\ g_4(X) &:= q_m^\alpha(x)h + \omega_m^\alpha(x),\\ g_5(X) &:= k_m^\alpha(x)t. \end{aligned}$$

From the analysis of section (2.4.3) we observe that the sequence $\hat{\lambda}^{\ell}_{i,N}(\overline{R})$, $i = 1, 2$ converges to $\hat{\lambda}^{\infty}_{i,N}(\overline{R})$, $i = 1, 2$, where

$$\hat{\lambda}^{\infty}_{i,N}(\overline{R}) = \frac{2R_2^{m+1}\overline{R}^{m-1}}{\sigma_1\left(R_2^{2m} + \overline{R}^{2m}\right) + \sigma_2\left(R_2^{2m} - \overline{R}^{2m}\right)}\psi_i$$

with

$$\psi_1 = (\sigma_1 m + \alpha\overline{R}) \quad \text{and} \quad \psi_2 = (\sigma_1 m - \alpha\overline{R}).$$

Similarly, the sequence $\hat{\lambda}^{\ell}_{i,D}(\overline{R})$, $i = 1, 2$ converges to $\hat{\lambda}^{\infty}_{i,D}(\overline{R})$, $i = 1, 2$, where

$$\hat{\lambda}^{\infty}_{i,D}(\overline{R}) = \frac{2\sigma_2 C_f R_2^{m}\overline{R}^{m-1}}{\sigma_1\left(R_2^{2m} - \overline{R}^{2m}\right) + \sigma_2\left(R_2^{2m} + \overline{R}^{2m}\right)}\psi_i.$$

Moreover, we have

$$\begin{cases} \hat{\lambda}^{\infty}_{1,N}(\overline{R}) = p^{\alpha}_m(\overline{R})\hat{\lambda}^{\infty}_{2,N}(\overline{R}) + \eta^{\alpha}_m(\overline{R}), \\ \hat{\lambda}^{\infty}_{2,N}(\overline{R}) = k^{\alpha}_m(\overline{R})\hat{\lambda}^{\infty}_{1,N}(\overline{R}), \\ \hat{\lambda}^{\infty}_{1,D}(\overline{R}) = q^{\alpha}_m(\overline{R})\hat{\lambda}^{\infty}_{2,D}(\overline{R}) + w^{\alpha}_m(\overline{R}), \\ \hat{\lambda}^{\infty}_{2,D}(\overline{R}) = k^{\alpha}_m(\overline{R})\hat{\lambda}^{\infty}_{1,D}(\overline{R}). \end{cases}$$

Using the expression of C_f given by (1.46) one can easily check that $\hat{\lambda}^{\infty}_{i,N}(\overline{R}) = \hat{\lambda}^{\infty}_{i,D}(\overline{R})$ and then $\overline{X} = \left(\overline{R}, \hat{\lambda}^{\infty}_{1,N}(\overline{R}), \hat{\lambda}^{\infty}_{2,N}(\overline{R}), \hat{\lambda}^{\infty}_{1,D}(\overline{R}), \hat{\lambda}^{\infty}_{2,D}(\overline{R})\right) = \left(\overline{R}, \hat{\lambda}^{\infty}_{1,N}(\overline{R}), \hat{\lambda}^{\infty}_{2,N}(\overline{R}), \hat{\lambda}^{\infty}_{1,N}(\overline{R}), \hat{\lambda}^{\infty}_{2,N}(\overline{R})\right)$ is a fixed point of G. We first establish in the following lemma that $\overline{X}$ is the unique fixed point of G.

Lemma 3.3.3. *The point $\overline{X}$ defined above is the unique fixed point of G.*

Proof. Let $X = (x, y, z, t, h)$ a fixed point of G, then we have:

$$\begin{cases} t = y, \\ y = p^{\alpha}_m(x)z + \eta^{\alpha}_m(x), \\ z = k^{\alpha}_m(x)y, \\ t = q^{\alpha}_m(x)h + w^{\alpha}_m(x), \\ h = k^{\alpha}_m(x)t. \end{cases}$$

Consequently

$$\begin{pmatrix} y \\ \\ z \end{pmatrix} = \begin{pmatrix} 0 & p^{\alpha}_m(x) \\ \\ k^{\alpha}_m(x) & 0 \end{pmatrix} \begin{pmatrix} y \\ \\ z \end{pmatrix} + \begin{pmatrix} \eta^{\alpha}_m(x) \\ \\ 0 \end{pmatrix}.$$

and

$$\begin{pmatrix} t \\ \\ h \end{pmatrix} = \begin{pmatrix} 0 & q_m^\alpha(x) \\ \\ k_m^\alpha(x) & 0 \end{pmatrix} \begin{pmatrix} t \\ \\ h \end{pmatrix} + \begin{pmatrix} w_m^\alpha(x) \\ \\ 0 \end{pmatrix},$$

then we have:

$$\begin{cases} y = \dfrac{2R_2^{m+1}x^{m-1}(\sigma_1 m + \alpha x)}{\sigma_1\left(R_2^{2m} + x^{2m}\right) + \sigma_2\left(R_2^{2m} - x^{2m}\right)}, \\ \\ t = \dfrac{2\sigma_2 C_f R_2^m x^{m-1}(\sigma_1 m + \alpha x)}{\sigma_1\left(R_2^{2m} - x^{2m}\right) + \sigma_2\left(R_2^{2m} + x^{2m}\right)}. \end{cases}$$

Therefore,

$$C_f = \frac{R_2}{\sigma_2}\frac{[\sigma_1(R_2^{2m} - x^{2m}) + \sigma_2(R_2^{2m} + x^{2m})]}{[\sigma_1(R_2^{2m} + x^{2m}) + \sigma_2(R_2^{2m} - x^{2m})]}.$$

where the mapping defined on $]0, R_2[$ by :

$$g(x) = \frac{R_2}{\sigma_2}\frac{[\sigma_1(R_2^{2m} - x^{2m}) + \sigma_2(R_2^{2m} + x^{2m})]}{[\sigma_1(R_2^{2m} + x^{2m}) + \sigma_2(R_2^{2m} - x^{2m})]}$$

is one to one. We deduce that, $x = \overline{R}$, and then

$$X = \left(\overline{R}, \hat{\lambda}_{1,N}^\infty(\overline{R}), \hat{\lambda}_{2,N}^\infty(\overline{R}), \hat{\lambda}_{1,D}^\infty(\overline{R}), \hat{\lambda}_{2,D}^\infty(\overline{R})\right) = \overline{X}.$$

□

Theorem 3.3.5. *There exists $\alpha_0 > 0$ such that for all $\alpha \in]0, \alpha_0[$ Algorithm 2 with $L = 1$ is locally convergent for all $\tau \in]0, \delta_\alpha[$ for some $\delta_\alpha > 0$.*

Proof. For short notation, let us set $\overline{x} = \overline{R}$, $\overline{y} = \hat{\lambda}_{1,N}^\infty$, and

$$k := k_m^\alpha(\overline{x}) = \frac{\sigma_1 m - \alpha\overline{x}}{\sigma_1 m + \alpha\overline{x}} = \frac{\psi_2}{\psi_1}. \tag{3.41}$$

Then from the previous Lemma, $\overline{X} = (\overline{x}, \overline{y}, k\overline{y}, \overline{y}, k\overline{y})$ is the unique fixed point of G. In order to prove the local convergence we shall establish that G is a contraction in a neighborhood

of $\overline{X}$. This requires the study of the Jacobian matrix $DG(\overline{X})$. The latter is given by

$$DG(\overline{X}) = \begin{pmatrix} 1 & d\tau & 0 & -d\tau & 0 \\ a & 0 & p & 0 & 0 \\ b & k & 0 & 0 & 0 \\ c & 0 & 0 & 0 & q \\ b & 0 & 0 & k & 0 \end{pmatrix}$$

where we have set for short notation

$$d := \frac{1}{\tau}\frac{\partial g_1}{\partial y}(\overline{X}) = \frac{2\pi m^2(\sigma_1^2 - \sigma_2^2)\overline{x}}{\sigma_2(\sigma_1 m + \alpha\overline{x})^2}\overline{y}, \tag{3.42}$$

$$a := \frac{\partial g_2}{\partial x}(\overline{X}) = \frac{-2m\alpha\sigma_2(4mR_2^{2m}\overline{x}^{2m} - \overline{x}^{4m} + R_2^{4m})}{\left[\sigma_2 m(R_2^{2m} - \overline{x}^{2m}) + \alpha\overline{x}(R_2^{2m} + \overline{x}^{2m})\right]^2}k\overline{y} \tag{3.43}$$

$$+ \frac{4m\alpha R_2^{m+1}\overline{x}^{m-1}\left[(\sigma_2 m^2 - \alpha\overline{x})(R_2^{2m} + \overline{x}^{2m}) + \alpha\overline{x}m(R_2^{2m} - \overline{x}^{2m})\right]}{\left[\sigma_2 m(R_2^{2m} - \overline{x}^{2m}) + \alpha\overline{x}(R_2^{2m} + \overline{x}^{2m})\right]^2} \tag{3.44}$$

$$p := \frac{\partial g_2}{\partial z}(\overline{X}) = p_m^{\alpha}(\overline{x}), \tag{3.45}$$

$$b := \frac{\partial g_3}{\partial x}(\overline{X}) = \frac{-2\sigma_1 m\alpha}{(\sigma_1 m + \alpha\overline{x})^2}\overline{y} \tag{3.46}$$

$$c := \frac{\partial g_4}{\partial x}(\overline{X}) = \frac{2m\alpha\sigma_2(4mR_2^{2m}\overline{x}^{2m} + \overline{x}^{4m} - R_2^{4m})}{\left[\sigma_2 m(R_2^{2m} + \overline{x}^{2m}) + \alpha\overline{x}(R_2^{2m} - \overline{x}^{2m})\right]^2}k\overline{y} \tag{3.47}$$

$$+ \frac{4m\sigma_2\alpha C_f R_2^m\overline{x}^{m-1}\left[(\sigma_2 m^2 - \alpha\overline{x})(R_2^{2m} - \overline{x}^{2m}) + \alpha\overline{x}m(R_2^{2m} + \overline{x}^{2m})\right]}{\left[\sigma_2 m(R_2^{2m} + \overline{x}^{2m}) + \alpha\overline{x}(R_2^{2m} - \overline{x}^{2m})\right]^2}, \tag{3.48}$$

$$q := \frac{\partial g_4}{\partial h}(\overline{X}) = q_m^{\alpha}(\overline{x}). \tag{3.49}$$

For every $(\lambda, \tau) \in \mathbb{R} \times \mathbb{R}$, we define the characteristic polynomial of $DG(\overline{X})$

$$P(\lambda,\tau) := det(DG(\overline{X}) - \lambda I_5) = \begin{vmatrix} 1-\lambda & d\tau & 0 & -d\tau & 0 \\ a & -\lambda & p & 0 & 0 \\ b & k & -\lambda & 0 & 0 \\ c & 0 & 0 & -\lambda & q \\ b & 0 & 0 & k & -\lambda \end{vmatrix}$$

and we denote by $\lambda_i(\tau) \in \mathbb{C}$, $i = 1, \ldots, 5$, the eigenvalues of $DG(\overline{X})$. Then, we have

$$P(\lambda, \tau) = (1-\lambda)(\lambda^2 - kp)(\lambda^2 - kq) - \tau\, d\left[(c-a)\lambda^3 + b(q-p)\lambda^2 + (aq-cp)k\lambda\right], \quad (3.50)$$

and $P(\lambda_i(\tau), \tau) = 0$ for $i = 1, \ldots, 5$.

Let $\overline{\rho}(\tau) := \max\{|\lambda_i(\tau)|;\ \ i = 1, \ldots, 5\}$ be the spectral radius of $DG(\overline{X})$. We remark that for $\tau = 0$, we have

$$P(\lambda, 0) = (1-\lambda)(\lambda^2 - kp)(\lambda^2 - kq),$$

and therefore, the eigenvalues of the $DG(\overline{X})$ for $\tau = 0$ are given by

$$(\lambda_1(0), \lambda_2(0), \lambda_3(0), \lambda_4(0), \lambda_5(0)) = \left(1, \sqrt{kp}, -\sqrt{kq}, \sqrt{kq}, -\sqrt{kq}\right),$$

where $|kp| < 1$, $|kq| < 1$, and $kq \neq kp$ if α sufficiently small. Then, for $\tau = 0$ and α sufficiently small, all eigenvalues of $DG(\overline{X})$ are simple and verify:

$$|\lambda_1(0)| = 1, \text{ and } |\lambda_i(0)| < 1 \quad \forall\, i \in \{2, 3, 4, 5\}.$$

Consequently, there exists a small enough number $\delta > 0$ such that all eigenvalues of $DG(\overline{X})$ are simple for all $\tau \in]0, \delta[$ and

$$\lim_{\tau \to 0} \lambda_i(\tau) = \lambda_i(0) \ \ \forall\, i \in \{1, 2, 3, 4, 5\}.$$

Thus one can choose $\delta > 0$ sufficiently small such that $|\lambda_i(\tau)| < 1$ for $i \in \{2, 3, 4, 5\}$, $\overline{\rho}(\tau) = |\lambda_0(\tau)|$ for all $\tau \in]0, \delta[$. Moreover $\lim\limits_{\tau \longrightarrow 0} \overline{\rho}(\tau) = 1$. To show that if $\overline{\rho}(\tau) < 1$ for small enough $\tau > 0$, we use a first order Taylor expansion of $(\lambda, \tau) \mapsto P(\lambda, \tau)$ in a neighborhood of the point $(1, 0)$. Indeed

$$\begin{aligned} P(\lambda, \tau) &= P(1,0) + \frac{\partial P}{\partial \lambda}(1,0)\,(\lambda - 1) + \frac{\partial P}{\partial \tau}(1,0)\,\tau + \epsilon(\lambda, \tau) \\ &= C_1(1-\lambda) - C_2\tau + \epsilon(\lambda, \tau) \end{aligned}$$

where $\lim\limits_{(\lambda,\tau)\to(1,0)} \dfrac{|\epsilon(\lambda,\tau)|}{\sqrt{(1-\lambda)^2 + \tau^2}} = 0$, and

$$\begin{cases} C_1 := (1-kp)(1-kq), \\ C_2 := d\Big[(c-a)(1-kp) + (q-p)(b+ak)\Big]. \end{cases} \quad (3.51)$$

This shows that for τ sufficiently small

$$\lambda_0(\tau) = 1 - \frac{C_2}{C_1}\tau + o(\tau). \tag{3.52}$$

Clearly $C_1 > 0$ from the conditions $|kp| < 1$ and $|kq| < 1$. Let $\alpha \in]0, \alpha_0[$ where α_0 is as in Lemma 3.3.4. Then we also have that $C_2 > 0$. We then infer from equation (3.52) the existence of $\delta_\alpha > 0$ such that $\overline{\rho}(\tau) = |\lambda_0(\tau)| < 1$ for all $\tau \in]0, \delta_\alpha[$. This proves that G is a contraction for $\tau \in]0, \delta_\alpha[$, which gives the desired result.

□

Lemma 3.3.4. *There exists $\alpha_0 > 0$ such that $C_2 > 0$ for all $0 < \alpha < \alpha_0$ where $C_2 = C_2(\alpha)$ is given by* (3.51).

Proof. We first observe that

$$\overline{y} \sim k\overline{y} \sim \frac{2m\sigma_1 R_2^{m+1}\overline{R}^{m-1}}{\sigma_1\left(R_2^{2m} + \overline{R}^{2m}\right) + \sigma_2\left(R_2^{2m} - \overline{R}^{2m}\right)} \text{ as } \alpha \to 0.$$

Then, using a first order Taylor expansion of $a,\ b,\ c,\ d,\ k,\ p,\ q$, in a neighborhood of $\alpha = 0$ we get the following equivalences as $\alpha \to 0$

$$d \sim \frac{2\pi\left(\sigma_1^2 - \sigma_2^2\right)\overline{x}}{\sigma_1^2\sigma_2}\overline{y} \sim \frac{4m\pi(\sigma_1^2 - \sigma_2^2)R_2^{m+1}\overline{R}^m}{\sigma_1\sigma_2\left[\sigma_1\left(R_2^{2m} + \overline{R}^{2m}\right) + \sigma_2\left(R_2^{2m} - \overline{R}^{2m}\right)\right]}, \tag{3.53}$$

$$
\begin{aligned}
b &\sim \frac{-2\alpha}{m\sigma_1}\overline{y} \sim \frac{-4\alpha R_2^{m+1}\overline{R}^{m-1}}{\sigma_1\left(R_2^{2m}+\overline{R}^{2m}\right)+\sigma_2\left(R_2^{2m}-\overline{R}^{2m}\right)},\\
k &\sim 1-\frac{2\alpha\overline{R}}{m\sigma_1},\\
p &\sim 1-\frac{2\alpha\overline{R}\left(R_2^{2m}+\overline{R}^{2m}\right)}{m\sigma_2\left(R_2^{2m}-\overline{R}^{2m}\right)},\\
q &\sim 1-\frac{2\alpha\overline{R}\left(R_2^{2m}-\overline{R}^{2m}\right)}{m\sigma_2\left(R_2^{2m}+\overline{R}^{2m}\right)},\\
a &\sim \frac{-2\alpha\left(4mR_2^{2m}\overline{R}^{2m}-\overline{R}^{4m}+\overline{R_2}^{4m}\right)}{m\sigma_2\left(R_2^{2m}-\overline{R}^{2m}\right)^2}\overline{y}+\frac{4m\alpha R_2^{m+1}\overline{R}^{m-1}\left(R_2^{2m}+\overline{R}^{2m}\right)}{\sigma_2\left(R_2^{2m}-\overline{R}^{2m}\right)^2},\\
&\sim \frac{4\alpha R_2^{m+1}\overline{R}^{m-1}\left[m\sigma_1\left(R_2^{2m}-\overline{R}^{2m}\right)+(m\sigma_2-\sigma_1)\left(R_2^{2m}+\overline{R}^{2m}\right)\right]}{\sigma_2\left(R_2^{2m}-\overline{R}^{2m}\right)\left[\sigma_1\left(R_2^{2m}+\overline{R}^{2m}\right)+\sigma_2\left(R_2^{2m}-\overline{R}^{2m}\right)\right]},\\
c &\sim \frac{2\alpha\left(4mR_2^{2m}\overline{R}^{2m}+\overline{R}^{4m}-\overline{R_2}^{4m}\right)}{m\sigma_2\left(R_2^{2m}+\overline{R}^{2m}\right)^2}\overline{y}+\frac{4m\alpha C_f R_2^m\overline{R}^{m-1}\left(R_2^{2m}-\overline{R}^{2m}\right)}{\left(R_2^{2m}+\overline{R}^{2m}\right)^2},\\
&\sim \frac{4\alpha R_2^{m+1}\overline{R}^{m-1}\left[m\sigma_1\left(R_2^{2m}+\overline{R}^{2m}\right)+(m\sigma_2-\sigma_1)\left(R_2^{2m}-\overline{R}^{2m}\right)\right]}{\sigma_2\left(R_2^{2m}+\overline{R}^{2m}\right)\left[\sigma_1\left(R_2^{2m}+\overline{R}^{2m}\right)+\sigma_2\left(R_2^{2m}-\overline{R}^{2m}\right)\right]}.
\end{aligned}
$$

Then we infer that

$$
c-a \sim \frac{16\alpha(\sigma_1-m\sigma_2)R_2^{3m+1}\overline{R}^{3m-1}}{\sigma_2\left(R_2^{4m}-\overline{R}^{4m}\right)\left[\sigma_1\left(R_2^{2m}+\overline{R}^{2m}\right)+\sigma_2\left(R_2^{2m}-\overline{R}^{2m}\right)\right]},
$$

$$
1-kp \sim \frac{2\alpha\overline{R}\left[\sigma_1\left(R_2^{2m}+\overline{R}^{2m}\right)+\sigma_2\left(R_2^{2m}-\overline{R}^{2m}\right)\right]}{m\sigma_1\sigma_2\left(R_2^{2m}-\overline{R}^{2m}\right)}, \tag{3.54}
$$

$$
1-kq \sim \frac{2\alpha\overline{R}\left[\sigma_1\left(R_2^{2m}-\overline{R}^{2m}\right)+\sigma_2\left(R_2^{2m}+\overline{R}^{2m}\right)\right]}{m\sigma_1\sigma_2\left(R_2^{2m}+\overline{R}^{2m}\right)}, \tag{3.55}
$$

$$
\begin{aligned}
q-p &\sim \frac{8\alpha R_2^{2m}\overline{R}^{2m+1}}{m\sigma_2\left(R_2^{4m}-\overline{R}^{4m}\right)},\\
b+ak\sim b+a &\sim \frac{4\alpha R_2^{m+1}\overline{R}^{m-1}\left[(m\sigma_1-\sigma_2)\left(R_2^{2m}-\overline{R}^{2m}\right)+(m\sigma_2-\sigma_1)\left(R_2^{2m}+\overline{R}^{2m}\right)\right]}{\sigma_2\left(R_2^{2m}-\overline{R}^{2m}\right)\left[\sigma_1\left(R_2^{2m}+\overline{R}^{2m}\right)+\sigma_2\left(R_2^{2m}-\overline{R}^{2m}\right)\right]}.
\end{aligned}
$$

Consequently,

$$
\begin{aligned}
(c-a)(1-kp) &\sim \frac{32\alpha^2(\sigma_1-m\sigma_2)R_2^{3m+1}\overline{R}^{3m}}{m\sigma_1\sigma_2^2\left(R_2^{4m}-\overline{R}^{4m}\right)\left(R_2^{2m}-\overline{R}^{2m}\right)},\\
(q-p)(b+ak) &\sim \frac{32\alpha^2 R_2^{3m+1}\overline{R}^{3m}\left[(m\sigma_1-\sigma_2)\left(R_2^{2m}-\overline{R}^{2m}\right)+(m\sigma_2-\sigma_1)\left(R_2^{2m}+\overline{R}^{2m}\right)\right]}{m\sigma_2^2\left(R_2^{4m}-\overline{R}^{4m}\right)\left(R_2^{2m}-\overline{R}^{2m}\right)\left[\sigma_1\left(R_2^{2m}+\overline{R}^{2m}\right)+\sigma_2\left(R_2^{2m}-\overline{R}^{2m}\right)\right]},
\end{aligned}
$$

and from equations (3.51) and (3.53), we obtain

$$
C_2 \sim \frac{128\pi\alpha^2 m\left(\sigma_1^2-\sigma_2^2\right)^2 R_2^{4m+2}\overline{R}^{4m}}{\sigma_1^2\sigma_2^3\left(R_2^{4m}-\overline{R}^{4m}\right)\left[\sigma_1\left(R_2^{2m}+\overline{R}^{2m}\right)+\sigma_2\left(R_2^{2m}-\overline{R}^{2m}\right)\right]^2}>0.
$$

□

Remark 3.3.6. *C_1, C_2 and $DG(\overline{X})$ deserve a few remarks.*

1. *Using equations (3.51), (3.54) and (3.55), we obtain*

$$
C_1 \sim \frac{4\alpha^2\overline{R}^2\left[\sigma_1\left(R_2^{2m}+\overline{R}^{2m}\right)+\sigma_2\left(R_2^{2m}-\overline{R}^{2m}\right)\right]\left[\sigma_1\left(R_2^{2m}-\overline{R}^{2m}\right)+\sigma_2\left(R_2^{2m}+\overline{R}^{2m}\right)\right]}{m^2\sigma_1^2\sigma_2^2\left(R_2^{4m}-\overline{R}^{4m}\right)},
$$

   as $\alpha\to 0$. Therefore,

$$
\frac{C_2}{C_1} \sim \mathcal{J}''(\overline{R}) \text{ as } \alpha\to 0. \tag{3.56}
$$

   This shows that the local convergence of Algorithm 2 is equivalent to the local convergence of Algorithm 1, as described in Section 1.7.3 for this specific case.

2. *We conjecture that the exact equality $\dfrac{C_2}{C_1}=\mathcal{J}''(\overline{R})$ also holds true for all $\alpha>0$.*

3. We observe that

$$DG(\overline{X}) \sim A = \begin{pmatrix} 1 & 0 & 0 & 0 & 0 \\ 0 & 0 & 1 & 0 & 0 \\ 0 & 1 & 0 & 0 & 0 \\ 0 & 0 & 0 & 0 & 1 \\ 0 & 0 & 0 & 1 & 0 \end{pmatrix} \text{ as } m \to +\infty$$

and the spectral radius of the matrix A is equal 1. *Consequently*

$$\lim_{m \to +\infty} \overline{\rho}(DG(\overline{X})) = 1.$$

The following proposition proves the conjecture of the above Remark in the particular case where $\sigma_1 = 1$, $\sigma_2 = 2$, $R_2 = 1$ and $m = 1$.

Proposition 3.3.5. *Let us fix $\sigma_1 = 1$, $\sigma_2 = 2$, $R_2 = 1$ and $m = 1$. Then, for all $\alpha > 0$ and $\overline{R} \in]0, R_2[$, we have the following equality:*

$$\frac{C_2}{C_1} = \mathcal{J}''(\overline{R}). \tag{3.57}$$

Proof. Let $m = 1$, $\sigma_1 = 1$, $\sigma_2 = 2$, and $R_2 = 1$, we first observe that

$$\begin{aligned} C_f &= \frac{3 + \overline{R}}{2(3 - \overline{R})}, \\ \overline{y} &= \frac{2(1 + \alpha\overline{R})}{3 - \overline{R}^2}. \end{aligned}$$

According to equations (3.41), (3.45), (3.49), (3.42), (3.47), (3.43), and (3.46), we can obtain the simplified expressions for k, p, q, d, c, a, and b as follows:

$$d = \frac{6\pi\overline{R}}{(1 + \alpha\overline{R})(3 - \overline{R}^2)},$$

$$
\begin{aligned}
b &= -\frac{4\alpha}{(1+\alpha\overline{R})(3-\overline{R}^2)},\\
p &= \frac{2(1-\overline{R}^2)-\alpha\overline{R}(1+\overline{R}^2)}{2(1-\overline{R}^2)+\alpha\overline{R}(1+\overline{R}^2)},\\
q &= \frac{2(1+\overline{R}^2)-\alpha\overline{R}(1-\overline{R}^2)}{2(1+\overline{R}^2)+\alpha\overline{R}(1-\overline{R}^2)},\\
a &= \frac{8\alpha}{(3-\overline{R}^2)\left[\alpha\overline{R}(1+\overline{R}^2)+2(1-\overline{R}^2)\right]},\\
c &= \frac{8\alpha}{(3-\overline{R}^2)\left[\alpha\overline{R}(1-\overline{R}^2)+2(1+\overline{R}^2)\right]}.
\end{aligned}
$$

Then we infer that

$$
\begin{aligned}
c-a &= \frac{16\alpha\overline{R}^2(\alpha\overline{R}-2)}{(3-\overline{R}^2)\left[\alpha\overline{R}(1-\overline{R}^2)+2(1+\overline{R}^2)\right]\left[\alpha\overline{R}(1+\overline{R}^2)+2(1-\overline{R}^2)\right]},\\
1-kp &= \frac{2\alpha\overline{R}(3-\overline{R}^2)}{(1+\alpha\overline{R})\left[\alpha\overline{R}(1+\overline{R}^2)+2(1-\overline{R}^2)\right]},\\
1-kq &= \frac{2\alpha\overline{R}(3+\overline{R}^2)}{(1+\alpha\overline{R})\left[\alpha\overline{R}(1-\overline{R}^2)+2(1+\overline{R}^2)\right]},\\
q-p &= \frac{16\alpha\overline{R}^3}{\left[\alpha\overline{R}(1+\overline{R}^2)+2(1-\overline{R}^2)\right]\left[\alpha\overline{R}(1-\overline{R}^2)+2(1+\overline{R}^2)\right]},\\
b+ak &= \frac{4\alpha\overline{R}\left[2\overline{R}-\alpha(3+\overline{R}^2)\right]}{(3-\overline{R}^2)(1+\alpha\overline{R})\left[\alpha\overline{R}(1+\overline{R}^2)+2(1-\overline{R}^2)\right]}.
\end{aligned}
$$

Consequently,

$$
\begin{aligned}
C_1 := (1-kp)(1-kq) &= \frac{4\alpha^2\overline{R}^2(9-\overline{R}^4)}{(1+\alpha\overline{R})^2\left[\alpha\overline{R}(1+\overline{R}^2)+2(1-\overline{R}^2)\right]\left[\alpha\overline{R}(1-\overline{R}^2)+2(1+\overline{R}^2)\right]},\\
(c-a)(1-kp) &= \frac{32\alpha^2\overline{R}^3(\alpha\overline{R}-2)}{(1+\alpha\overline{R})\left[\alpha\overline{R}(1+\overline{R}^2)+2(1-\overline{R}^2)\right]^2\left[\alpha\overline{R}(1-\overline{R}^2)+2(1+\overline{R}^2)\right]},
\end{aligned}
$$

$$(q-p)(b+ak) = \frac{64\alpha^2\overline{R}^4\left[2\overline{R}-\alpha(3+\overline{R}^2)\right]}{(3-\overline{R}^2)(1+\alpha\overline{R})\left[\alpha\overline{R}(1+\overline{R}^2)+2(1-\overline{R}^2)\right]^2\left[\alpha\overline{R}(1-\overline{R}^2)+2(1+\overline{R}^2)\right]},$$

and from equation (3.51), we obtain

$$C_2 = \frac{576\ \alpha^2\pi\overline{R}^4}{(3-\overline{R}^2)^2(1+\alpha\overline{R})^2\left[\alpha\overline{R}(1+\overline{R}^2)+2(1-\overline{R}^2)\right]\left[\alpha\overline{R}(1-\overline{R}^2)+2(1+\overline{R}^2)\right]}.$$

Hence,

$$\frac{C_2}{C_1} = \frac{144\pi\overline{R}^2}{(3+\overline{R}^2)(3-\overline{R}^2)^3} > 0 \ \ \forall\ \alpha > 0 \text{ and } \overline{R} \in]0, R_2[,$$

and from equation (1.49), we deduce that

$$\frac{C_2}{C_1} = \mathcal{J}''(\overline{R}).$$

□

3.4 Numerical experiments and validation

The goal of this section is to test the efficiency of Algorithm 2 in comparison with the standard descent gradient described in Algorithm 1. We shall employ synthetic data numerically generated using a finite elements solver designed with the help of FreeFem++ [35]. Indeed, we use a direct solver to generate the data, while the OSM is used in the inversion for Algorithm 2. We further avoid any inverse crime by making sure that the meshes used for generating the data have no connections with the ones used in the inversion. Actually, the latter vary during iterations since the interface Σ changes. Moreover, in most of the examples below the geometry of Σ can not be exactly represented by the parametrization (1.29) used in the inversion algorithms.

For all the examples below, the domain Ω is the open disk of center $(0,0)$ and radius $R_2 = 2$, the current flux $\phi(\theta) = \cos(\theta)$, $\theta \in [0, 2\pi]$, the conductivity parameters $\sigma_1 = 1$, $\sigma_2 = 2$ and the OSM parameter $\alpha = 1$. The measured data f is represented by the values f_i, $i = 1, \ldots, N_\Gamma$ of the numerical solution u_{num} at the nodes belonging to Γ. In order to simulate noise in the data f we artificially corrupt the computed values f_i with random noise as follows

$$f_i^\epsilon := f_i + \epsilon(1-2r_i)f_i,\ i = 1, \ldots, N_\Gamma,$$

where r_i are randomly chosen between 0 and 1 and ϵ denotes the noise level. In addition to representing the obtained geometrical reconstructions we shall also give the evolution of the dimensionless square-root cost functional $\sqrt{\mathcal{J}/\mathcal{J}_0}$ during iterations where $\mathcal{J}$ is given by (1.30) and

$$\mathcal{J}_0 := \int_\Omega \sigma |\nabla u_{\text{num}}|^2 dx.$$

3.4.1 Discussion of Algorithm 2 for a kite shape

In the first example we choose Σ to be a kite defined by

$$x(t) = \cos(t) + 0.5\cos(2t) - 0.4 \text{ and } y(t) = 1.2\sin(t),\ t \in [0, 2\pi]. \tag{3.58}$$

For the inversion algorithms we use the parametrization (1.29) with $n = 19$. The initial guess is $R_j^0 = 1.8$, for $j = 0, \ldots, n-1$. The results of the inversion are given in Figure 3.1(b) for Algorithm 1 and Figure 3.1(c) for Algorithm 2 with $L = 1$, i.e only one OSM step is used at each gradient descent iteration. We observe that we qualitatively obtain the same accuracy for both algorithms. The evolution of the cost functional is depicted in Figure 3.2(left). We remark that the cost functional increases in the first iterations for Algorithm 2, which means that the approximated OSM solution is not yet sufficiently close to the exact one and therefore the approximate gradient is not yet a descent direction. This is corrected as the iteration number increases. Whence the iteration number is sufficiently large we notice that the speed of convergence represented by the slope of the curves is roughly the same between the two algorithms. This indeed shows the superiority and relevance of Algorithm 2 which achieves comparative performances with potentially much cheaper numerical cost per iteration. Figure 3.2(middle) and (right) show the effect of increasing the number L of OSM steps. We naturally observe that as this number increases, Algorithm 2 becomes closer to Algorithm 1. Let us also mention that, other numerical tests not reported here suggest that this observation also holds when we fix L, for instance $L = 1$, and decrease the descent step τ (see also Figure 3.7(right)).

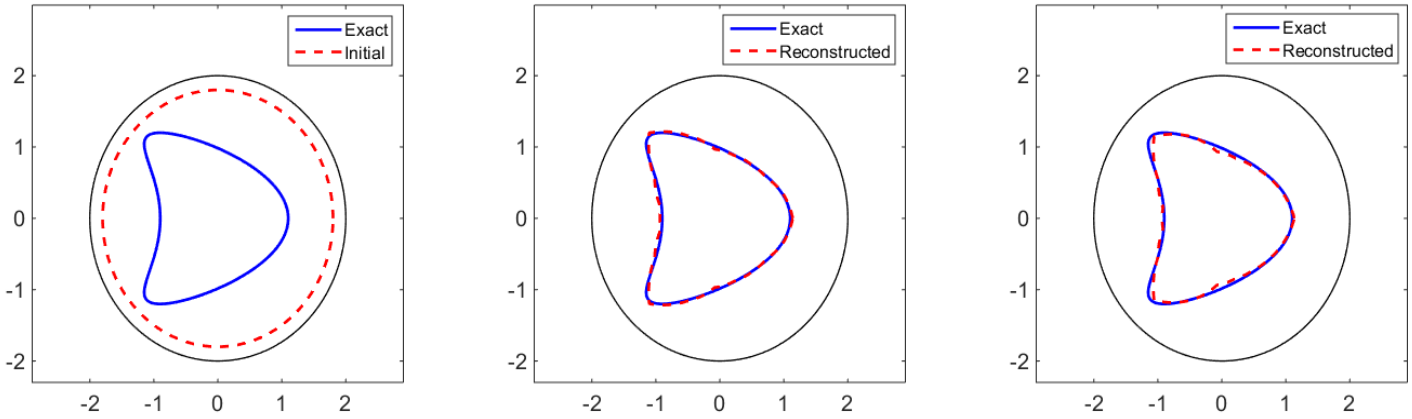

(a) Initial guess (b) Algorithm 1 (c) Algorithm 2

Figure 3.1: Comparison between Algorithm 1 and Algorithm 2 with $L = 1$ for the case of the kite parameterized by (3.58) and for noise free data. The exact shape and initial guess are shown in Figure (a). The gradient descent parameter $\tau = 0.05$ for both algorithms.

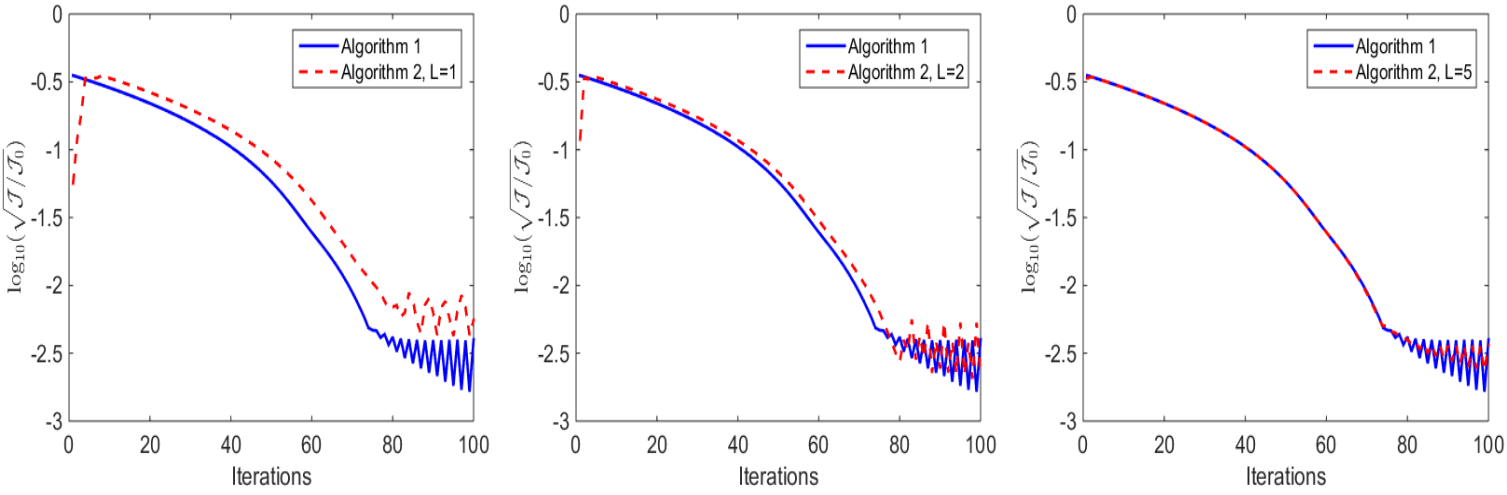

Figure 3.2: Comparison of the evolution of $\log_{10}(\sqrt{\mathcal{J}/\mathcal{J}_0})$ between Algorithm 1 and Algorithm 2 with $L = 1$ (left), $L = 2$ (middle) and $L = 5$ (right) for the example shown in Figure 3.1. The gradient descent parameter is $\tau = 0.05$.

Figure 3.3 shows the reconstructions obtained by Algorithm 2 for the example discussed in Figure 3.1 but for noisy data with noise level $\epsilon = 1\%$ (left), $\epsilon = 3\%$ (middle) and $\epsilon = 5\%$ (right). We observe robustness of the obtained results and a good accuracy which is very

similar to the one obtains with Algorithm 1.

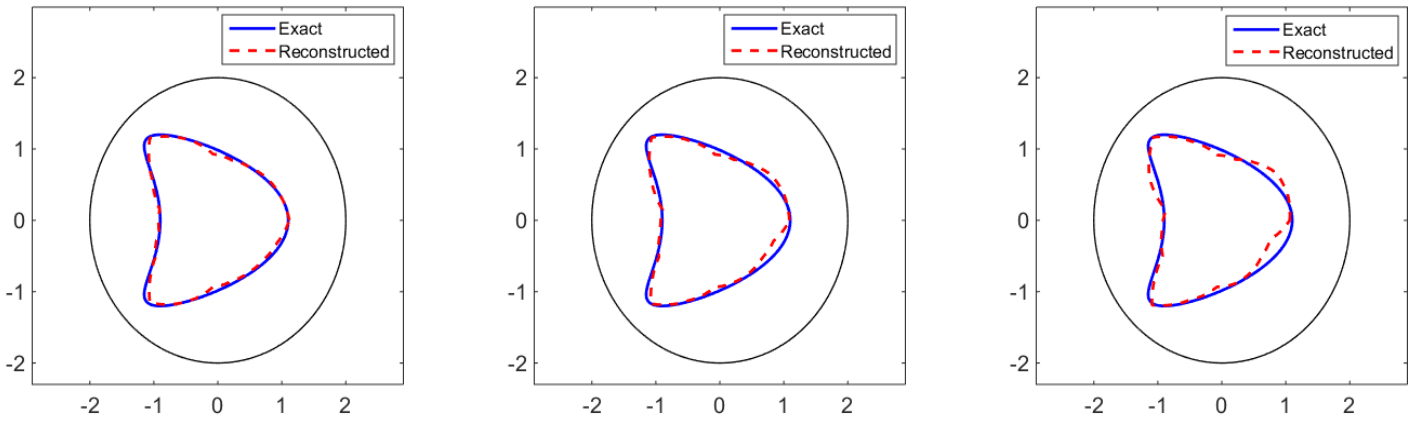

Figure 3.3: Reconstructions obtained by Algorithm 2 with $L = 1$ for the example discussed in Figure 3.1 but for noisy data with noise level $\epsilon = 1\%$ (left), $\epsilon = 3\%$ (middle) and $\epsilon = 5\%$ (right).

3.4.2 The example of other geometries

We report in Figure 3.4 and Figure 3.5 the reconstructions obtained by Algorithm 2, $L = 1$ for other geometries, keeping the same parameters as in Example 3.4.1 and with noise levels $\epsilon = 3\%$ and $\epsilon = 5\%$. The parametrizations of these geometries are given by Table 3.1.

Geometry type	Parametrization $(x(t), y(t))$
Peanut shaped	$1.5\sqrt{\cos^2(t) + 0.23\sin^2(t)}(\cos(t), \sin(t))$
Pear	$\frac{5.5 + \sin(3t)}{5}(\cos(t), \sin(t))$
Star	$(1.2 + 0.4\sin(5t))(\cos(t), \sin(t))$

Table 3.1: The boundary parametrization of the geometries.

We clearly observe good performances in terms of robustness and accuracy.

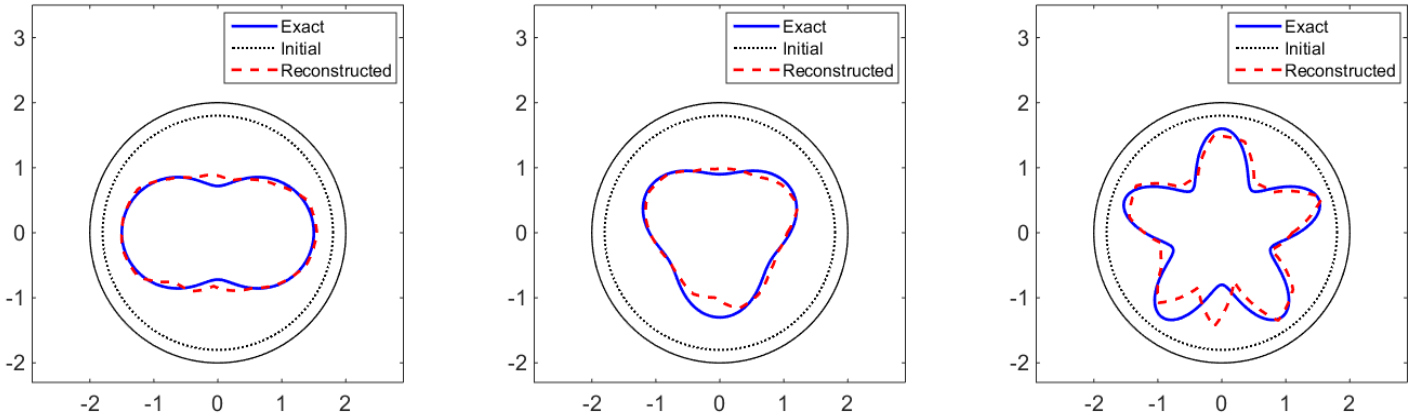

Figure 3.4: Reconstructions obtained by Algorithm 2 for the geometries discussed in Table 3.1 but for noisy data with noise level $\epsilon = 3\%$.

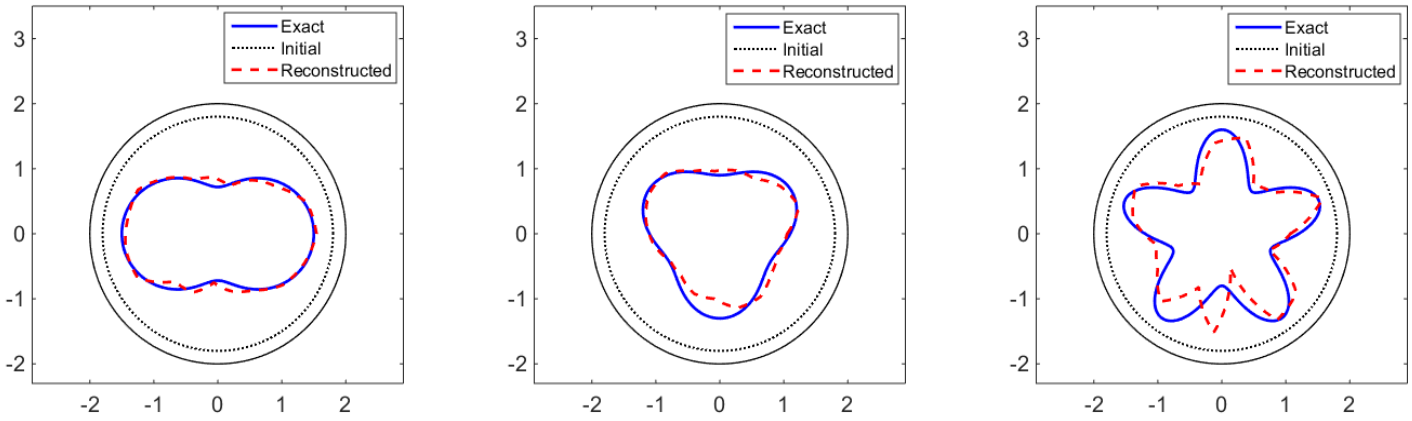

Figure 3.5: Reconstructions obtained by Algorithm 2 for the geometries discussed in Table 3.1 but for noisy data with noise level $\epsilon = 5\%$.

3.4.3 Discussion on the choice of L and τ

As mentioned earlier for a given τ, it is not clear which value of L would lead to potentially best performances of Algorithm 2. We provide here some elementary numerical investigations in the case where the exact geometry is given by the parametrization $\mathcal{T}_n$ (1.29) for given n. In that case it is possible to use a stopping rule related to the accuracy of the reconstruction,

e^k defined as

$$e^k = \frac{\|\overline{R} - R^k\|_2}{\|\overline{R}\|_2},$$

where $\Sigma_{\overline{R}}$ is the exact interface.

In the example below we choose $n = 9$, $\overline{R} = (1, 0.8, 0.7, 0.9, 1, 1.7, 1.6, 1.5, 1.4)$ and the initial guess $R^0 = (1.7, 1.6, 1.55, 1.4, 1.3, 1.3, 1.2, 1.4, 1.5)$ (see Figure 3.6(a)).

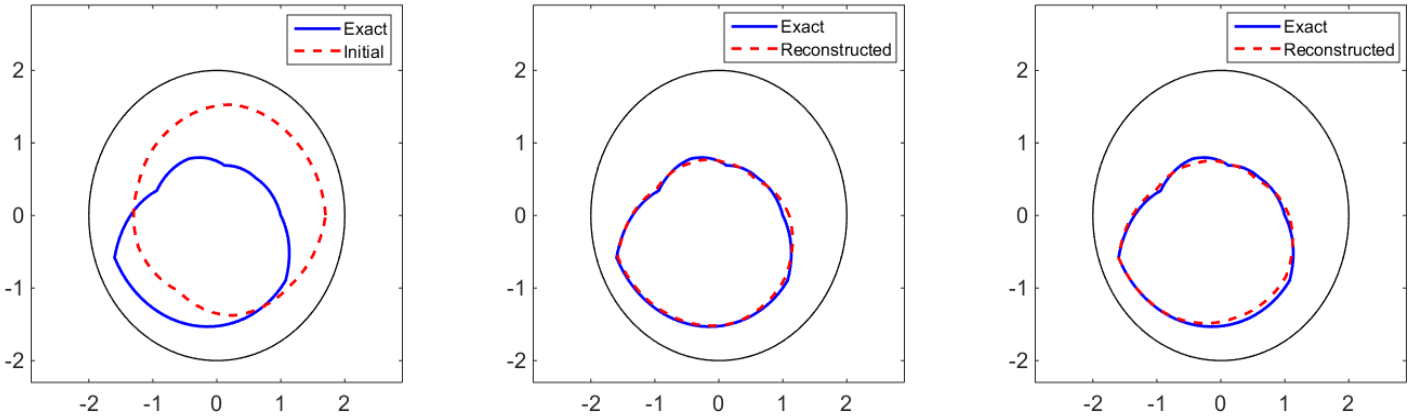

(a) Initial guess (b) Algorithm 1 (c) Algorithm 2

Figure 3.6: Comparison between Algorithm 1 and Algorithm 2 with $L = 1$ to achieve 5% relative accuracy in the case of the geometry given by Figure (a) and for noise free data. The gradient descent parameter $\tau = 0.1$ for both algorithms.

Table 3.2 gives the number of iterations K and the CPU time needed to achieve an accuracy $e^k \simeq 5\%$ for noise free data. We also indicate the virtually total cost $2KL$ that represents the total number of iterations for direct problems. We observe that $L = 1$ provides the lowest values for KL and $L = 2$ or $L = 3$ comparative performances. Figure 3.7 display the evolution of the cost functional for different values of τ indicating that the number of iterations K becomes closer to the one for gradient descent (Algorithm 1) as $\tau \to 0$. These observations show again the relevance of Algorithm 2 and that a few OSM iterations are sufficient to provide good solution for the inverse problem.

	$\tau = 0.1$			$\tau = 0.05$			$\tau = 0.005$		
L	K	$2KL$	CPU time	K	$2KL$	CPU time	K	$2KL$	CPU time
1	53	106	35.782	55	110	38.055	359	718	245.219
2	29	116	19.482	41	164	27.711	355	1420	240.439
3	29	174	20.314	39	234	26.006	355	2130	243.784
4	30	240	22.305	41	328	28.919	354	2832	259.115
5	30	300	24.263	39	390	30.149	354	3540	253.93

Table 3.2: Total number of iterations and CPU time for Algorithm 2 to achieve 5% relative accuracy in the case of the geometry given by Figure 3.6 and for noise free data.

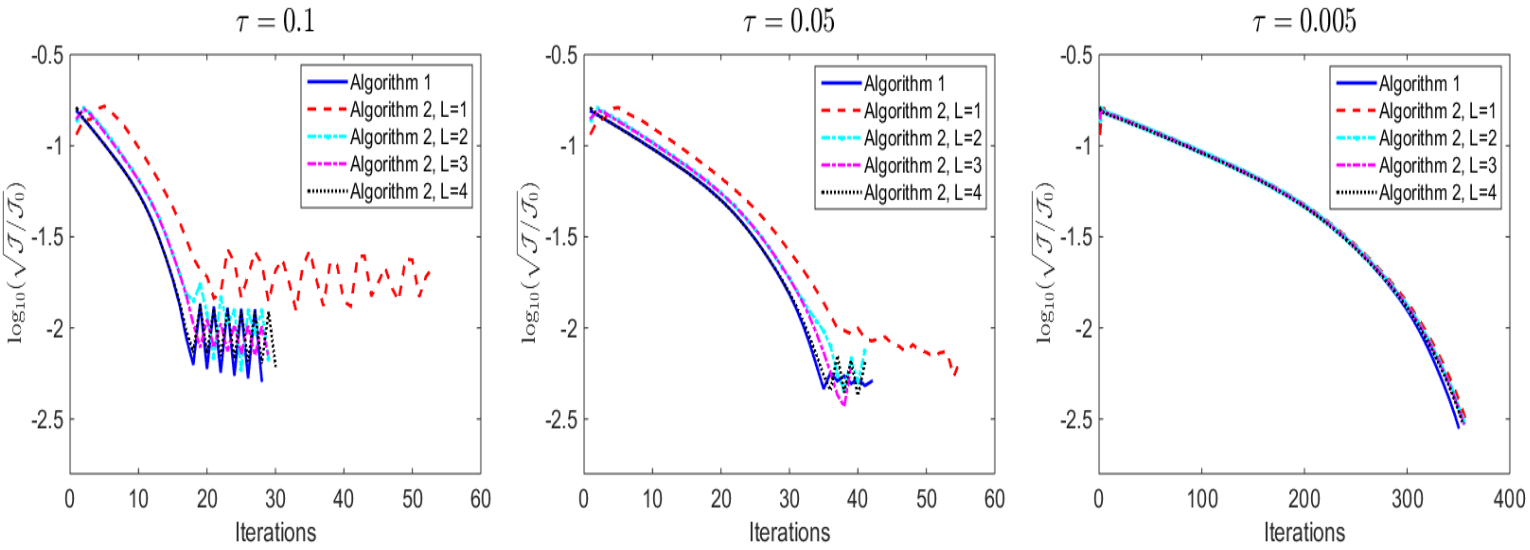

Figure 3.7: Comparison of the evolution of $\log_{10}(\sqrt{\mathcal{J}/\mathcal{J}_0})$ between Algorithm 1 and Algorithm 2 applied to the example of Figure 3.6 with different gradient descent parameter $\tau = 0.1$ (left), $\tau = 0.05$ (middle) and $\tau = 0.005$ (right).

Remark 3.4.1. *Figure 3.7 shows that the combined algorithm has almost the same number of iterations as the full gradient descent. This clearly indicates that the combined algorithm is potentially more cost-effective than the full gradient algorithm. However, the difference in execution time indicated in Table 3.2 is considerably similar. This can be explained by the fact that the direct problems we considered have small discrete systems. This may no longer be the case for large-scale problems, such as 3D problems.*

3.5 Conclusion

In this chapter, we have considered the geometric inverse conductivity problem. We have developed a combined inversion algorithm, summarized in Algorithm 2, to identify the singularity curve Σ of σ. This algorithm consists in mixing a gradient descent algorithm, summarized in Algorithm 1, with an Optimized Schwarz Method described in Chapter 2. We have proved the local convergence of Algorithm 2 in some simplified cases of domains. We complemented these results by showcasing some two-dimensional experiments to test the efficiency of the combined algorithm and compare it with the classical one.

CHAPTER 4

A combined inversion method for the full inverse conductivity problem

4.1 Introduction

In this chapter, we extend the approach proposed in the previous one to a more complex case involving iteration on the conductivity value. More precisely, we assume that σ_2 is known, and we aim to identify the conductivity σ_1 and the interface Σ by developing an alternating inversion algorithm that incorporates both the geometry and the conductivity value with an adaptive step descent to enhance its performance.

The chapter is organized as follows. We first discuss the issue of identifiability in the case of a piecewise constant conductivity, where we present a counterexample to illustrate that a single or two pairs (ϕ, f) are not sufficient to uniquely determine the unknown parameter σ_1 and the geometry Σ. To address this, one needs to increase the number of linearly independent used pairs of measurements. These additional measurements would enable a more reliable and accurate resolution of the inverse problem. In this context, we reformulate the Kohn-Vogelius cost function in order to develop an alternating inversion descent algorithm, which alternates between updating the geometry Σ and the conductivity value σ_1 using an adaptive step descent. This algorithm is summarized in Algorithm 3, which is detailed in Subsection 4.3.1. Additionally, in Subsection 4.3.2, we introduce a combined inversion algorithm summarized in Algorithm 4 that incorporates the coupling with OSM. In Subsection 4.3.3, a qualitative theoretical study is given in a simplified configuration. To assess the performance

and convergence of the proposed algorithms, we conduct several numerical experiments in Section 4.4 and compare the efficiency of the combined algorithm (Algorithm 4) to the full gradient algorithm (Algorithm 3).

4.2 Identifiability

We consider in this section the inverse conductivity problem that consists in recovering the conductivity value $\overline{\sigma_1}$ and the discontinuity interface $\overline{\Sigma}$ of an electrical conductivity $\overline{\sigma} \in S_{ad}$ from the knowledge of the flux ϕ together with the potential $f = u_{\overline{\sigma}_{|\Gamma}}$, where $u_{\overline{\sigma}}$ is the solution of $(N_{\overline{\sigma}})$. We give a counterexample proving that a single couple (ϕ, f) is not sufficient in general to uniquely determine the unknown parameter σ_1 and the interface Σ.

Example 4.2.1. *Consider the particular case where the domain Ω is the open disk of center $(0,0)$ and radius $R_2 = 3$. We denote by Σ and Σ' the following interfaces:*

$$\Sigma = \{(x,y) \in \mathbb{R}^2 \text{ such that } x^2 + y^2 = R_\Sigma^2 = 3\},$$

$$\Sigma' = \{(x,y) \in \mathbb{R}^2 \text{ such that } x^2 + y^2 = R_{\Sigma'}^2 = 7\},$$

and by Ω_i respectively Ω_i', $i \in \{1,2\}$ the subdomains of Ω limited by Γ and Σ, respectively Γ and Σ' as shown in the following two figures:

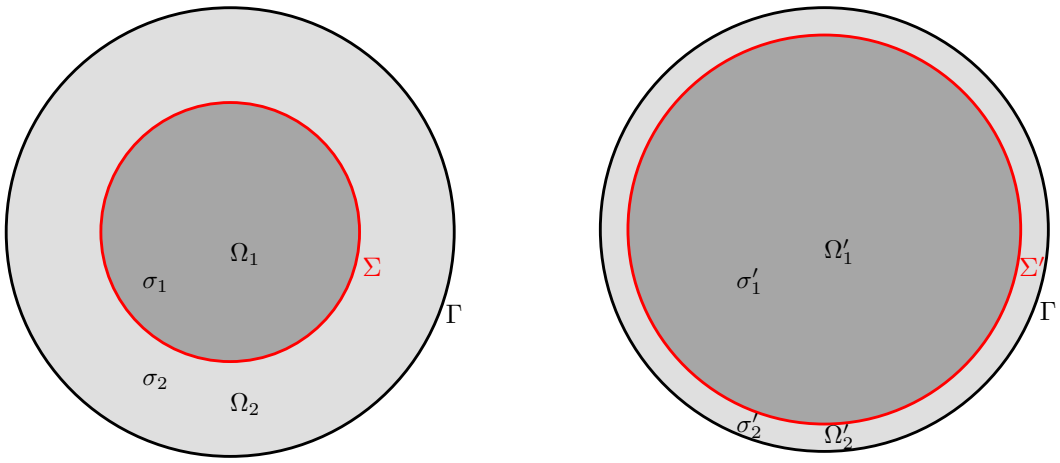

$\sigma = \sigma_1 \chi_{\Omega_1} + \sigma_2 \chi_{\Omega_2}$ $\qquad$ $\sigma' = \sigma_1' \chi_{\Omega_1'} + \sigma_2' \chi_{\Omega_2'}$

Figure 4.1: The two partitions of Ω for the counterexample.

Let (ϕ, f) a single couple of measurement defined by

$$\begin{array}{rccc} \phi: & [0,2\pi] & \longrightarrow & \mathbb{R} \\ & \theta & \longmapsto & \dfrac{8}{9}cos(\theta) \end{array} \quad ; \quad \begin{array}{rccc} f: & [0,2\pi] & \longrightarrow & \mathbb{R} \\ & \theta & \longmapsto & \dfrac{10}{3}cos(\theta), \end{array}$$

we see that

$$u_\sigma(r,\theta) = \begin{cases} u_1(r,\theta) = \dfrac{4}{3} r\cos(\theta) & \text{in } \Omega_1, \\ u_2(r,\theta) = \left(r + \dfrac{1}{r}\right)\cos(\theta) & \text{in } \Omega_2, \end{cases}$$

is the unique solution of the problem (N_σ) for $\sigma_1 = 1$, $\sigma_2 = 2$ and $R_\Sigma = \sqrt{3}$, and

$$u_{\sigma'}(r,\theta) = \begin{cases} u_1(r,\theta) = \dfrac{8}{7} r\cos(\theta) & \text{in } \Omega_1', \\ u_2(r,\theta) = \left(r + \dfrac{1}{r}\right)\cos(\theta) & \text{in } \Omega_2', \end{cases}$$

is the unique solution of the problem $(N_{\sigma'})$ for $\sigma_1' = \dfrac{3}{2}$, $\sigma_2' = \sigma_2$ and $R_{\Sigma'} = \sqrt{7}$.

Consequently, only one measurement is not sufficient to determine the unknown parameter $\overline{\sigma}$. In fact, even two linearly independent pairs of measurements (ϕ_1, f_1), (ϕ_2, f_2) are not sufficient to determine the piecewise constant conductivity $\overline{\sigma}$ (take the same example below replacing $\cos(\theta)$ by $\sin(\theta)$).

4.3 Numerical algorithm in the case of starlike domains

As a preparatory step for the combined algorithm, we first present the gradient descent algorithm in the case of starlike interfaces Σ (see Figure 1.2 for an illustration), similar to Section 1.7, which is detailed in Chapter 1.

4.3.1 An alternating gradient descent algorithm

Recall that the unknown of the inverse problem is $\overline{\sigma_1}$ and $\overline{R} \in (\mathbb{R}_+^*)^n$, $n \in \mathbb{N}^*$ that serve to define the starlike interface $\overline{\Sigma} = \Sigma_{\overline{R}}$. The Kohn-Vogelius cost function J given by formula (1.15) can then be seen as a function of σ_1 and R_i, $i = 0, \ldots, n-1$ with $R_n = R_0$.

Let us set $\sigma(\sigma_1, R) := \sigma_1 \chi_{\Omega_{1,R}} + \sigma_2 \chi_{\Omega_{2,R}}$ and define the function $\mathcal{J}_\phi$ by

$$\begin{array}{rccl} \mathcal{J}_\phi : & [\sigma_*, \infty[\times (\mathbb{R}_+^*)^n & \longrightarrow & \mathbb{R} \\ & (\sigma_1, R) & \longmapsto & \mathcal{J}_\phi(\sigma_1, R) = J(\sigma(\sigma_1, R)), \end{array} \tag{4.1}$$

The partial derivative $\dfrac{\partial \mathcal{J}_\phi}{\partial R_i}$, $i = 0, \ldots, n-1$, can be evaluated by applying Theorem 1.6.5 to a deformation field $\zeta = \zeta_i \nu$ on Σ_R where ζ_i is hat function defined by

$$\zeta_i(M) = t \chi_{\{M = \hat{M}_{i-1}(t) \in S_{i-1}\}} + (1-t) \chi_{\{M = \hat{M}_i(t) \in S_i\}}$$

with $S_{-1} = S_{n-1}$, $\hat{M}_i(t)$ is defined in (1.28) and ν is the outward normal vector to $\Omega_{1,R}$. We then get, by using Theorem 1.6.5 that the derivative of the cost function $\mathcal{J}_\phi$ with respect to R_i is given by the following formula:

$$\begin{aligned} \frac{\partial \mathcal{J}_\phi}{\partial R_i}(\sigma_1, R) = [\sigma(\sigma_1, R)] \int_{\Sigma_R} \Bigg[\frac{1}{\sigma_1 \sigma_2} \left(\left| \sigma(\sigma_1, R) \frac{\partial v_{\sigma(\sigma_1,R)}}{\partial \nu} \right|^2 - \left| \sigma(\sigma_1, R) \frac{\partial u_{\sigma(\sigma_1,R)}}{\partial \nu} \right|^2 \right) \\ + \left(|\nabla_\tau v_{\sigma(\sigma_1,R)}|^2 - |\nabla_\tau u_{\sigma(\sigma_1,R)}|^2 \right) \Bigg] \zeta_i \, ds, \end{aligned} \tag{4.2}$$

and by using Corollary 1.6.4, the derivative of the cost function $\mathcal{J}_\phi$ with respect to $\sigma_1 \in [\sigma_*, \infty[$ is given by the following formula:

$$\frac{\partial \mathcal{J}_\phi}{\partial \sigma_1}(\sigma_1, R) := \frac{\partial \psi}{\partial \sigma_1}(\sigma_1, \sigma_2) = \int_{\Omega_{1,R}} (|\nabla v_{\sigma(\sigma_1,R)}|^2 - |\nabla u_{\sigma(\sigma_1,R)}|^2) \, dx. \tag{4.3}$$

Our algorithm is based on minimizing the cost functional $\mathcal{J}_\phi$, one also has to avoid (as much as possible) the presence of local minima. We numerically observed that this can be done by increasing the number of used fluxes ϕ. More specifically, given N_ϕ linearly independent fluxes $\phi_1, \phi_2, \ldots, \phi_{N_\phi}$, the cost functional $\mathcal{J}(\sigma_1, R)$ that we shall consider is

$$\mathcal{J}(\sigma_1, R) := \sum_{j=1}^{N_\phi} \mathcal{J}_{\phi_j}(\sigma_1, R).$$

The derivative of $\mathcal{J}$ with respect to σ_1 and R can be written as

$$\frac{\partial \mathcal{J}}{\partial \sigma_1} = \sum_{j=1}^{N_\phi} \frac{\partial \mathcal{J}_{\phi_j}}{\partial \sigma_1}, \tag{4.4}$$

and

$$\frac{\partial \mathcal{J}}{\partial R_i} = \sum_{j=1}^{N_\phi} \frac{\partial \mathcal{J}_{\phi_j}}{\partial R_i}, \text{ for } i = 0, \ldots, n-1, \tag{4.5}$$

where $\frac{\partial \mathcal{J}_{\phi_j}}{\partial \sigma_1}$ is given by formula (4.3), and $\frac{\partial \mathcal{J}_{\phi_j}}{\partial R_i}$ is given by formula (4.2), which is based on Theorem 1.6.5.

The gradient descent algorithm, which alternates iterations on σ_1 and R_i, is summarized in Algorithm 3.

Algorithm 3: An alternating gradient descent algorithm with an exact direct solver

- Given N_ϕ linearly independent fluxes $\phi_1, \phi_2, \ldots, \phi_{N_\phi}$.
- Fix the number of parameters $n \in \mathbb{N}^*$ that serve to define the starlike interface.
- Consider an initial guesses σ_1^0 and $R^0 \in (\mathbb{R}_+^*)^n$, the initial interface $\Sigma = \Sigma_{R^0} = \mathcal{T}_n(R^0)$ and the corresponding conductivity $\sigma(\sigma_1^0, R^0) = \sigma_1^0 \chi_{\Omega_{1,R^0}} + \sigma_2 \chi_{\Omega_{2,R^0}}$.
- $k = 0$.

repeat *until* $k \leq$ *maximum number of iterations*

- Use a direct solver to calculate $u_{\sigma(\sigma_1^k, R^k)}$ and $v_{\sigma(\sigma_1^k, R^k)}$, the respective solutions of $(N_{\sigma(\sigma_1^k, R^k)})$ and $(D_{\sigma(\sigma_1^k, R^k)})$.
- Calculate $\dfrac{\partial \mathcal{J}}{\partial R_j}(\sigma_1^k, R^k)$, for $j = 0, \ldots, n-1$ using formula (4.2).
- Update $\Sigma = \mathcal{T}_n(R^{k+1})$ with

$$R_j^{k+1} := R_j^k - \tau_\Sigma \frac{\partial \mathcal{J}}{\partial R_j}(\sigma_1^k, R^k),\ j = 0, \ldots, n-1,$$

  where $\tau_\Sigma > 0$ is chosen sufficiently small that the cost functional decreases (a step adaptation can be incorporated here).
- Calculate $u_{\sigma(\sigma_1^k, R^{k+1})}$ and $v_{\sigma(\sigma_1^k, R^{k+1})}$, the respective solutions of $(N_{\sigma(\sigma_1^k, R^{k+1})})$ and $(D_{\sigma(\sigma_1^k, R^{k+1})})$.
- Calculate $\dfrac{\partial \mathcal{J}}{\partial \sigma_1}(\sigma_1^k, R^{k+1})$ using formula (4.3).
- Update for σ_1^{k+1}

$$\sigma_1^{k+1} = \sigma_1^k - \tau_{\sigma_1} \frac{\partial \mathcal{J}}{\partial \sigma_1}(\sigma_1^k, R^{k+1}),$$

  where $\tau_{\sigma_1} > 0$ is chosen sufficiently small that the cost functional decreases (a step adaptation can be incorporated here).
- $R^k = R^{k+1}$.
- $\sigma_1^k = \sigma_1^{k+1}$.
- $k = k + 1$.

end

A non-alternating scheme would consist of using an iteration step as follows:

$$\begin{cases} R_j^{k+1} = R_j^k - \tau \dfrac{\partial \mathcal{J}}{\partial R_j}(\sigma_1^k, R^k), \\ \sigma_1^{k+1} = \sigma_1^k - \tau \dfrac{\partial \mathcal{J}}{\partial \sigma_1}(\sigma_1^k, R^k), \end{cases} \tag{4.6}$$

where τ is a sufficiently small step. The inconvenience of this scheme is that it may converge slowly if σ_1 and R are not of the same order of magnitude.

4.3.2 An alternating combined inversion algorithm

We now introduce an alternative combined inversion algorithm, which combines Algorithm 3 with OSM. While this algorithm shares similarities with the combined algorithm explored in Chapter 3 for the inverse geometric problem, it differs in that we now assume knowledge of only σ_2. Our objective is to simultaneously determine both the conductivity σ_1 and the interface Σ. To achieve this, we present an improved alternating inversion algorithm that effectively incorporates both geometric and conductivity information associated with σ_1.

Given an integer $L > 0$, an initial guess σ_1^0, an interface Σ and an initial guess $\lambda_{i,N}^0 \in L^2(\Sigma)$, $i = 1, 2$ we denote by $N^L(\sigma_1, \Sigma, \lambda_{1,N}, \lambda_{2,N})$ the L^{th} iterate of (2.7). More precisely, we set

$$\begin{cases} N^L(\sigma_1^0, \Sigma, \lambda_{1,N}^0, \lambda_{2,N}^0) := u_1^L & \text{in } \Omega_1, \\ N^L(\sigma_1^0, \Sigma, \lambda_{1,N}^0, \lambda_{2,N}^0) := u_2^L & \text{in } \Omega_2, \end{cases}$$

where (u_1^ℓ) and (u_2^ℓ), $\ell = 1, \ldots, L$ verify the induction (2.7). We also set

$$\Lambda_{i,N}^L(\sigma_1^0, \Sigma, \lambda_{1,N}^0, \lambda_{2,N}^0) := \lambda_{i,N}^L \text{ on } \Sigma, \ i = 1, 2,$$

where $\lambda_{i,N}^L$ is the iterate number L of (2.7).

Similarly, for some initial guess $\lambda_{i,D}^0 \in L^2(\Sigma)$, $i = 1, 2$ we define:

$$\begin{cases} D^L(\sigma_1^0, \Sigma, \lambda_{1,D}^0, \lambda_{2,D}^0) := v_1^L & \text{in } \Omega_1, \\ D^L(\sigma_1^0, \Sigma, \lambda_{1,D}^0, \lambda_{2,D}^0) := v_2^L & \text{in } \Omega_2, \end{cases}$$

where (v_1^ℓ) and (v_2^ℓ), $\ell = 1, \ldots, L$ verify the induction (2.9) and by

$$\Lambda_{i,D}^L(\sigma_1^0, \Sigma, \lambda_{1,D}^0, \lambda_{2,D}^0) := \lambda_{i,D}^L \text{ on } \Sigma, \ i = 1, 2,$$

where $\lambda_{i,D}^L$ is the iterate number L of (2.9).

Algorithm 4: An alternating combined inversion algorithm

- Given N_ϕ linearly independent fluxes $\phi_1, \phi_2, \ldots, \phi_{N_\phi}$.
- Fix the number of parameters $n \in \mathbb{N}^*$ that serve to define the starlike interface.
- Consider an initial guesses σ_1^0 and $R^0 \in (\mathbb{R}_+^*)^n$, such that $\Sigma = \Sigma_{R^0} = \mathcal{T}_n(R^0)$ and the corresponding conductivity $\sigma(\sigma_1^0, R^0) = \sigma_1^0 \chi_{\Omega_{1,R^0}} + \sigma_2 \chi_{\Omega_{2,R^0}}$.
- Choose as initial boundary values: $\lambda_{i,N}(\Sigma) = 0,\ \lambda_{i,D}(\Sigma) = 0$ on $\Sigma,\ i = 1, 2$.
- k=0;

repeat *until* $k \leq$ *maximum number of iterations*

1. Set $\lambda_{i,N}^0 = \lambda_{i,N}(\Sigma),\ \lambda_{i,D}^0 = \lambda_{i,D}(\Sigma)$ on $\Sigma,\ i = 1, 2$.
2. Use L iterations of OSM to evaluate

$$u_{\sigma(\sigma_1^k, R^k)} = N^L(\sigma_1^k, \Sigma, \lambda_{1,N}^0, \lambda_{2,N}^0),\ \lambda_{i,N}^L(\sigma_1^k, R^k) = \Lambda_{i,N}^L(\sigma_1^k, \Sigma, \lambda_{1,N}^0, \lambda_{2,N}^0).$$

$$v_{\sigma(\sigma_1^k, R^k)} = D^L(\sigma_1^k, \Sigma, \lambda_{1,D}^0, \lambda_{2,D}^0),\ \lambda_{i,D}^L(\sigma_1^k, R^k) = \Lambda_{i,D}^L(\sigma_1^k, \Sigma, \lambda_{1,D}^0, \lambda_{2,D}^0).$$

3. Evaluate $\dfrac{\partial \mathcal{J}}{\partial R_j}(\sigma_1^k, R^k)$, for $j = 0, \ldots, n-1$ using formula (4.2) where the boundary values are calculated using $u_{\sigma(\sigma_1^k, R^k)_{|\Omega_1}}$ and $v_{\sigma(\sigma_1^k, R^k)_{|\Omega_1}}$.
4. Update $\Sigma = \mathcal{T}_n(R^{k+1})$ with $R_j^{k+1} := R_j^k - \tau_\Sigma \dfrac{\partial \mathcal{J}}{\partial R_j}(\sigma_1^k, R^k),\ j = 0, \ldots, n-1$, where $\tau_\Sigma > 0$ is chosen sufficiently small (A step adaptation can be incorporated here but only after a few iterations, when the gradient becomes sufficiently accurate and provides a descent direction).
5. Update the interface values on S_j as $\lambda_{i,N}(\Sigma)(\hat{M}_j(t)) = \lambda_{i,N}^L(\sigma_1^k, R^k)(t)$, $\lambda_{i,D}(\Sigma)(\hat{M}_j(t)) = \lambda_{i,D}^L(\sigma_1^k, R^k)(t)$, $t \in [0, 1]$, following the identification (3.1).
6. Repeat step 2 with $\Sigma = \mathcal{T}_n(R^{k+1})$.
7. Evaluate $\dfrac{\partial \mathcal{J}}{\partial \sigma_1}(\sigma_1^k, R^{k+1})$ using formula (4.3).
8. Update for σ_1: $\sigma_1^{k+1} = \sigma_1^k - \tau_{\sigma_1} \dfrac{\partial \mathcal{J}}{\partial \sigma_1}(\sigma_1^k, R^{k+1})$, where $\tau_{\sigma_1} > 0$ is chosen sufficiently small (A step adaptation can be incorporated here).

- $R^k = R^{k+1}$.
- $\sigma_1^k = \sigma_1^{k+1}$.
- $k = k + 1$.

end

A non-alternating scheme would consist of using an iteration step as follows:

$$\begin{cases} R_j^{k+1} = R_j^k - \tau \dfrac{\partial \mathcal{J}}{\partial R_j}(\sigma_1^k, R^k), \\ \sigma_1^{k+1} = \sigma_1^k - \tau \dfrac{\partial \mathcal{J}}{\partial \sigma_1}(\sigma_1^k, R^k), \end{cases} \tag{4.7}$$

where τ is a sufficiently small step. The inconvenience of this scheme is that it may converge slowly if σ_1 and R are not of the same order of magnitude.

4.3.3 On the local convergence study of the non-alternating version of Algorithm 4.

We will investigate the convergence of the non-alternating version of Algorithm 4 (see system (4.7)) in the simplified one-dimensional case where $\Omega =]0,1[$ and the number of OSM iterations $L = 1$, meaning we perform only one OSM step per iteration. In particular, we prove that with only one flux ($N_\phi = 1$), the algorithm may not converge (consistent with the non-uniqueness issue mentioned in Section 4.2).

In this part, we consider the configuration studied in Section 3.3.1 and use the same notation. From Theorem 1.6.5 and equation (1.36), we have

$$\frac{\partial \mathcal{J}}{\partial \delta}(\sigma_1, \delta) = \frac{(\sigma_1 - \sigma_2)}{\sigma_1 \sigma_2} \left(|\sigma_1 v'_{\sigma(\sigma_1,\delta)}(\sigma_1, \delta)|^2 - |\sigma_1 u'_{\sigma(\sigma_1,\delta)}(\sigma_1, \delta)|^2 \right),$$

and from formula (4.3), we have

$$\frac{\partial \mathcal{J}}{\partial \sigma_1}(\sigma_1, \delta) = \int_0^\delta |v'_{\sigma(\sigma_1,\delta)}(\sigma_1, \delta)|^2 - |u'_{\sigma(\sigma_1,\delta)}(\sigma_1, \delta)|^2 \, dx,$$

Moreover, the solutions after only one OSM step iterate are given in $]0, \delta[$ by

$$\begin{cases} u_{\sigma(\sigma_1^k,\delta^k)}(x) = \alpha_N^L(\sigma_1^k, \delta^k)x, \\ v_{\sigma(\sigma_1^k,\delta^k)}(x) = \alpha_D^L(\sigma_1^k, \delta^k)x, \end{cases}$$

where

$$\begin{cases} \alpha_N^L(\sigma_1, \delta) := \dfrac{\lambda_{1,N}^L(\sigma_1, \delta)}{(\sigma_1 + \alpha\delta)}, \\ \alpha_D^L(\sigma_1, \delta) := \dfrac{\lambda_{1,D}^L(\sigma_1, \delta)}{(\sigma_1 + \alpha\delta)}. \end{cases}$$

Hence, the gradient of $\mathcal{J}$ with respect to $\delta \in]0,1[$ and with respect to σ_1 are approximated by

$$\frac{\partial \mathcal{J}}{\partial \sigma_1}(\sigma_1^k, \delta^k) \simeq \frac{\delta^k}{(\sigma_1^k + \alpha\delta^k)^2} \left(|\lambda_{1,D}^L(\sigma_1^k, \delta^k)|^2 - |\lambda_{1,N}^L(\sigma_1^k, \delta^k)|^2 \right),$$

$$\frac{\partial \mathcal{J}}{\partial \delta}(\sigma_1^k, \delta^k) \simeq \frac{\sigma_1^k(\sigma_1^k - \sigma_2)}{\sigma_2(\sigma_1^k + \alpha\delta^k)^2} \left(|\lambda_{1,D}^L(\sigma_1^k, \delta^k)|^2 - |\lambda_{1,N}^L(\sigma_1^k, \delta^k)|^2 \right).$$

Our non-alternating version of Algorithm 4 (see system (4.7)) can be written as:

$$\delta^{k+1} = \delta^k - \tau \frac{\sigma_1^k(\sigma_1^k - \sigma_2)}{\sigma_2(\sigma_1^k + \alpha\delta^k)^2} \left(|\lambda_{1,D}^L(\sigma_1^k, \delta^k)|^2 - |\lambda_{1,N}^L(\sigma_1^k, \delta^k)|^2 \right), \tag{4.8}$$

$$\sigma_1^{k+1} = \sigma_1^k - \tau \frac{\delta^k}{(\sigma_1^k + \alpha\delta^k)^2} \left(|\lambda_{1,D}^L(\sigma_1^k, \delta^k)|^2 - |\lambda_{1,N}^L(\sigma_1^k, \delta^k)|^2 \right), \tag{4.9}$$

and the updates for the boundary values are given by

$$\begin{aligned}
\lambda_{1,N}^L(\sigma_1^{k+1}, \delta^{k+1}) &= p^\alpha(\sigma_1^k, \delta^k)\ \lambda_{2,N}^L(\sigma_1^k, \delta^k) + \eta^\alpha(\sigma_1^k, \delta^k), && (4.10)\\
\lambda_{2,N}^L(\sigma_1^{k+1}, \delta^{k+1}) &= k^\alpha(\sigma_1^k, \delta^k)\ \lambda_{1,N}^L(\sigma_1^k, \delta^k), && (4.11)\\
\lambda_{1,D}^L(\sigma_1^{k+1}, \delta^{k+1}) &= q^\alpha(\sigma_1^k, \delta^k)\ \lambda_{2,D}^L(\sigma_1^k, \delta^k) + \omega^\alpha(\sigma_1^k, \delta^k), && (4.12)\\
\lambda_{2,D}^L(\sigma_1^{k+1}, \delta^{k+1}) &= k^\alpha(\sigma_1^k, \delta^k)\ \lambda_{1,D}^L(\sigma_1^k, \delta^k), && (4.13)
\end{aligned}$$

where

$$\begin{aligned}
p^\alpha(\sigma_1^k, \delta^k) &:= -1,\\
\eta^\alpha(\sigma_1^k, \delta^k) &:= 2\phi,\\
k^\alpha(\sigma_1^k, \delta^k) &= \frac{\sigma_1^k - \alpha\delta^k}{\sigma_1^k + \alpha\delta^k},\\
q^\alpha(\sigma_1^k, \delta^k) &= \frac{\sigma_2 - \alpha(1-\delta^k)}{\sigma_2 + \alpha(1-\delta^k)},\\
w^\alpha(\sigma_1^k, \delta^k) &= \frac{2\alpha\sigma_2 f}{\sigma_2 + \alpha(1-\delta^k)},
\end{aligned}$$

and

$$f = \frac{\phi}{\overline{\sigma_1}\sigma_2} \left[\overline{\sigma_1}(1-\overline{\delta}) + \sigma_2\overline{\delta} \right]. \tag{4.14}$$

If we set $X^k := (\sigma_1^k, \delta^k, \lambda_{1,N}^L(\sigma_1^k, \delta^k), \lambda_{2,N}^L(\sigma_1^k, \delta^k), \lambda_{1,D}^L(\sigma_1^k, \delta^k), \lambda_{2,D}^L(\sigma_1^k, \delta^k))$, then the iterative scheme formed by (4.9)...(4.13) can be synthetically written as

$$X^{k+1} = G(X^k),$$

where the function G is given by

$$\begin{array}{rccl} G: & \mathbb{R}^6 & \longrightarrow & \mathbb{R}^6 \\ & X=(x_0,x,y,z,t,h) & \longmapsto & G(X)=(g_0(X),g_1(X),g_2(X),g_3(X),g_4(X),g_5(X)), \end{array}$$

such that:

$$\begin{aligned} g_0(X) &:= x_0-\tau\frac{x}{(x_0+\alpha x)^2}(t^2-y^2), \\ g_1(X) &:= x-\tau\frac{x_0(x_0-\sigma_2)}{\sigma_2(x_0+\alpha x)^2}(t^2-y^2), \\ g_2(X) &:= -z+2\phi, \\ g_3(X) &:= k^\alpha(x_0,x)y, \\ g_4(X) &:= q^\alpha(x_0,x)h+\omega^\alpha(x_0,x), \\ g_5(X) &:= k^\alpha(x_0,x)t. \end{aligned}$$

From the analysis of Section 2.4.1, we observe that the sequence $\lambda^\ell_{i,N}(\overline{\sigma_1},\overline{\delta})$, $i=1,2$ converges to $\lambda^\infty_{i,N}(\overline{\sigma_1},\overline{\delta})$, $i=1,2$, where

$$\lambda^\infty_{i,N}(\overline{\sigma_1},\overline{\delta})=\frac{\phi}{\overline{\sigma_1}}\psi_i,$$

with

$$\psi_1=(\overline{\sigma_1}+\alpha\overline{\delta}) \quad \text{and} \quad \psi_2=(\overline{\sigma_1}-\alpha\overline{\delta}).$$

Similarly, the sequence $\lambda^\ell_{i,D}(\overline{\sigma_1},\overline{\delta})$, $i=1,2$ converges to $\lambda^\infty_{i,D}(\overline{\sigma_1},\overline{\delta})$, $i=1,2$, where

$$\lambda^\infty_{i,D}(\overline{\sigma_1},\overline{\delta})=\frac{\sigma_2 f}{\sigma_2\overline{\delta}+\overline{\sigma_1}(1-\overline{\delta})}\psi_i.$$

Moreover, we have

$$\left\{\begin{array}{l} \lambda^\infty_{1,N}(\overline{\sigma_1},\overline{\delta})=-\lambda^\infty_{2,N}(\overline{\sigma_1},\overline{\delta})+2\phi, \\ \lambda^\infty_{2,N}(\overline{\sigma_1},\overline{\delta})=k^\alpha(\overline{\sigma_1},\overline{\delta})\lambda^\infty_{1,N}(\overline{\sigma_1},\overline{\delta}), \\ \lambda^\infty_{1,D}(\overline{\sigma_1},\overline{\delta})=q^\alpha(\overline{\sigma_1},\overline{\delta})\lambda^\infty_{2,D}(\overline{\sigma_1},\overline{\delta})+w^\alpha(\overline{\sigma_1},\overline{\delta}), \\ \lambda^\infty_{2,D}(\overline{\sigma_1},\overline{\delta})=k^\alpha(\overline{\sigma_1},\overline{\delta})\lambda^\infty_{1,D}(\overline{\sigma_1},\overline{\delta}). \end{array}\right.$$

Using the expression of f given by (4.14), one can easily check that $\lambda^\infty_{i,N}(\overline{\sigma_1},\overline{\delta})=\lambda^\infty_{i,D}(\overline{\sigma_1},\overline{\delta})$ and then

$$\begin{aligned} \overline{X} &= (\overline{\sigma_1},\overline{\delta},\lambda^\infty_{1,N}(\overline{\sigma_1},\overline{\delta}),\lambda^\infty_{2,N}(\overline{\sigma_1},\overline{\delta}),\lambda^\infty_{1,D}(\overline{\sigma_1},\overline{\delta}),\lambda^\infty_{2,D}(\overline{\sigma_1},\overline{\delta})) \\ &= (\overline{\sigma_1},\overline{\delta},\lambda^\infty_{1,N}(\overline{\sigma_1},\overline{\delta}),\lambda^\infty_{2,N}(\overline{\sigma_1},\overline{\delta}),\lambda^\infty_{1,N}(\overline{\sigma_1},\overline{\delta}),\lambda^\infty_{2,N}(\overline{\sigma_1},\overline{\delta})) \end{aligned}$$

is a fixed point of G.
For short notation, let us set $\overline{x} = \overline{\delta}$, $\overline{x_0} = \overline{\sigma_1}$ $\overline{y} = \lambda^{\infty}_{1,N}(\overline{\sigma_1}, \overline{\delta})$, and

$$k := k^{\alpha}(\overline{x_0}, \overline{x}) = \frac{\overline{x_0} - \alpha\overline{x}}{\overline{x_0} + \alpha\overline{x}} = \frac{\psi_2}{\psi_1}. \tag{4.15}$$

Since $\overline{X} = (\overline{x_0}, \overline{x}, \overline{y}, k\overline{y}, \overline{y}, k\overline{y})$ is a fixed point of G and the Jacobian matrix $DG(\overline{X})$ of G is given by

$$DG(\overline{X}) = \begin{pmatrix} 1 & 0 & s\tau & 0 & -s\tau & 0 \\ 0 & 1 & d\tau & 0 & -d\tau & 0 \\ 0 & 0 & 0 & -1 & 0 & 0 \\ r & b & k & 0 & 0 & 0 \\ 0 & c & 0 & 0 & 0 & q \\ r & b & 0 & 0 & k & 0 \end{pmatrix}$$

where we have set for short notation

$$\begin{aligned} s &:= \frac{1}{\tau}\frac{\partial g_0}{\partial y}(\overline{X}) = \frac{2\overline{x}\ \overline{y}}{(\overline{x_0} + \alpha\overline{x})^2}, \\ d &:= \frac{1}{\tau}\frac{\partial g_1}{\partial y}(\overline{X}) = \frac{2x_0(\overline{x_0} - \sigma_2)}{\sigma_2(\overline{x_0} + \alpha x)}, \\ r &:= \frac{\partial g_3}{\partial x_0}(\overline{X}) = \frac{2\alpha\overline{x}\ \overline{y}}{(\overline{x_0} + \alpha\overline{x})^2}, \\ b &:= \frac{\partial g_3}{\partial x}(\overline{X}) = \frac{-2\alpha\phi}{(\overline{x_0} + \alpha\overline{x})}, \\ c &:= \frac{\partial g_4}{\partial x}(\overline{X}) = \frac{2\alpha\phi}{(\sigma_2 + \alpha(1 - \overline{x}))}, \\ q &:= \frac{\partial g_4}{\partial h}(\overline{X}) = q^{\alpha}(\overline{x_0}, \overline{x}). \end{aligned}$$

For every $\tau > 0$, we denote by $\overline{\rho}(\tau)$, the spectral radius of the Jacobian matrix $DG(\overline{X})$.

The following proposition proves that the non-alternating version of Algorithm 4 (see equations (4.8) and (4.9)) cannot be convergent in general for any $\tau > 0$.

Proposition 4.3.1. $\overline{\rho}(\tau) \geq 1$ *for any* $\tau > 0$.

Proof. For every $(\lambda, \tau) \in \mathbb{R} \times \mathbb{R}$, we define the characteristic polynomial of $DG(\overline{X})$

$$P(\lambda,\tau) \;:=\; det(DG(\overline{X}) - \lambda I_6) = \begin{vmatrix} 1-\lambda & 0 & s\tau & 0 & -s\tau & 0 \\ 0 & 1-\lambda & d\tau & 0 & -d\tau & 0 \\ 0 & 0 & -\lambda & -1 & 0 & 0 \\ r & b & k & -\lambda & 0 & 0 \\ 0 & c & 0 & 0 & -\lambda & q \\ r & b & 0 & 0 & k & -\lambda \end{vmatrix}$$

Then, we have

$$P(\lambda,\tau) \;=\; (\lambda-1)\left(\lambda^5 - \lambda^4 + a_3(\tau)\lambda^3 + a_2(\tau)\lambda^2 + a_1(\tau)\lambda + a_0\right),$$

where

$$\begin{aligned} a_3(\tau) :&= cd\tau - k(q-1), \\ a_2(\tau) :&= (q+1)(db+sr)\tau + k(q-1), \\ a_1(\tau) :&= kcd\tau - k^2 q, \\ a_0 :&= k^2 q. \end{aligned}$$

Consequently, for all $\tau > 0$, $\lambda_0 = 1$ is an eigenvalue of $DG(\overline{X})$.

□

Remark 4.3.1. *Let us remark that despite this non-convergence issue, we have numerically observed that for geometries other than circles, the algorithm may converge with only one flux (but eventually to a local minimum). The convergence study in the case of multiple fluxes is more complicated and is still in progress.*

4.4 Numerical validation and results

The goal of this section is to test the efficiency of Algorithm 4 in comparison with the full gradient descent algorithm described in Algorithm 3. For our numerical validation example, we choose an open disk of center $(0, 0)$ and radius $R_2 = 2$. The exact conductivity values are given by $\overline{\sigma_1} = 1$, $\overline{\sigma_2} = 2$, and the OSM parameter $\alpha = 1$. As for the fluxes, we choose $\phi_1 = \cos(\theta)$ and $\phi_2 = \sin(\theta)$, $\theta \in [0, 2\pi]$, defined on the boundary Γ. Additionally, we select

$\overline{\Sigma}$ to be a kite defined by

$$x(t) = \cos(t) + 0.5\cos(2t) - 0.4 \;\text{ and }\; y(t) = 1.2\sin(t),\; t \in [0, 2\pi]. \tag{4.16}$$

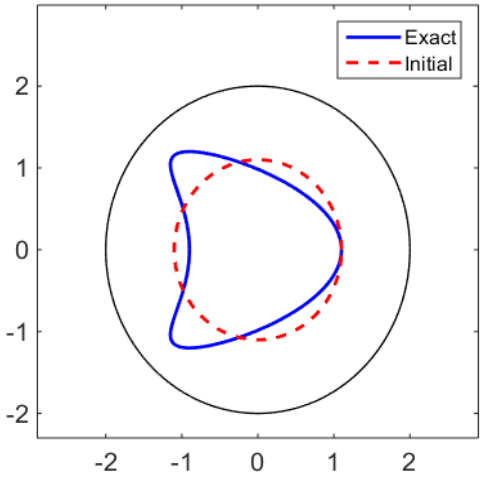

Figure 4.2: Description of the geometry for the kite parameterized by (4.16)

For the inversion algorithms, we utilize the parametrization (1.29) with $n = 19$. The initial guess is set to $R_j^0 = 1.1$ for $j = 0, \ldots, n-1$. The results of the inversion when we use only one flux ϕ are given in Figure 4.3 for Algorithm 3 and Figure 4.4 for Algorithm 4 with $L = 1$ (i.e., only one OSM step is used at each gradient descent iteration). We observe that both algorithms yield qualitatively similar accuracy, and both may converge with only one flux. The results when we use two fluxes ϕ_1 and ϕ_2 are shown in Figure 4.5 for Algorithm 3 and in Figure 4.6 for Algorithm 4 with $L = 1$. The evolution of the cost functional for both algorithm in the case of two fluxes is depicted in Figure 4.7. We clearly observe improvement in the reconstructions for both algorithms with qualitatively the some accuracy and number of iterations. This is once again a clear demonstration on the relevance of combined algorithm for solving this type of inverse problems.

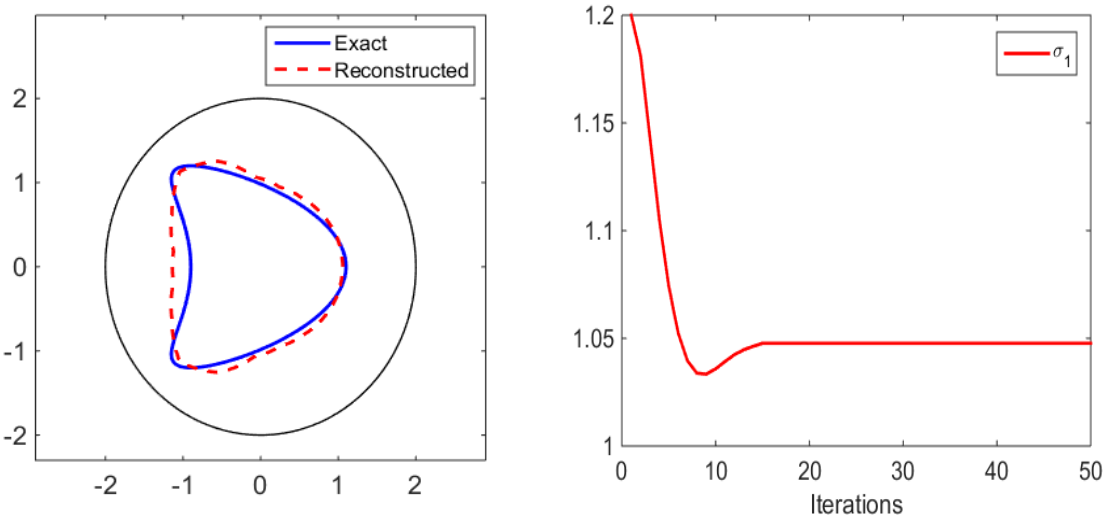

Figure 4.3: Reconstructions obtained by Algorithm 3 using flux ϕ_1 and for noise-free data. The initial guess is shown in Figure 4.2.

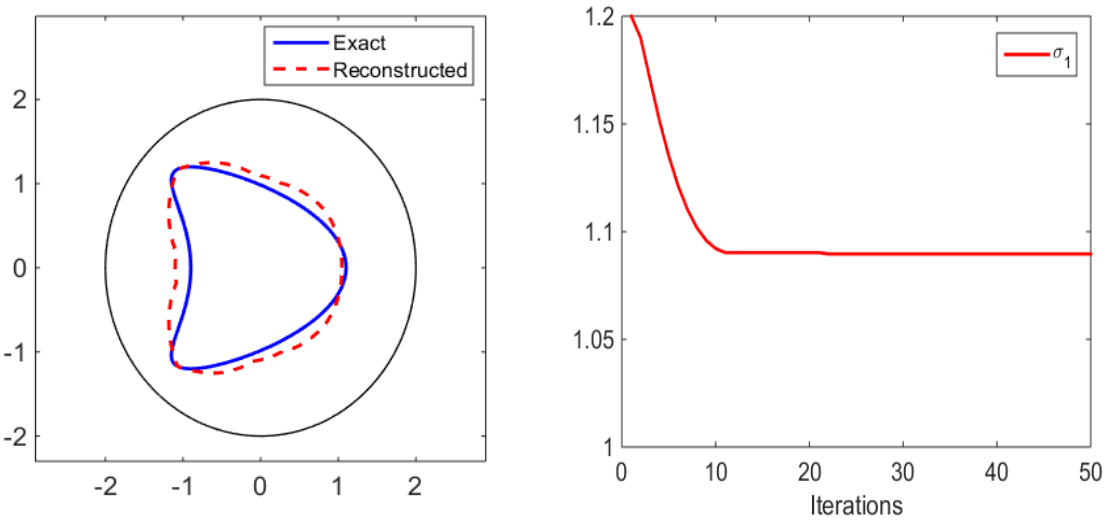

Figure 4.4: Reconstructions obtained by Algorithm 4 with $L = 1$ using flux ϕ_1 and for noise-free data. The initial guess is shown in Figure 4.2.

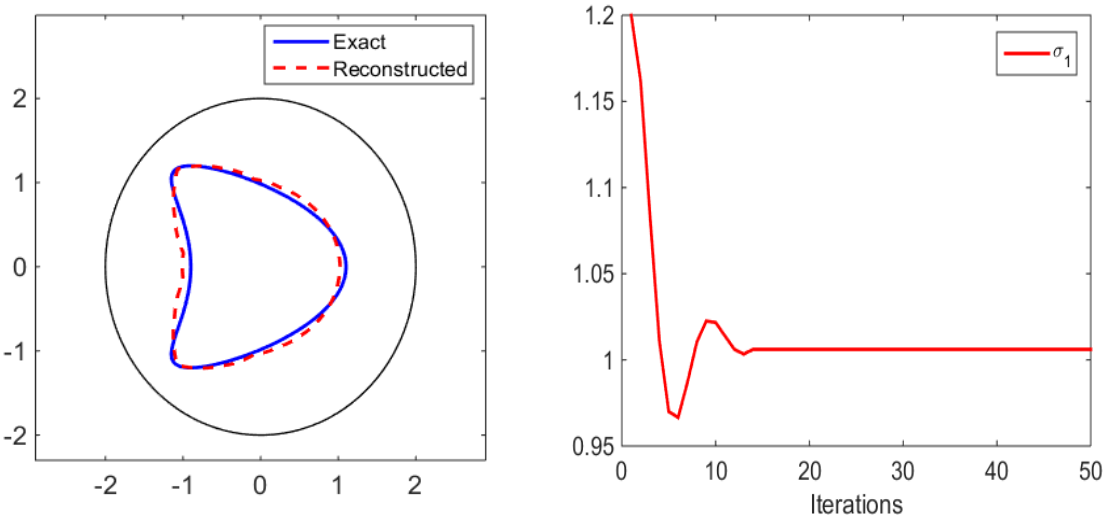

Figure 4.5: Reconstructions obtained by Algorithm 3 using two fluxes ϕ_1 and ϕ_2, and for noise-free data. The initial guess is shown in Figure 4.2.

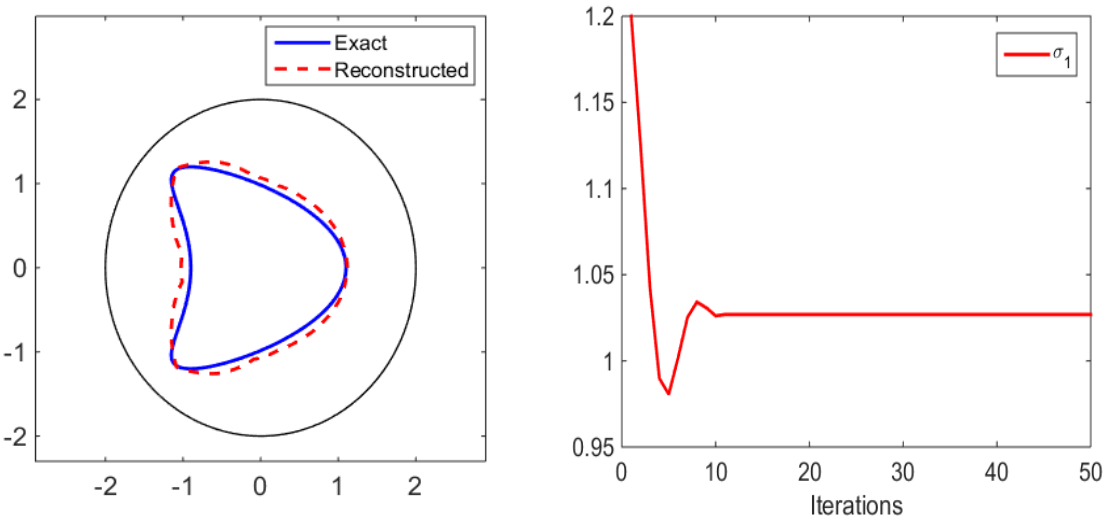

Figure 4.6: Reconstructions obtained by Algorithm 4 with $L = 1$ using two fluxes ϕ_1 and ϕ_2, and for noise-free data. The initial guess is shown in Figure 4.2.

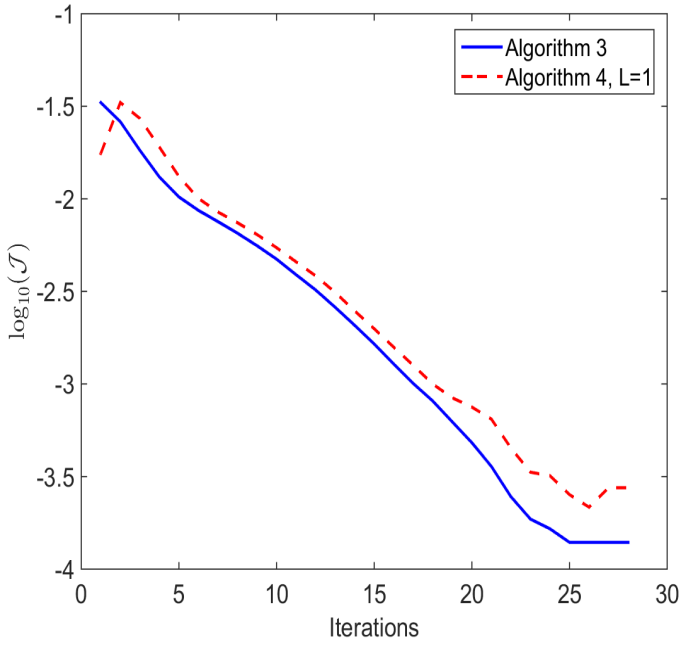

Figure 4.7: Comparison of the evolution of $\log_{10}(\mathcal{J})$ between Algorithm 3 and Algorithm 4 with $L = 1$ for the example shown in Figures 4.5 and 4.6.

4.5 Conclusion

In this chapter, we have extended the combined inversion method proposed in the previous one to address more complex cases involving iteration on the conductivity value. Specifically, we assume that σ_2 is known, and our objective is to identify the conductivity σ_1 and the interface Σ. We first discussed the issue of identifiability in the case of piecewise constant conductivity. We presented a counterexample to illustrate that a single or two pairs of measurements (ϕ, f) are insufficient to uniquely determine the unknown parameters σ_1 and Σ. To overcome this limitation, we emphasized the need to increase the number of linearly independent measurement pairs. Furthermore, we introduced a combined inversion algorithm, Algorithm 4, which incorporates the coupling with OSM. For the convergence analysis, we have specifically proved in the one-dimensional case that with only one flux, the algorithm may not converge. However, the convergence behavior in cases with multiple fluxes is more complex and is still under investigation. We conducted several numerical experiments comparing the efficiency of Algorithm 4 against the full gradient algorithm, summarized in Algorithm 3. The numerical observations showed that the algorithm may converge with only one flux for geometries other than circles, but it may lead to a local minimum. For multiple

fluxes, the combined algorithm has comparable performances as the full gradient one, but indeed with the potential of being much more cheap.

Conclusions and perspectives

In this thesis, we have developed a combined inversion algorithm that mixes the use of the Kohn-Vogelius cost functional and the Optimized Schwarz Method to solve an inverse geometrical problem in connection with impedance tomography. The latter consists of retrieving the interface discontinuity of the conductivity from measurements of Cauchy data. The proposed algorithm uses an incomplete OSM iteration at each gradient descent step for the interface. We have proved the convergence of the scheme for some simplified configurations of the geometry. We have also demonstrated the efficiency and relevance of the method through some 2D numerical experiments. These examples showed, in particular, that only one OSM iteration is sufficient to obtain comparable accuracy performances as the full gradient method. A full demonstration of the potential of this combined method can only be done through 3D experiments, for which the solution of the forward problem is costly. This is one of the perspectives of this work.

In the last part of this manuscript, we started the investigations of the inverse problem where the inner values of the conductivity are also unknown. We proposed an extension of the combined algorithm through alternate gradient steps on the geometry and the conductivity values. Preliminary numerical results confirm our conclusions on the efficiency of the combined algorithm. The theoretical investigations on the convergence are more challenging as we are faced with non-uniqueness issues in the case of one Cauchy pair of measurements. These aspects are also part of the perspectives of this work.

Bibliography

[1] R. A. Adams. *Sobolev Spaces*. Academic press New York, 1970.

[2] L. Afraites, M. Dambrine and D. Kateb. *Shape Methods for the Transmission Problem with a Single Measurement.* Numer. Funct. Anal. Optim., 28(5-6), 519-551, 2007.

[3] L. Afraites, M. Dambrine and D. Kateb. *On second order shape optimization methods for electrical impedance tomography*. SIAM J. Control Optim., 47(3), 1556-1590, 2008.

[4] G. Alessandrini and S. Vessella. *Lipschitz stability for the inverse conductivity problem*. Adv. Appl. Math., 35, 207-241, 2005.

[5] G. Allaire G. and F. Alouges. *Analyse variationnelle des équations aux dérivées partielles*. Cours MAP 431, Editions de École Polytechnique, Palaiseau, 109, 2016.

[6] A. Aspri, E. Beretta, E. Francini and S. Vessella. *Lipschitz Stable Determination of Polyhedral Conductivity Inclusions from Local Boundary Measurements*. SIAM Journal on Mathematical Analysis, 54(5), 5182-5222, 2022.

[7] K. Astala and L. Päivärinta. *Calderón's inverse conductivity problem in the plane.* Ann. of Math., 163, 265-299, 2006.

[8] E. Beretta and E. Francini. *Lipschitz stability for the electrical impedance tomography problem: The complex case.* Comm. Partial Differential Equations, 36, 1723–1749, 2011.

[9] E. Beretta and E. Francini. *Global Lipschitz stability estimates for polygonal conductivity inclusions from boundary measurements.* Appl. Anal., 01(10), 35363549, 2022.

[10] M. Bonazzoli. *Efficient high order and domain decomposition methods for the time-harmonic Maxwell's equations.* PhD thesis. Université Côte d'Azur, 2017.

[11] M. Bonazzoli, H. Haddar and T. A. Vu. *Convergence analysis of multi-step one-shot methods for linear inverse problems.* [Research Report] RR-9477, Inria Saclay; ENSTA ParisTech, 2022.

[12] L. Borcea. *Electrical impedance tomography.* Inverse Problems, 18(6), R99–R136, 2002.

[13] H. Brezis. *Analyse fonctionnelle: théorie et applications.* Masson, 1983.

[14] M. Burger and W. Mühlhuber. *Iterative regularization of parameter identification problems by sequential quadratic programming methods.* Inverse Problems, 18(4), 943–969, 2002.

[15] S. Chaabane, B. Charfi and H. Haddar. *Reconstruction of discontinuous parameters in a second order impedance boundary operator.* Inverse Problems, 32(10), 105004, 2016.

[16] S. Chaabane, C. Elhechmi and M. Jaoua. *A stable recovery algorithm for the Robin inverse problem.* IMACS, Math. Comput. Simul., 66(4-5), 367-383, 2004.

[17] S. Chaabane, I. Feki and N. Mars. *Numerical reconstruction of a piecewise constant Robin parameter in the two-or three-dimensional case.* Inverse Problems, 28(6), 065016, 2012.

[18] S. Chaabane and M. Jaoua. *Un algorithme d'identification de frontières soumises à des conditions aux limites de Signorini.* M2AN, 34(3), 707-722, 2000.

[19] S. Chaabane, H. Haddar and R. Jerbi. *A combination of Kohn-Vogelius and DDM methods for a geometrical inverse problem.* Inverse Problems, 39(9), 095001, 2023.

[20] B. Desprès. *Décomposition de domaine et problème de Helmholtz.* C.R. Acad. Sci. Paris, 1(6):313–316, 1990

[21] V. Dolean, P. Jolivet and F. Nataf. *An Introduction to Domain Decomposition Methods.* SIAM, Philadelphia, 2015.

[22] O. Dubois. *Optimized Schwarz methods for the advection-diffusion equation and for problems with discontinuous coefficients.* PhD thesis. McGill University, 2007.

[23] A. Friedman and B. Gustafsson. *Identification of the Conductivity Coefficient in an Elliptic Equation*, Siam J. Math. Anal, 777-787, 1987.

[24] R. Gaburro and E. Sinchich. *Lipschitz stability for the inverse conductivity problem for a conformal class of anisotropic conductivities.* Inverse Problems, 31(1), 2015.

[25] M. J. Gander. *Optimized Schwarz methods.* SIAM J. Numer. Anal., 44(2), 699-731, 2006.

[26] M. J. Gander. *Schwarz methods in the course of time.* Electronic Transactions on Numerical Analysis, 31 :228–255, 2008.

[27] N. Gauger, A. Griewank, A. Hamdi, C. Kratzenstein, E. Özkaya and T. Slawig. *Automated extension of fixed point PDE solvers for optimal design with bounded retardation.* In: Constrained Optimization and Optimal Control for Partial Differential Equations. International Series of Numerical Mathematics, 160, 99–122, Springer Basel, Basel, 2012.

[28] L. Gerardo-Giorda and F. Nataf. *Optimized Schwarz methods for unsymmetric layered problems with strongly discontinuous and anisotropic coefficients.* Technical report, 561, submitted. Ecole Polytechnique, CMAP, CNRS UMR 7641, Paris, France, 2004.

[29] A. Griewank. *Projected Hessians for Preconditioning in One-Step One-Shot Design Optimization.* In: Large-Scale Nonlinear Optimization. Nonconvex Optimization and Its Applications, 83, 151–171, Springer US, Boston, MA, 2006.

[30] E. Haber and U. M. Ascher. *Preconditioned all-at-once methods for large, sparse parameter estimation problems.* Inverse Problems, 17(6), 1847–1864, 2001.

[31] H. Haddar and R. Kress. *Conformal mapping and impedance tomography.* Inverse Problems, 26(7), 074002, 2010.

[32] A. Hamdi and A. Griewank. *Reduced quasi-Newton method for simultaneous design and optimization.* Computational Optimization and Applications, 49(3), 521–548, 2009.

[33] M. Hanke, B. Harrach and N. Hyvönen. *Justification of point electrode models in electrical impedance tomography.* Math. Models Methods Appl. Sci., 21(6), 1395-1413, 2011.

[34] M. Hassine and I. Kallel. *Kohn–Vogelius formulation and topological sensitivity analysis based method for solving geometric inverse problems.* Arab. J. Math. Sci., 24(1), 43–62, 2018.

[35] F. Hecht. *New development in FreeFem++.* J. Numer. Math., 20(3-4), 251–265, 2012.

[36] F. Hettlich and W. Rundell. *The determination of a discontinuity in a conductivity from a single boundary measurement.* Inverse Problems, 14(1), 67-82, 1998.

[37] B. Hofmann. *Approximation of the inverse electrical impedance tomography problem by an inverse transmission problem.* Inverse Problems, 14, 1171-1187, 1998.

[38] V. Isakov. *Inverse Problems for Partial Differential Equations.* Applied Mathematical Sciences, 127, Springer, 2017.

[39] C. Japhet and F. Nataf. *The best interface conditions for domain decomposition methods: Absorbing boundary conditions*. In: Absorbing Boundaries and Layers, Domain Decomposition Methods: Applications to Large Scale Computations, 348-373, Nova Science, New York, 2001.

[40] C. Japhet, F. Nataf and F. Rogier. *The optimized order 2 method. Application to convection-diffusion problems.* Future Gener. Comput. Sys., 18(1), 17-30, 2001.

[41] R. Jerbi. *Identification du support singulier d'une conductivité électrique.* Master's dissertation. University of Sfax, 2019.

[42] B. Kaltenbacher, A. Kirchner and B. Vexler. *Goal oriented adaptivity in the IRGNM for parameter identification in PDEs II: all-at-once formulations.* Inverse Problems, 30(4), 045002, 2014.

[43] T. A. Khan. *Review on Electrical Impedance Tomography: Artificial Intelligence Methods and its Applications.* Algorithms, 12(5), 88, 2019.

[44] R. V. Kohn and M. Vogelius. *Identification of an unknown conductivity by means of measurements at the boundary.* SIAM - AMS Proceedings; Vol. 14, pp.113-123, 1984.

[45] R. V. Kohn and M. Vogelius. *Determining conductivity by boundary measurements II. Interior results.* Communications on Pure and Applied Mathematics, 38(5), 643-667, 1985.

[46] R. V. Kohn and M. Vogelius. *Relaxation of a variational method for impedance computed tomography.* Communications on Pure and Applied Mathematics, 40(6), 745-777, 1987.

[47] M. Lecouvez. *Méthodes itératives de décomposition de domaine sans recouvrement avec convergence géométrique pour l'equation de Helmholtz.* Analyse numérique [math.NA]. PhD thesis. Ecole Polytechnique, Palaiseau, 2015.

[48] P.-L. Lions. *On the Schwarz alternating method. III. A variant for nonoverlapping subdomains.* In: Third International Symposium on Domain Decomposition Methods for Partial Differential Equations. SIAM, 202-223, 1990.

[49] M. Marden. *Geometry of Polynomial*, 2nd edition, Mathematical Surveys-Number 3, American Mathematical Society 1966.

[50] J. L. Mueller and S. Siltanen. *Linear and Nonlinear Inverse Problems with Practical Applications.* SIAM, 2012.

[51] A.I. Nachmann. *Reconstruction from boundary measurements.* Ann. of Math., 128, 531-576, 1988.

[52] A.I. Nachmann. *Global uniqueness for a two dimensional inverse boundary value problem.* Ann. of Math., 143, 71-96, 1996.

[53] R.G. Novikov. *A multidimensional inverse spectral problem for the equation* $\Delta\psi + (v(x) - Eu(x))\psi = 0$. Funktsional. Anal. i Prilozhen., 22(4), 11-22, 96, 1988 (in Russian); English Transl.: Funct. Anal. and Appl., 22(4), 263–272, 1988.

[54] H. A. Schwarz. *Über einen Grenzübergang durch alternierendes Verfahren.* Vierteljahrss chrift der Naturforschenden Gesellschaft in Zürich, 15:272–286, 1870.

[55] J. Sylvester and G. Uhlmann. *A global uniqueness for an inverse boundary value problem.* Ann. of Math., 125, 153-169, 1987.